MICROCOPY RESOLUTION TEST CHART
NATIONAL BUREAU OF STANDARDS-1963-A

SRI International

AD-A141 196

AFOSR-TR- 84 - 0 3 4 2

April 5, 1984

Final Scientific Report
Covering the Period 15 November 1980 through
28 February 1984

ION PHOTOFRAGMENT SPECTROSCOPY: STRUCTURE AND
DISSOCIATION OF MOLECULAR IONS

By: P. C. Cosby
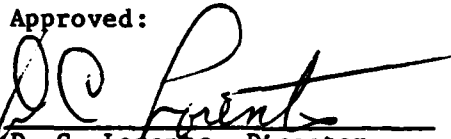
SRI Project No. 2422
AFOSR Contract No. F49620-81-K-0006
MP 84-057

Prepared for:

U.S. AIR FORCE OFFICE OF SCIENTIFIC RESEARCH
Bolling Air Force Base
Washington, DC 20332

Attention: Directorate of Chemical and
Atmospheric Sciences

Approved:

D. C. Lorents, Director
Chemical Physics Laboratory

G. R. Abrahamson
Vice President
Physical Sciences Division

MAY 1 0 1984

A

84 05 15 224

SECURITY CLASSIFICATION OF THIS PAGE *(When Data Entered)*

REPORT DOCUMENTATION PAGE		READ INSTRUCTIONS BEFORE COMPLETING FORM
1. REPORT NUMBER AFOSR-TR- 84-0342	2. GOVT ACCESSION NO. AD-A196 196	3. RECIPIENT'S CATALOG NUMBER
4. TITLE *(and Subtitle)* ION PHOTOFRAGMENT SPECTROSCOPY: STRUCTURE AND DISSOCIATION OF MOLECULAR IONS		5. TYPE OF REPORT & PERIOD COVERED Final Scientific
		6. PERFORMING ORG. REPORT NUMBER
7. AUTHOR*(s)* P. C. Cosby		8. CONTRACT OR GRANT NUMBER*(s)* F49620-81-K-0006
9. PERFORMING ORGANIZATION NAME AND ADDRESS SRI International 333 Ravenswood Avenue Menlo Park, CA 94025		10. PROGRAM ELEMENT PROJECT. TASK AREA & WORK UNIT NUMBERS 61102F 9303/B1
11. CONTROLLING OFFICE NAME AND ADDRESS Air Force Office of Scientific Research /NC. Bolling Air Force Base Washington, DC 20332		12. REPORT DATE 5 April 1984
		13. NUMBER OF PAGES 122
14. MONITORING AGENCY NAME & ADDRESS*(if different from Controlling Office)*		15. SECURITY CLASS *(of this report)* Unclassified
		15a. DECLASSIFICATION. DOWNGRADING SCHEDULE

16. DISTRIBUTION STATEMENT *(of this Report)*

Approved for public release; distribution unlimited.

17. DISTRIBUTION STATEMENT *(of the abstract entered in Block 20, if different from Report)*

N/A

18. SUPPLEMENTARY NOTES

The findings in this report are not to be construed as an official Department of the Air Force position, unless so designated by other authorized documents.

19. KEY WORDS *(Continue on reverse side if necessary and identify by block number)*

Photodissociation, Ions, Potential curves, Photofragment Spectroscopy, Molecular Structure, Lifetimes, Molecular Constants, N_2^{++}, NO^+, OH^+, SO^+, O_2^+, SH^+, CH_3I^+

20. ABSTRACT *(Continue on reverse side if necessary and identify by block number)*

Photodissociation of the postive molecular ions of NO, OH, SO, SH, oxygen, and methyliodide and the doubly-charged molecular ion of nitrogen is observed at visible and ultraviolet laser wavelengths using ion photofragment spectroscopy. The wavelength dependence for the production of photofragments from each of these species reflects highly structured absorption spectra of electronic transitions into predissociated excited states lying in the region of their lowest energy dissociation asymptotes. The absorption spectra, coupled with

DD FORM 1473 EDITION OF 1 NOV 65 IS OBSOLETE

kinetic energy analysis of the photofragments produced in the dissociations, allow identification of the absorbing and dissociating states in these ions and determination of their molecular constants.

CONTENTS

APPENDICES

i

I INTRODUCTION

Molecular ions are prevalent in a wide range of gaseous media, including the earth's and other planetary atmospheres and ionospheres, interstellar space, gas discharges and lasers, MHD power generators, rocket exhaust plumes, and ballistic missile reentry wakes. A detailed knowledge of their structure and reactions is required in the development of both diagnostic techniques and theoretical models of the media.

The goal of the research on Contract F49620-81-K-0006 was to apply the unique technique of photofragment spectroscopy to determine the structure and dissociation dynamics of small molecular ions. Our implementation of photofragment spectroscopy under this contract simultaneously employed sub-Doppler optical resolution and high dissociation fragment kinetic energy resolution. The technique is demonstrated to yield the identification, potential energy curves, and molecular constants of ion electronic states, precise bond dissociation energies and ionization potentials, excited state lifetimes, and product branching ratios. In particular, this research provides detailed information on the interactions among molecular electronic states and the partitioning of internal and translational energy in the dissociation process.

This research was begun on 15 November 1980. Over the course of this research, we have applied the technique of photofragment spectroscopy to the ions O_2^+, NO^+, N_2^{++}, SO^+, OH^+, SH^+, and CH_3I^+. Our work on each of these species has provided new insights into the process of molecular dissociation dynamics and the inverse process of ion-atom collisions. One of the more notable achievements of this research was to observe for the first time a marked selectivity among atomic fine-structure states in a molecular dissociation, which has stimulated the introduction of new theoretical models to describe this process. The research has also provided the first experimental observation of a strong rotational dependence in the angular distribution of dissociation fragments, verifying a theoretical model introduced two decades earlier. In addition, it provided the first definitive evidence for the existence of a stable doubly-charged diatomic ion that had been postulated

1

nearly three decades ago, as well as spectroscopic identification of long-lived excited electronic states in ions produced by electron-impact ionization. Our work has further found that assumptions regarding the randomization of internal energy should not be routinely applied to all polyatomic ions.

A brief discription of the experimental technique used in this research is given in the next section. This is followed by a summary of the research results for individual ionic species.

II EXPERIMENTAL APPROACH

The high reactivity of molecular ions and the very low densities with which they can be produced preclude direct application of the traditional spectroscopic techniques developed for neutral species to the study of molecular ion excited states. Consequently, current information on the structure and internal energy states of molecular ions is extremely limited and, before the inception of our research, the dynamic evolution of these states could only be indirectly inferred. We have found that photodissociation can be used as a particularly sensitive probe to obtain detailed information on molecular ion energy levels. This information is analogous to, and indeed surpasses, that obtained for neutral molecules using absorption spectroscopy.

In our technique, a laser is used to pump the molecular ion from specific vibrational, rotational, and fine-structure levels in a bound electronic state to levels in an excited state of the ion that lie in energy above its dissociation limit. If these levels are predissociated (as is generally the case), the absorption of photons can be detected with high efficiency by the appearance of a fragment ion. Moreover, the kinetic energy and angular distribution of the fragment ion are directly measured. This technique is termed photofragment spectroscopy.

To implement this technique, we constructed (under our previous AFOSR contract) an unique laser-ion coaxial beams photofragment spectrometer,[1] shown schematically in Figure 1. The ions are produced in an electron impact ion source, extracted to form a beam, and accelerated under collision-free conditions to several thousand electron volts of energy. The desired mass species is selected by a magnetic sector, collimated to 2 mrad angular divergence, and bent by 90 degrees into the photon interaction region by a two-dimensional electrostatic quadrupole field. In this region the ions are intersected by a coaxial laser beam. Fragment ions produced in this region are directed by a second quadrupole field either into a high resolution
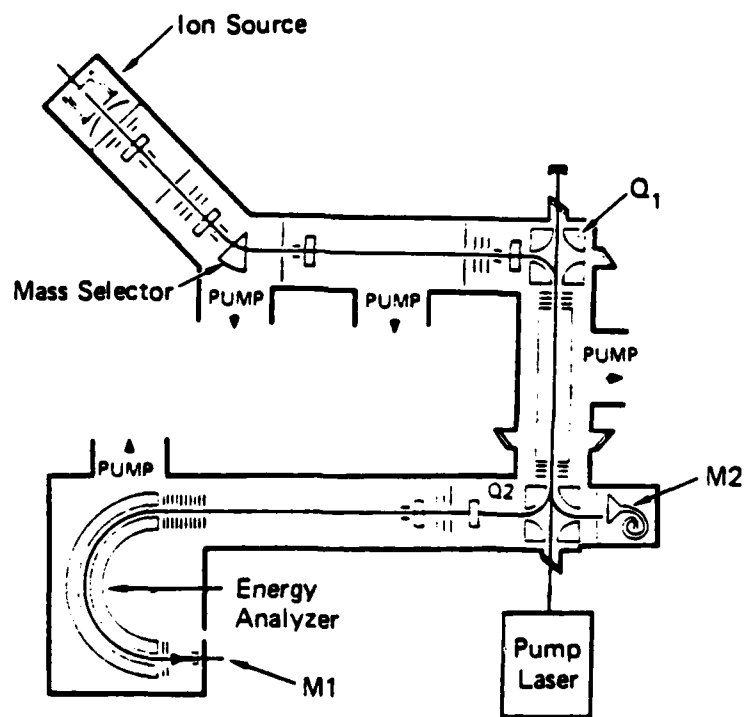
FIGURE 1   SRI LASER-ION COAXIAL BEAMS PHOTOFRAGMENT
SPECTROMETER

JA-330583-74E

4

hemispherical electrostatic energy analyzer and detected by electron multiplier M1, or directly into electron multiplier M2.

There are two basic methods for observing the photodissociation process with this apparatus, depending on whether the frequency of the irradiating laser is fixed or scanned. In the first method, the ion beam is irradiated with a fixed laser wavelength and the transmission maxima of both the second quadrupole and the electrostatic energy analyzer are scanned. The resulting kinetic energy spectrum of the photofragment ions identifies the locations of both the absorbing and dissociating ion states relative to the molecules' dissociation limit (rather than only relative to each other as in purely optical techniques), the mass of the fragment ions, the angular distribution of the fragment ions, and the internal energy states of the fragment ions.

In the second approach, the wavelength of the laser is scanned and the current of photofragments produced at each increment of laser wavelength is detected by either a fixed setting of the energy analyzer or by the multiplier M2. Using the energy analyzer as the detector, one observes only photofragments produced with a given energy relative to the dissociation limit. This yields the absorption spectrum of the ion for transitions that terminate only in the selected range of predissociating levels in the upper electronic state, but requires many wavelength scans with different energy analyzer settings to detect all of the dissociating levels in the upper electronic state. On the other hand, by directing the fragments produced in the photon interaction region onto multiplier M2, we can reduce the energy selectivity of the apparatus by several orders of magnitude, allowing a wide range of upper state levels to be observed in single wavelength scans.

As mentioned above, the laser is directed coaxial to the molecular ion beam. This has the advantage of providing a large region of overlap between the beams, thus increasing the sensitivity of the apparatus for detecting the production of photofragments. More importantly, the coaxial geometry allows us to take advantage of the Doppler effect both to vary the frequency of line-tunable lasers and to use velocity compression of the absorption linewidths. The frequency of the irradiating laser ν_0, when observed by the molecular ion beam, is Doppler-shifted to a new value $\nu_\pm = \nu_0(1 \pm v/c)/[1-(v/c)^2]^{1/2}$, where + refers to photons counterpropagating with the ion beam direction, - refers to copropagating photons, and v is the

5

velocity of the ion beam. Thus, by applying a variable voltage to the photon interaction region, the velocity of the ion beam is scanned, thereby scanning the effective frequency of a fixed-frequency laser. This is generally applied to ion lasers, but can also be used with advantage on tunable dye lasers because the resulting scan is far more linear than can be achieved by the laser itself.

The second advantage of the coaxial geometry is that it leads to very small Doppler-width contributions to the absorption lineshapes. Although the kinetic energy spread of the ions produced in the source is large ($\sim$ 1 eV) compared with that of a room temperature gas, the magnitude of this energy spread (in the laboratory system) remains unchanged as the beam is accelerated to several thousand electron volts. This results in the well-known kinematic compression in the ion beam velocity spread and permits Doppler widths equivalent to those of a gas at a temperature of 1 K or less for absorptions in the coaxial laser ion beam configuration. The predissociation lifetimes of discrete vibrational, rotational, and fine-structure levels can thus be measured directly from the broadened absorption linewidths of transitions into the predissociated level.

III   RESEARCH ACCOMPLISHMENTS

Research under this contract has entailed study of the photodissociative processes in N_2^{++}, NO^+, OH^+, SO^+, O_2^+, SH^+, and CH_3I^+. The results for each of these species are summarized below.

A. N_2^{++}

The doubly charged ions of N_2, O_2, and NO are known to occur in ionized atmospheric gases, but because of their very high reactivity, only limited experimental knowledge of their structure and properties exists. Theory predicts that the large Coulombic repulsion between their single-charged constituent atoms is overcome by chemical bonding forces only at short inter-nuclear distances. Consequently, even the ground electronic states of these species are metastable with respect to dissociation into two single-charged atoms. However, several of the electronic states in these species are pre-dicted to exhibit energetic barriers with respect to dissociation. These barriers can be wide enough that the predissociation lifetimes of the lower vibrational levels may be nearly infinite in the absence of external perturba-tion. Nevertheless, these species had been uniquely identified only in mass spectrometers, where they were observed to spontaneously dissociate. Before our research, there existed only one tentative optical measurement of a doubly charged diatomic ion: Carroll[2] in 1958 observed a single vibrational band within the vuv emission spectrum of a N_2-He discharge that he suggested might be the $D^1\Sigma_u^+(v=0) \rightarrow X^1\Sigma_g^+(v=0)$ transition in N_2^{++}, primarily because the rotational constants in this band did not agree with the known electronic states in either N_2 or N_2^+.

We observe N_2^{++} to photodissociate into $N^+ + N^+$ in a series of structured bands over the wavelength region of 6700 - 5100 Å. Rotational analysis of five of these bands identifies the absorption as $1^1\Pi_u \leftarrow X^1\Sigma_g^+(v=0,1,2)$. Figure 2 shows the potential energy curves for these states. Three vibra-tional levels of the $1^1\Pi_u$ state are observed to predissociate. The upper two levels predissociate by tunneling through the Coulombic barrier, whereas the

7
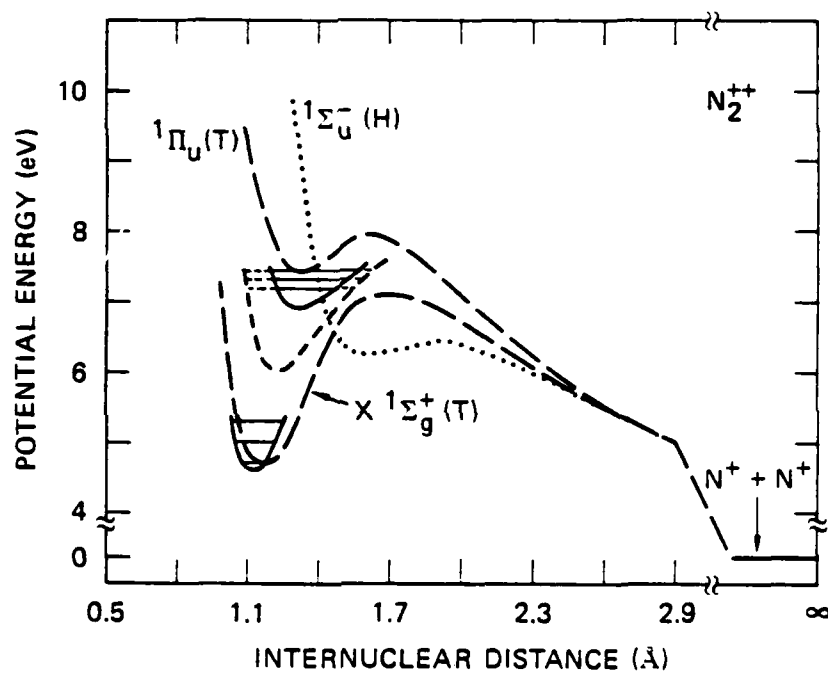
JA-2422-14

FIGURE 2 POTENTIAL ENERGY CURVES OF N_2^{++}

Lower solid curve is the RKR potential of the $X^1\Sigma_g^+$ state
derived in this work. Upper solid and short-dashed curves
are the RKR potentials of the $1^1\Pi_u$ state obtained assuming
the vibrational numbering of the observed levels was 1,2,3
and 6,7,8, respectively. The long-dashed curves are those
calculated by theory. The dotted curve is a theoretical
estimate for the location of the predissociating state.

8

lowest level is predissociated by spin-orbit coupling to the $1^1\Sigma_u^-$ state. The molecular constants for the ground state confirm the tentative identification of Carroll's emission band. Potential energy curves are constructed for the $X^1\Sigma_g^+$ and $1^1\Pi_u$ states and are used to resolve the conflicting results from three independent theoretical calculations of the N_2^{++} electronic states. Kinetic energy analysis of the N^+ photofragments also allowed us to establish the first definitive value for the appearance potential of N_2^{++}. A complete discription of this work has been published in The Physical Review and is attached as Appendix A to this report.

In addition to the work discussed above, we observe a structured band in the photofragment spectrum of N_2^{++} near 6600 Å that is not related to the $1^1\Pi_u$ ← $X^1\Sigma_g^+$ transition (see Fig. 1 of Appendix A). It is likely that this band accesses the lowest triplet manifold of N_2^{++}, which would warrant further study of this ion at longer wavelengths. Moreover, the technique of photofragment spectroscopy, which is so successfully applied here to N_2^{++}, is directly applicable to the other atmospheric doubly charged ions NO^{++} and O_2^{++}, for which absolutely no spectroscopic information is yet available.

B. NO^+

We observe the NO^+ ion to selectively photodissociate into O^+ and N^+ fragments in several extensive series of electronic absorptions over the wavelength region of 6950 – 5200 Å. These transitions are summarized in Figure 3, which shows the measured locations of the vibrational levels in the upper and lower electronic states involved in the transitions relative to the energy of $NO(X^2\Pi,v=0)$.

In the band system labelled I in Figure 3, three vibrational levels of the $b'^3\Sigma^-$ state are found to access 20 vibrational levels of the $2^3\Pi$ state, which predissociate to $O^+(^4S) + N(^4S)$ products. A complete discription of our work on this band system has been published in The Journal of Chemical Physics and is included as Appendix B to this report. In band systems labelled II and III in Figure 3, electronic transitions are observed from 10 vibrational levels of the $w^3\Delta$ state into four vibrational levels of a higher state, which predissociate into $O^+(^4S) + N(^4S)$ and two vibrational levels, which predissociate into $N^+(^3P) + O(^3P)$. The upper electronic state in both of
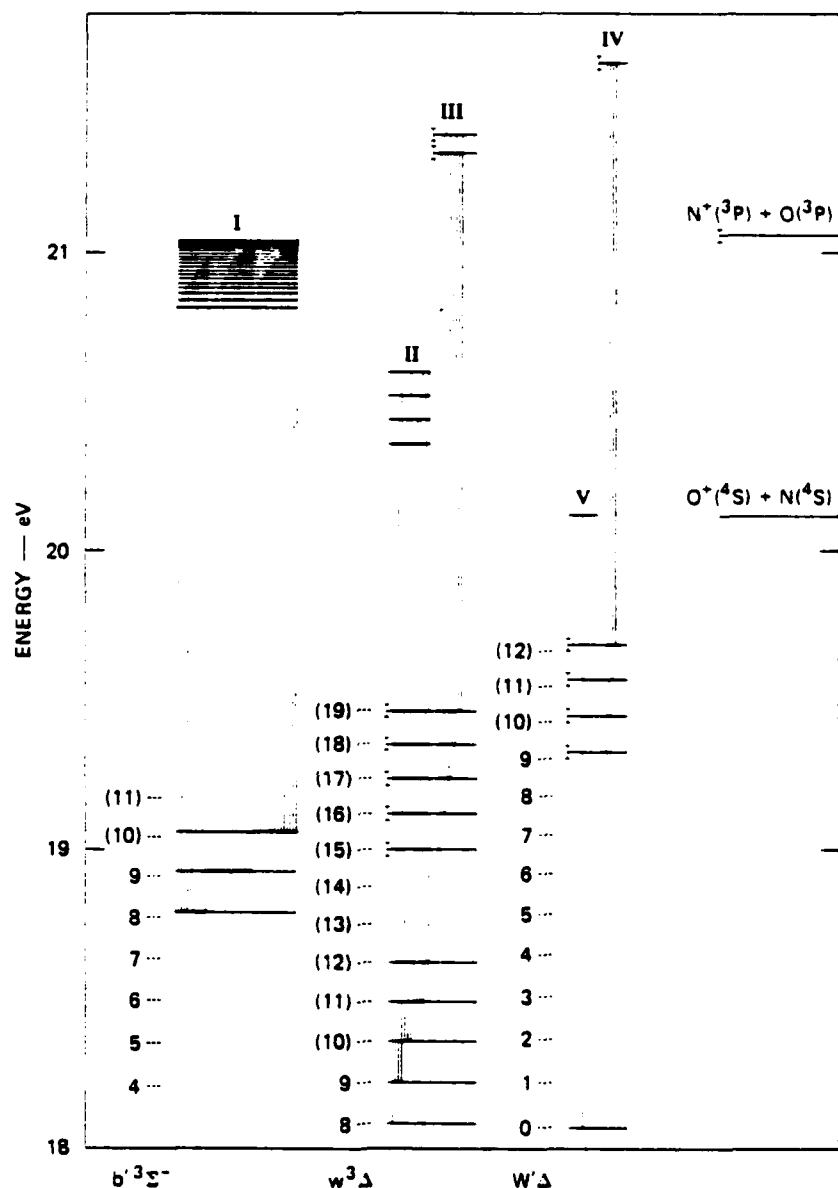
FIGURE 3 OBSERVED NO$^+$ ENERGY LEVELS

Transitions which result in predissociation of NO$^+$ are shown by the vertical lines. The horizontal lines connected by these transitions are the measured locations of the lower electronic state vibrational levels populated in the ion beam and the predissociated vibrational levels in the upper electronic states. The energy scale is relative to NO(X$^2\Pi$, v = 0). Expected locations for the levels in the b'$^3\Sigma^-$, w$^3\Delta$, and w'$^1\Delta$ states are shown by the dashed horizontal lines labelled by vibrational quantum numbers.

these systems is believed to be the $2'^3\Pi$ state, which is responsible for the homogeneous perturbation of the $2^3\Pi$ state observed in band system I.

A fourth band system, labelled IV in Figure 3, accesses a single level predissociating to $N^+ + O$ from four vibrational levels of the $W^1\Delta$ state. The predissociated state in this system is likely the $2^1\Pi$ state. In addition, one set of transitions into several predissociated rotational levels lying near the $O^+ + N$ dissociation limit is observed. The lower state in these transitions, labelled V in Figure 3, corresponds in energy to $v = 0$ of the $W^1\Delta$ state; the upper state is likely the $A^1\Pi(v=11)$ in high $(J\sim20)$ rotational levels, although reliable assignment of either state is impossible on the basis of system V alone. The details of our work on band systems II – V will be reported in a forthcoming publication.

Our study of the photofragment spectroscopy of NO^+ has yielded the first observation of three electronic states in the important region of this ion's lowest dissociation limits. The results should have significance in explaining the relative abundance of N^+ and O^+ in the ionosphere. In addition, the locations of the lower state levels observed in this work permit substantial improvement to the existing vibrational constants of the $b'^3\Sigma^-$, $w^3\Delta$, and $W^1\Delta$ states, which had hitherto only been observed by photoelectron spectroscopy. Finally, one of the most remarkable features of our work on NO^+ has been the detection of significant populations existing in the b', w, and W states more than 10 μs after this ion's formation by electron impact on NO gas. Clearly, the existence of numerous metastable electronic states in this species must be considered in any attempt to understand the reactions of nascent NO^+.

C. OH^+

The charge-transfer reaction $H^+ + O \rightarrow O^+ + H$ is the first step in the interstellar chemical cycle leading to the formation of OH. The reverse reaction represents the major ionization source for atomic hydrogen in the earth's ionosphere. The high rate at which this reaction proceeds in either direction derives in part from the accidental coincidence between the dissociation limits $O(^3P_1) + H^+$ and $O^+(^4S) + H(^2S)$, which are degenerate within the current knowledge of the ionization potentials of atomic oxygen and hydrogen. The effect of this degeneracy on the long-range behavior of the lower electronic states of OH^+ is shown in Figure 4a. The importance of the

11

charge-exchange reaction has triggered a number of theoretical investigations, the most fundamental being the close-coupling calculations of Chambaud et al.,[3] who explicitly included the fine-structure excitation in the charge-exchange channel. These authors showed that the charge-transfer event arises from dynamic coupling among the OH^+ molecular states at large internuclear separations (4 - 6 Å), with enhancement in the cross section at specific energies corresponding to shape resonances in the $A^3\Pi$ state.

Our work on this ion has allowed the first experimental study of two such resonances, which in a molecular picture may be viewed as quasibound levels of the adiabatic fine-structure states of $A^3\Pi$ shown in Figure 4a. These levels were excited from the $X^3\Sigma^-$ ground state in a mass-selected OH^+ beam with a cw UV laser. The observed transitions are shown by the vertical lines labelled I and II in Figure 4b. The dissociative decay of the A state resonances into O^+ + H was monitored by observation of the charged photofragments and measurement of their kinetic energy distribution. Analysis of the excitation spectrum, the photofragment separation energies and the excitation linewidths of the resonances allowed the assignment of quantum numbers to the resonances and a first direct measurement of the OH^+ dissociation energy. The details of this work have been reported in a paper that has been accepted for publication in The Physical Review. This paper is attached as Appendix C to this report.

Our observation of predissociated quasibound levels in the $A^3\Pi$ state now opens the possibility for an experimental study of the long-range interactions in OH^+. The observed fragmentation into the O^+ channel is direct evidence for the action of nonadiabatic couplings between the $^3\Pi$ and the $^{3,5}\Sigma^-$ states, which correlate to the $O^+(^4S)$ + $H(^2S)$ limit. A first search for photofragments reaching the H^+ + $O(^3P)$ channel has been unsuccessful; the low sensitivity of the present apparatus configuration did not allow discrimination between a light photofragment and a heavy diatomic molecular ion. Modifications of the detection s   uld permit observation of these photofragments in future work.

In addition to the $A^3\Pi \leftarrow X^3\Sigma^-$ ons discussed above, we have also observed two transitions in the region of 3500 Å that produce photofragments with kinetic energies 20 times higher than those from the A state. On the basis of the measured kinetic energy releases and the transition energies, we

12

(a)
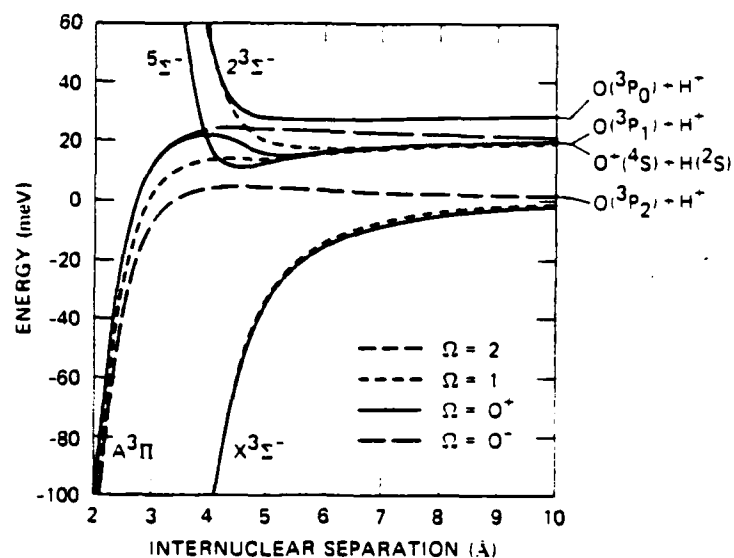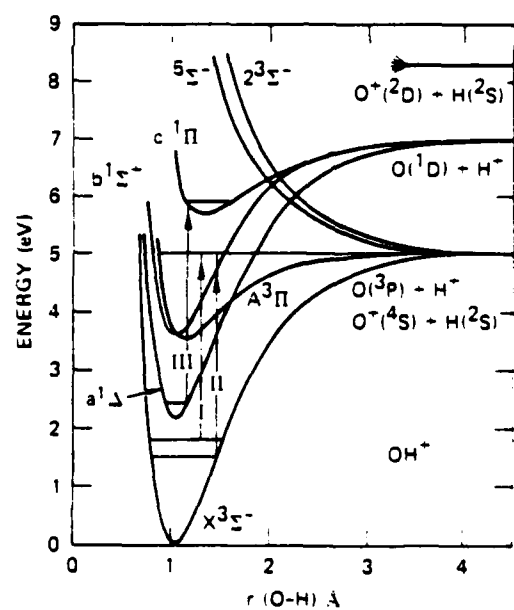
(b)

FIGURE 4 (a) Asymptotic rotationless potential curves for the lower
electronic states of OH$^+$ showing the correlation of their
spin-orbit components at large internuclear distances.

(b) Potential energy curves for the lower electronic states
of OH$^+$. The observed transitions are shown as the vertical
arrows labeled I, II, and III.

could tentatively assign these transitions to the $c^1\Pi(v=0) \leftarrow a^1\Delta(v=0)$ band. The c state had never previously been observed, but calculations[3] place it in the region of the upper state levels observed in the photodissociation. This state is apparently predissociated by spin-orbit coupling to the $^5\Sigma^-$, which is calculated to pass through this region. More definitive answers will require investigation of the 3500 Å region with a tunable laser.

D. SO^+

The SO^+ ion, which is isosteric with O_2^+, but lacks the g-u symmetry restrictions on its electronic states, had not been observed spectroscopically until recently. The photoelectron spectrum of the SO radical has been measured, but numerous features resulting from impurity species obscured the origins of the lowest quartet state $a^4\Pi$ and the first excited doublet state $A^2\Pi$. Tsuji, Nishimura, and coworkers[4] have made an extensive series of low resolution observations on the fluorescence from a He/SO_2 afterglow and identified the bands $A^2\Pi(v=0-11) \rightarrow X^2\Pi(v=0-10)$. This established the origin of the A state relative to that of the X. Their work has just been extended to longer wavelengths and higher resolution by Cossart, Lavendy, and Robbe,[5] who reported the first observation of emission from SO^+ quartet states. They observed and rotationally analyzed the $b^4\Sigma^-(v=0-2) \rightarrow a^4\Pi(v=0)$ progression, thus establishing the relative energies of the a and b states. They also give the theoretical and experimental potential energy curves for the lower electronic states of the SO^+ ion.

We have found that the SO^+ ion, produced from dissociative ionization of SO_2, undergoes photodissociation into $S^+ + O$ over the wavelength range of 6900 - 5750 Å. The photodissociation occurs in a series of structured bands that are assigned to absorptions in the $b^4\Sigma^- \leftarrow a^4\Pi$ system of SO^+, shown by the vertical lines in Figure 5. The predissociations occur from $v = 7-13$ of the b state. Higher vibrational levels extending to $>15000 \text{ cm}^{-1}$ above the origin of the b state also appear to predissociate. The predissociation lifetime of $b^4\Sigma^-(v=7)$ is found to be in the range $5 < \tau < 26$ ps, and is likely due to decay by spin-orbit coupling with the $^4\Sigma^+$ state arising from the $S^+(^4S) + O(^3P)$ separated atom limit.

JA-2422-21

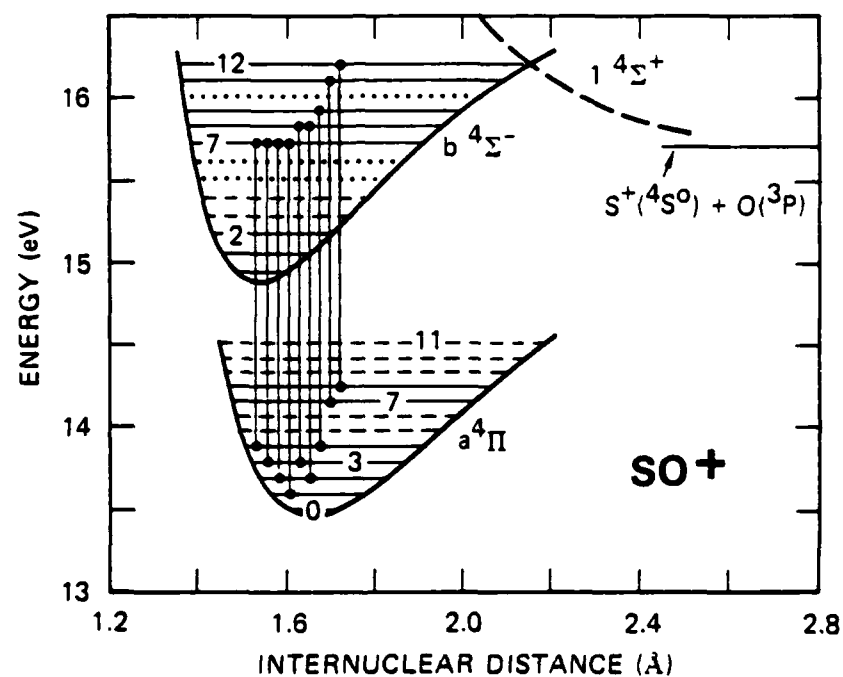FIGURE 5 POTENTIAL ENERGY CURVES FOR THE LOWER ELECTRONIC
STATES OF SO⁺

The observed transitions are shown by the vertical arrows.

15

Electronic absorptions into the b state are observed from v = 1-12 of the $a^4\Pi$ state. The population distribution in the a state is derived from the observed transitions. The a state is found to be nearly uniformly populated in its lower vibrational levels, in marked contrast to the distribution expected if the ion had been formed by direct ionization. The short predissociation lifetime of the b state prevented resolution of the complex rotational structure of the b ← a absorptions. However, moderate resolution (~ 1 cm^{-1}) spectra of the band envelopes and kinetic energy releases measured for the photofragments were combined with existing data from photoelectron spectra and high resolution emission spectra to yield an absolute measurement of the dissociation energies for the b and a states and vibrational constants for these states that are valid over an extensive range of their potentials were also obtained. This work is described in detail in a paper that has been accepted for publication in The Journal of Chemical Physics. This paper is attached as Appendix D to this report.

It is especially notable that the vibrational constants for the $a^4\Pi$ state obtained from our work differ greatly from those reported by Cossart et al., who apparently misassigned the weak $(v',v'') = (2,2)$ band in their emission spectrum. When we reassigned this band as the $(1,1)$, the data from Cossart et al., photoelectron spectroscopy, and photofragment spectroscopy are accurately described by a single set of vibrational constants. This demonstrates the unique advantage of photofragment spectroscopy to identify unambiguously the upper state in a transition on the basis of its photofragment kinetic energy.

E. O_2^+

The O_2^+ ion provides such a rich photodissociation spectrum that it has served over the years as a nearly ideal prototype species for the study of photofragment spectroscopy. The reasons for this are two-fold: (1) A high concentration of O_2^+, formed by direct ionization of O_2 gas, is produced in the $a^4\Pi_u$ state. This state is metastable and has a potential energy well shallow enough so that the first dissociation limit is accessible with visible photons, thus allowing the use of high power, cw tunable lasers. (2) This lowest dissociation limit, the $O^+(^4S) + O(^3P)$, gives rise to twelve molecular states that correlate to the three atomic fine-structure states of the O atom,

allowing the study of a wide range of short- and long-range interactions in both direct and predissociative photodissociation processes. Moreover, many of these electronic states have high multiplicities (quartets and sextets) not readily found in the neutral molecules that constitute the great body of traditional spectroscopic research.

Figure 6 shows the current of O^+ photofragments-- produced with kinetic energies in the range of 0 - 20 meV-- that is observed over the photon energy range of 14300 - 17500 cm^{-1}. The spectrum shows numerous structured bands superimposed on a continuum background. The background arises from direct photodissociation due to transitions from various vibrational and rotational levels of the $a^4\Pi_u$ state to the repulsive wall of the $f^4\Pi_g$ state. Figure 7 shows the potential energy curves of these states and others in the region of the lowest dissociation limit of O_2^+. This direct dissociation process has been studied by Tabche-Fouhaille et al.[6] and Grieman et al.[7] These studies allowed the first experimental observation of the f state, which had hitherto been predicted only by theory. The series of bands appearing in Figure 6 that are labelled b ← a arise from discrete transitions from the $a^4\Pi_u(v=4-7)$ into the $b^4\Sigma_g^-(v=4)$ level, which subsequently predissociates. We characterized this basic process under an earlier contract to obtain highly accurate molecular constants[8] for the a and b states and a precise measurement of the O_2 dissociation energy.[9] More recently, the study of this system has been extended under other support to higher vibrational levels of the b state,[10,11] allowing a unique determination of the predissociation mechanism and the first experimental observation of the location of the $^4\Sigma_g^+$ state.[12]

The photodissociation process of interest here is manifested by the series of structured bands in Figure 6 labelled f ← a. We have rotationally analyzed these bands at high resolution and established that they arise from transitions from $a^4\Pi_u(v=5-7)$ into the $f^4\Pi_g(v=1-3)$ levels. The f state had been predicted by a number of theoretical calculations to have a barrier in its potential energy curve. The presence of this barrier is evidenced by the abrupt cut-off in the direct dissociation process which gives rise to the humps in the photodissociation continuum that appear in Figure 6 to the blue of the discrete bands labeled (3,v"). We have found[13] that this barrier is sufficiently high to support two quasibound vibrational levels, v = 2 and 3, above the $O^+(^4S) + O(^3P_2)$ dissociation limit and that these levels are

17
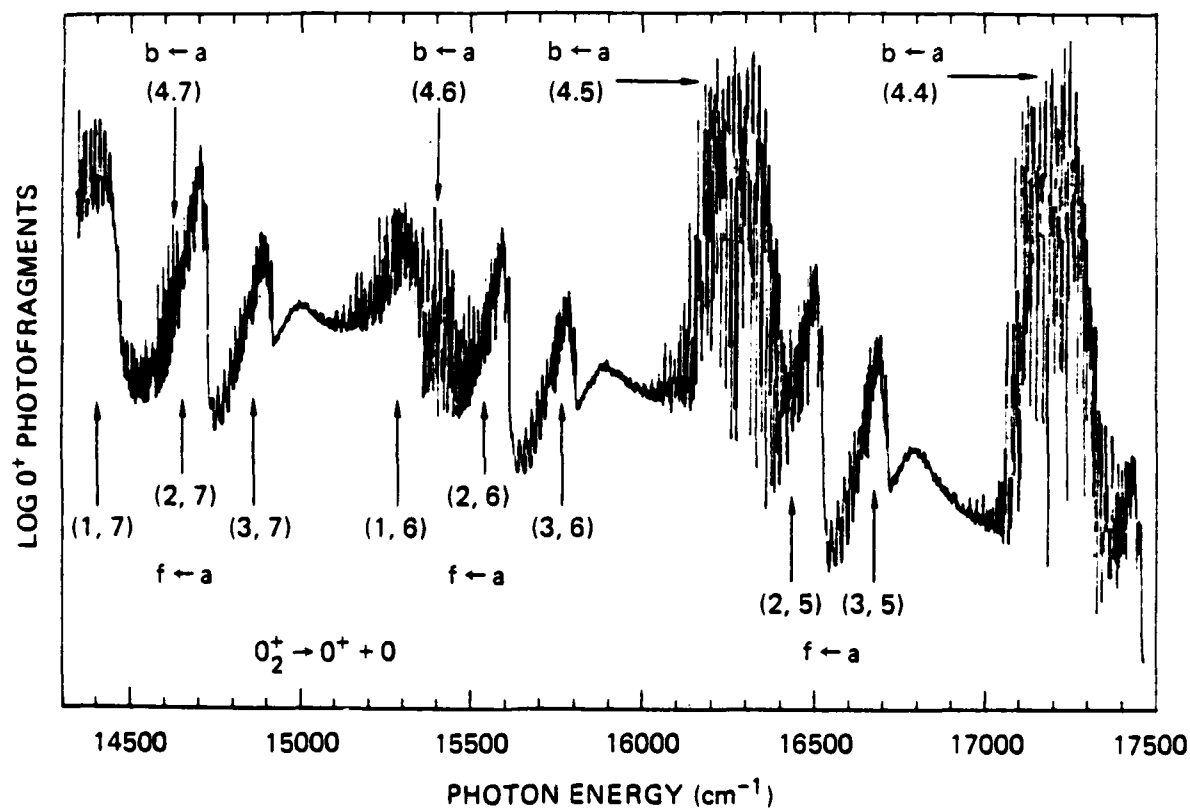
FIGURE 6 PHOTON ENERGY DEPENDENCE FOR THE PRODUCTION OF O^+ PHOTOFRAGMENTS WITH KINETIC ENERGIES IN THE RANGE 0 - 12 meV FROM THE PHOTODISSOCIATION OF O_2^+

JA-2422-23

18
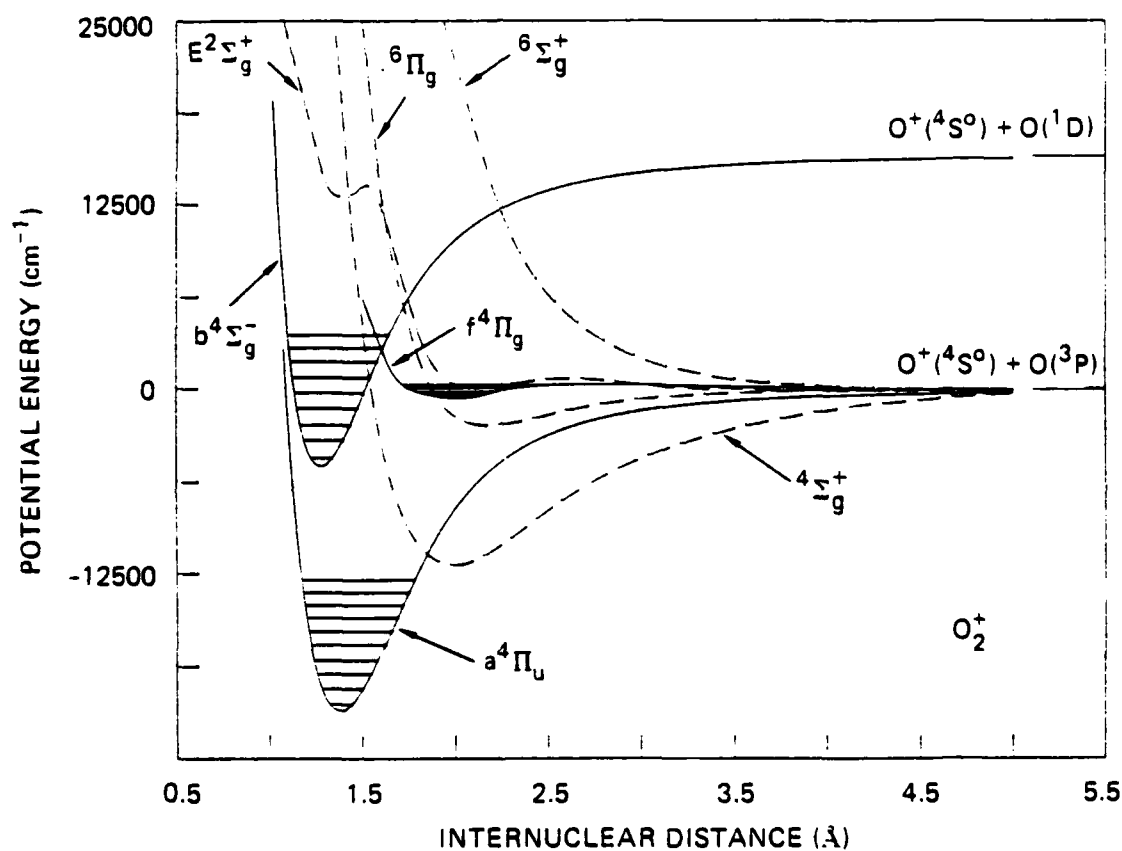
JA-2422-24

FIGURE 7 POTENTIAL ENERGY CURVES FOR THE ELECTRONIC STATES OF O_2^+ OBSERVED
BY PHOTOFRAGMENT SPECTROSCOPY

The solid curves are the RKR potentials derived in this work. The dashed curves are
theoretical locations for those electronic states identified as producing predissociation
in O_2^+. Experimentally observed levels are shown by the solid horizontal lines.

predissociated by several mechanisms, as discussed below. The v = 1 level lies below the dissociation limit; only its very highest rotational levels appear in the spectrum shown in Figure 6. The rotational lines in the Ω = 2.5 and 1.5 subbands of v = 2 and 3 were resolved by directly observing the photofragment spectrum generated by a single-mode dye laser. Because of extensive blending arising from their very rapid predissociation, the Ω = 0.5 and -0.5 subbands and all lines terminating in v = 1 could only be rotationally resolved through the use of an optical-optical double resonance technique.[14] Table I gives the merged molecular constants for the f state derived from these studies.

The very high optical resolution afforded by our technique allows the inhomogeneous linewidth for absorptions into the predissociated levels of the f state to be accurately determined, thereby establishing the predissociation mechanisms. These linewidths (Γ) are related to the predissociation lifetime (τ) of the pumped level by the uncertainty principle as $\Gamma = 1/2\pi\tau$. Figure 8 shows the linewidths and lifetimes measured for the rotational and fine-structure levels in v = 3 of the f state. The measurements were made on three isotopic combinations of O_2^+-- 16,16; 16,18; and 18,18-- where the effect of the heavier mass is to lower the energy of the vibrational level in the potential well. It is seen that the rotational dependence of these lifetimes is nearly exponential, demonstrating that v = 3 predissociates by tunnelling through the barrier in its potential energy curve. We have used an extension of the RKR technique, combining the rovibrational level locations (Table I) and tunnelling lifetimes, to determine the f state potential energy curve shown in Figure 7. The absorption linewidths measured for v = 2 of the f state are shown in Figure 9. In contrast with v = 3, the lifetimes in v = 2 are nearly independent of rotation. This level cannot predissociate by tunnelling; it lies too far in energy below the top of the barrier. Rather, v = 2 must be predissociated by spin-orbit coupling to the continuum of one or more other states arising from the $O^+(^4S) + O(^3P)$ dissociation limit.

The lifetimes measured for v = 2 and 3 in the four substates of the $f^4\Pi_u$ are summarized in Table II. Also shown in this table are the relative linewidths expected in these substates as a result of predissociation by spin-orbit coupling to the other _gerade_ states arising from the lowest dissociation limit. Only coupling to the $^6\Pi_g$ provides a reasonable

20

Table I. MOLECULAR CONSTANTS OF O_2^+ $f^4\Pi_g$ STATE

v	Isotope	ν_0[a]	A	$A_D(10^{-3})$	B	$D(10^{-6})$
1	16,16	15347.23(88)	−47.97(36)	−	0.5142(88)	[0.5087]
2	16,16	15604.057(53)	−45.726(37)	0.88(68)	0.50107(107)	1.65(13)
	16,18	15753.419(120)	−45.997(81)	1.79(88)	0.47465(139)	1.24(16)
	18,18	15907.657(133)	−46.275(93)	0.68(2.52)	0.4524(48)	2.9(3.0)
3	16,16	15789.677(34)	−40.148(24)	6.59(52)	0.42395(92)	4.46(47)
	16,18	15941.4887(84)	−41.0202(65)	5.97(29)	0.41124(50)	3.75(28)
	18,18	16097.2333(41)	−41.7790(33)	4.735(65)	0.395851(15)	2.86(8)

[a] Band origins are relative to $a^4\Pi_u(v=6)$. The origins of $f^4\Pi_g(v=3)$ lie 362.2 ± 1.8 cm^{-1}, 348.5 cm^{-1}, and 333.1 cm^{-1} above $O^+(^4S) + O(^3P_2)$ for $^{16,16}O_2^+$, $^{16,18}O_2^+$, and $^{18,18}O_2^+$, respectively.
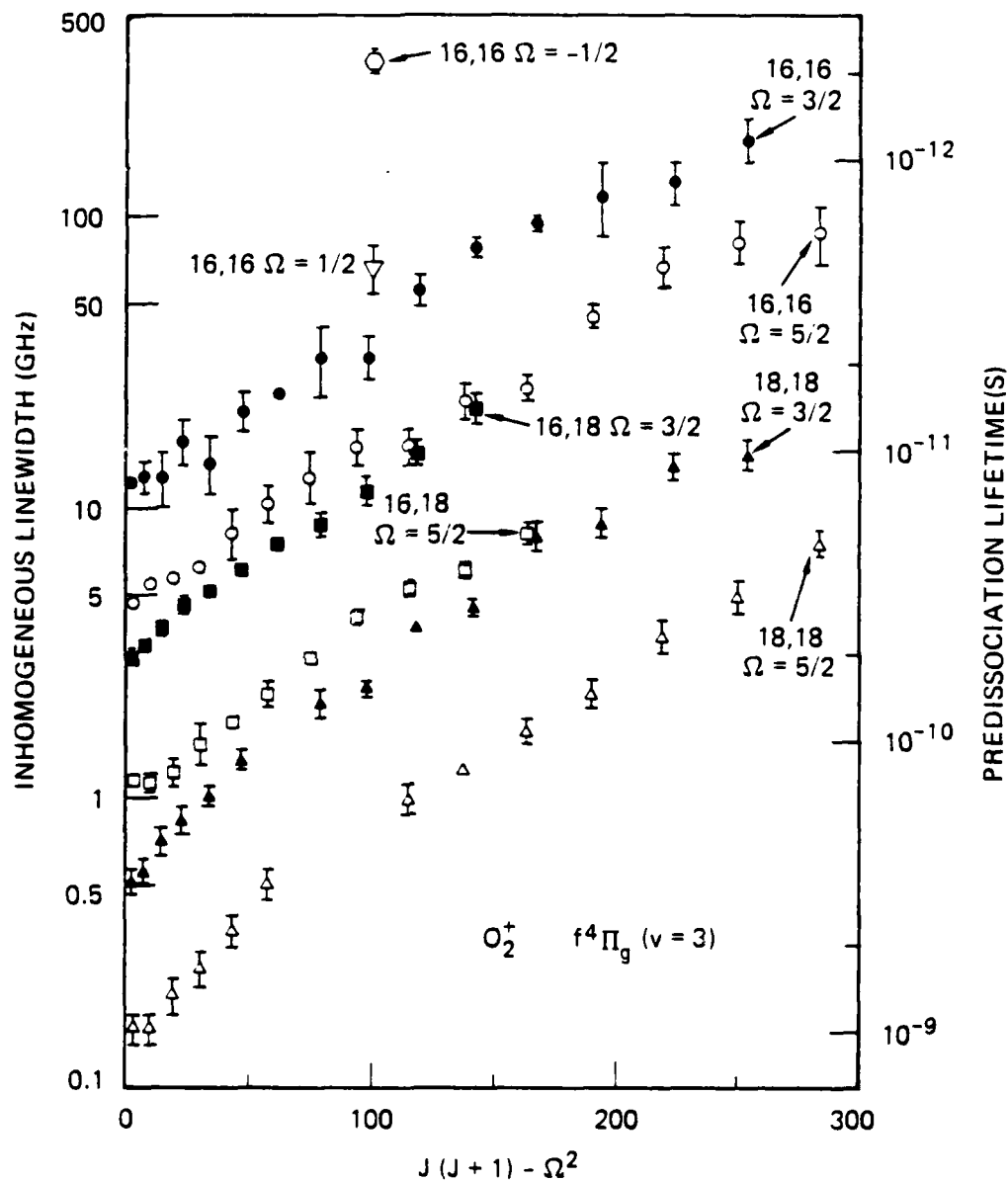
FIGURE 8 ABSORPTION LINEWIDTHS AND PREDISSOCIATION LIFETIMES MEASURED
FOR ROTATIONAL LEVELS IN v = 3 OF THE $f^4\Pi_g$ STATE OF O_2^+

Measurements are plotted for three isotopic combinations of the ion as a function
of the rotational level energy in cm^{-1} relative to its substate origin.
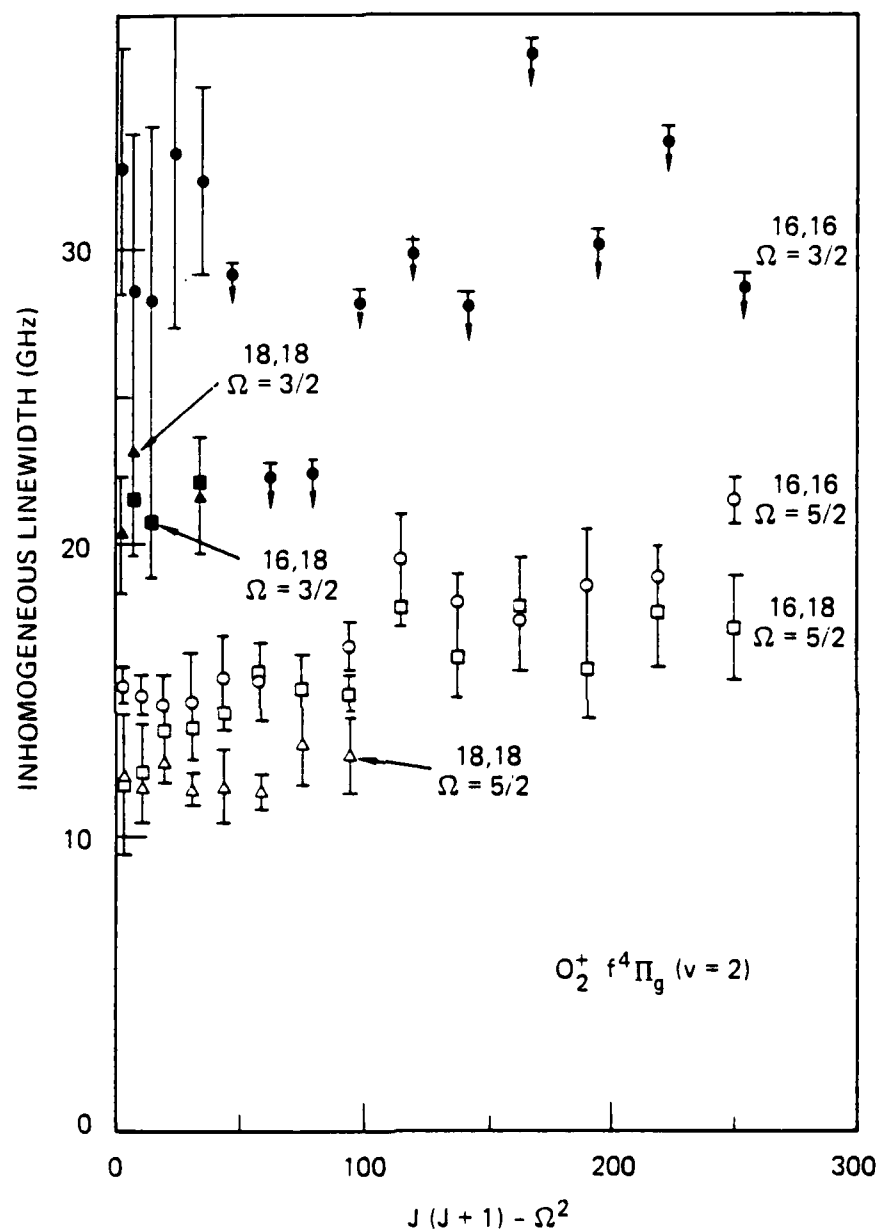
FIGURE 9 ABSORPTION LINEWIDTHS MEASURED FOR THE ROTATIONAL
LEVELS IN v = 2 OF THE O_2^+ $f^4\Pi_g$ STATE

The linewidths are plotted for the three isotopic combinations of this
ion as a function of the rotational level energy in cm^{-1} relative to its
substate origin. Predissociation lifetimes corresponding to the measured
linewidths range from 14 ps to 4 ps.

Table II. OBSERVED LINEWIDTHS (GHz) IN THE $f^4\Pi_\Omega$ SUBSTATES AND THE RELATIVE LINEWIDTHS EXPECTED DUE TO SPIN-ORBIT COUPLING TO VARIOUS O_2^+ <u>GERADE</u> STATES.

	Observed		Predicted Γ (relative)				
Ω	$\Gamma(v=2)$	$\Gamma(v=3)$	$X^2\Pi_g$	$^2\Sigma_g$	$^4\Sigma_g$	$^6\Pi_g$	$^6\Sigma_g$
2.5	14.9±0.4	4.8±0.2	0	0	~0	2	10
1.5	30.8±2.2	12.2±0.2	1	0	3	3	6
0.5	113±16	68±13	1	1	4	3	3
-.5	413±47	349±33	0	3	3	2	1

explanation for the observed linewidth ratio of 2.0 ± 0.3 for v = 2 in the Ω = 1.5 and 2.5 substates. Moreover, spin-orbit coupling to the $^2\Sigma_g^+$ must also occur to account for the very rapid predissociation of v = 2 and 3 in the Ω = ± 0.5 substates. The locations of the potential energy curves for both of these states given in Figure 7 are taken from the recent calculations of Marian et al.[15] It is clear from the observed lifetimes that either the actual location of the $^2\Sigma_g^+$ state must lie somewhat lower in energy than calculated or its potential barrier must be substantially smaller than calculated in order to effectively predissociate the f state. In principle, the locations of both predissociating states could be more accurately established on the basis of the observed lifetime ratios for v = 2 and 3 in the f state.

Figure 10 shows the photofragment kinetic energy spectra obtained for four completely resolved absorption lines that terminate in the lowest rotational level of v = 3 in the $f^4\Pi_{1.5}$ and $f^4\Pi_{2.5}$ substates. The different shapes of the Q and P branch lines arise from the different angular distributions of the photofragments; these distributions are produced by the change in angular momentum caused by the absorbed photon. We also find that the angular distributions observed in these branches and in the R branch change rapidly with increased rotation of the molecule. These effects were predicted by Zare[16] in 1964, but are only now experimentally observed. Figure 10 also shows that multiple photofragment kinetic energy releases are produced in the predissociation of the single rotational levels. This is due to the production of the neutral O fragment in different ^3P fine-structure states. We find that in v = 3, the Ω = 1.5 substate predissociates to $^3P_0$, $^3P_1$, and $^3P_2$ in the ratio 0.38:0.32:0.30. We further find that the Ω = 2.5 substate predissociates in the ratio 0:0.29:0.71. This observation of branching among the atomic fine-structure states is in marked contrast to our results for predissociation of the b state and for predissociation of all substates in v = 2 of the f state, where only the lowest energy atomic products are produced. Whereas the predissociation lifetimes reflect the coupling of the f state to the other gerade states at short internuclear distance, the final electronic states of the photofragments are determined by these couplings as well as the interaction with these states at larger internuclear separations. If the separation of the products proceeded adiabatically, the Ω = 2.5 substate would produce only $O(^3P_2)$ and the Ω = 1.5 substate would yield only $O(^3P_1)$. The observed yield of products suggests that spin-orbit
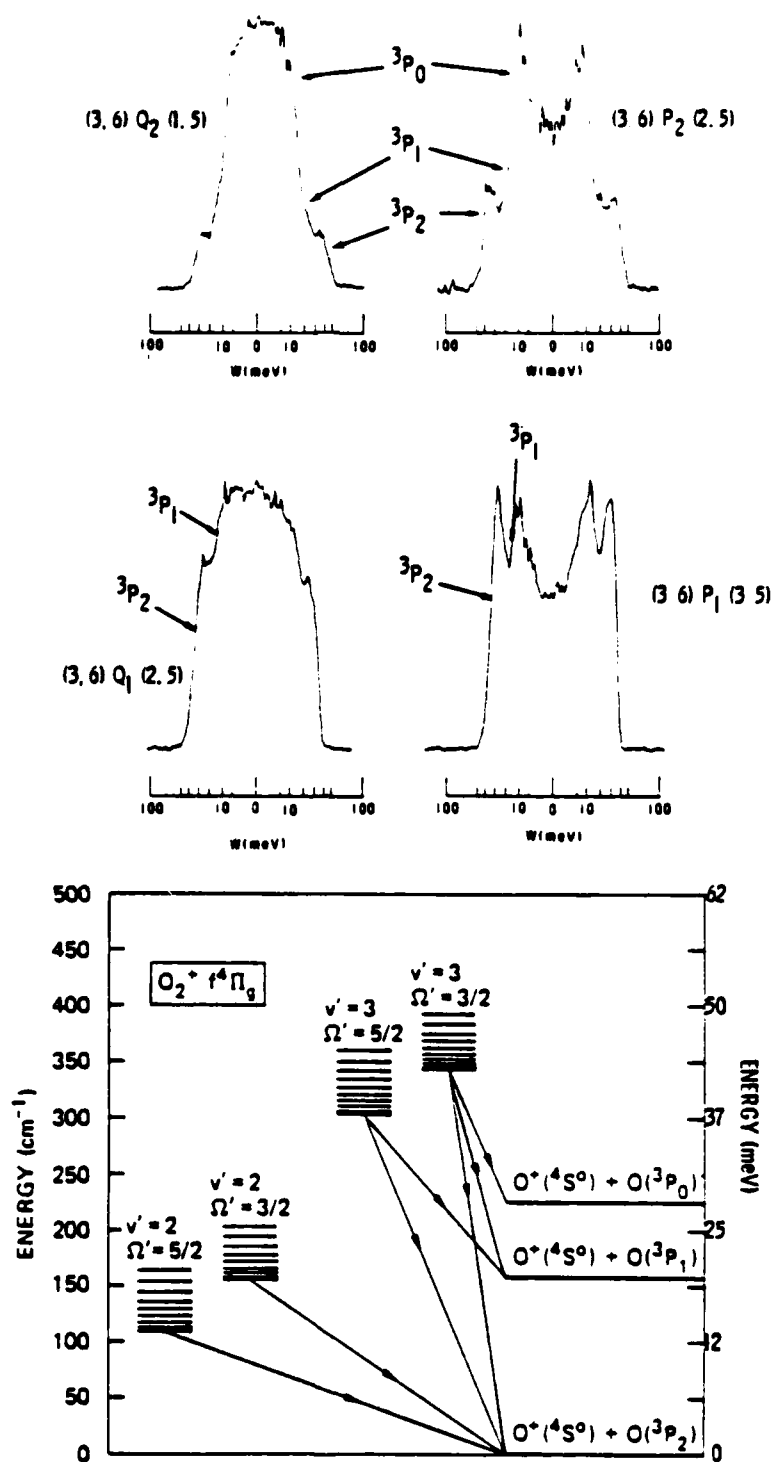
FIGURE 10 PHOTOFRAGMENT KINETIC ENERGY SPECTRA FROM THE
PREDISSOCIATION OF THE LOWEST ROTATIONAL LEVELS
IN THE $\Omega = 3/2$ (UPPER FIGURE) AND $\Omega = 5/2$ (CENTER
FIGURE) SUBSTATES OF O_2^+ $f^4\Pi_g$ ($v = 3$)

These levels produce markedly different photofragment angular
distributions when accessed by Q-branch ($\Delta J = 0$) and P-branch
($\Delta J = -1$) transitions. The observed final state distribution of the
$O(^3P)$ photofragments is summarized in the lower part of this
figure.

26

coupling of the f state to both the $X^2\Pi_g$ and the $^6\Sigma_g^+$ states must occur at intermediate internuclear distances. Durup[17] has treated these long-range interactions in O_2^+ in detail and finds reasonable agreement with the observed ratios.

In summary, our study of the predissociation of the O_2^+ $f^4\Pi_g$ state has yielded the first molecular constants and experimental potential energy curve for this state, a detailed understanding of its predissociation mechanisms, the first observation of variations in the angular distribution of photo-fragments as a function of rotation, and the first observation of branching among atomic fine-structure levels in a photodissociation. Two papers describing these results in more detail are in preparation.

F. $\underline{SH^+}$

The SH^+ ion plays a major role in the sulfur chemistry of the inter-stellar medium and can be expected to participate in combustion and plasmas containing sulfur or its compounds. The order of the lower electronic states in SH^+, shown by the potential energy curves in Figure 11, is similar to that of OH^+; however, the relative energies of these states and the limits to which they correlate have been greatly influenced by the much lower ionization potential of the sulfur atom.

The locations of the bound electronic states of SH^+ shown in Figure 11 have been established by photoelectron spectroscopy of the SH radical.[18] In addition, the transitions $A^3\Pi(v=0) \rightarrow X^3\Sigma^-(v=0-2)$ have been observed at moderate resolution in emission[19] and Edwards, Maclean, and Sarre[20] have recently reported observing predissociation of $v = 1$ of the A state in the (1,3) band of this system.

We have observed predissociation of SH^+ into $S^+ + H$ at moderate (1 cm^{-1}) resolution over the wavelength range of 6520 - 5800 Å in an extensive series of structured bands. By measuring the kinetic energies of the S^+ photo-fragments produced at discrete photon energies, we establish the energetic locations of the absorbing and predissociating states as given by the vertical arrows labelled I, II, and III in Figure 11. Rotational analysis of predisso-ciation band I identified the absorbing state as the $a^1\Delta(v\sim7)$ and the predissociating state as one vibrational level of the $c^1\Pi$. This level of the c state is found to predissociate to the $S^+(^4S)$ limit with a kinetic energy
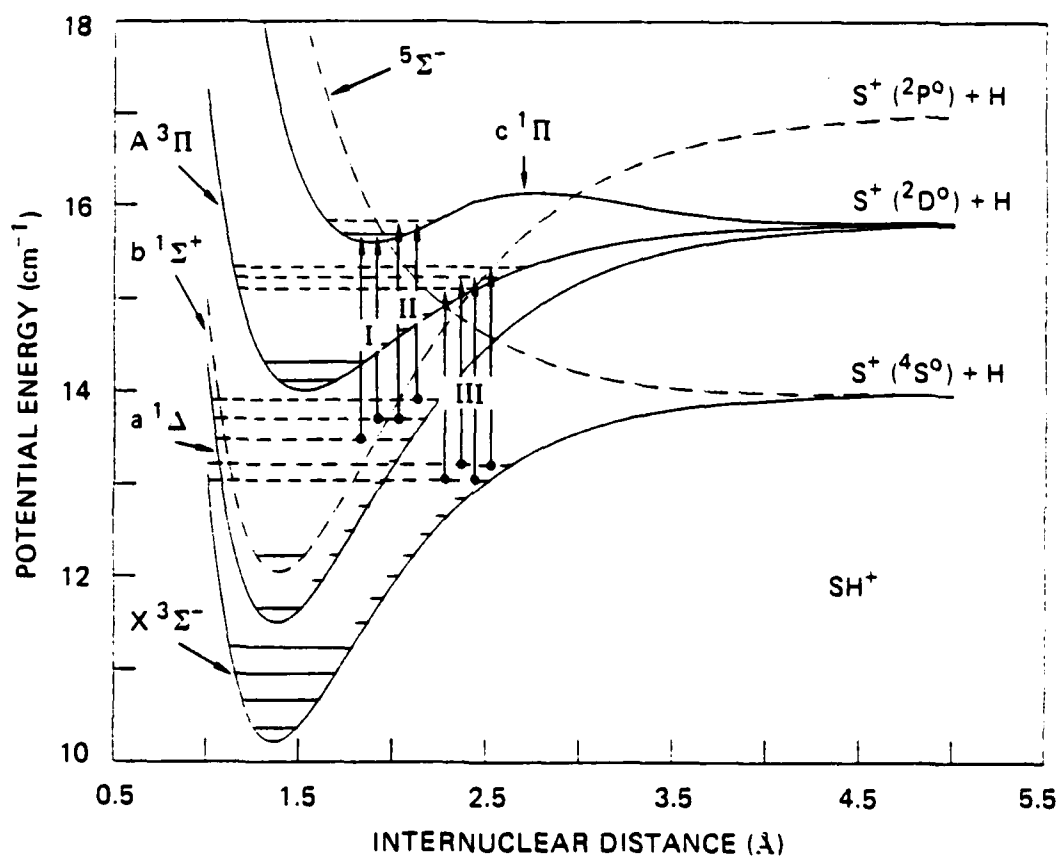
JA-2422-28

FIGURE 11 POTENTIAL ENERGY CURVES FOR THE LOWER ELECTRONIC STATES
IN SH⁺

Levels observed by photoelectron spectroscopy are shown as the full solid
horizontal lines. Transitions observed in this work are shown by the
vertical lines labeled I, II, and III.

release of ~ 1.8 eV. Since no lower kinetic energy releases were observed from this band system, we assume the predissociating level of the c state is v = 0. This is supported by the ionization potential measured for this state by photoelectron spectroscopy. Higher vibrational levels of the c state are not observed in the photoelectron spectrum because of overlap by intense impurity features. Consequently, the equilibrium internuclear distance for this state was not known. We have established this distance from the rotational analysis and used it to construct the potential energy curve for the c state shown in Figure 11.

Predissociation bands II exhibit an extensive, overlapping rotational structure that yields S^+ photofragments with kinetic energies ~ 50 meV. The most consistent explanation of these bands is that the absorptions occur from high vibrational levels of the $a^1\Delta$ state into v = 1 of the c state. The presumed dissociation mechanism for this level is tunneling; the c state is believed to be largely quasibound, with a barrier at large internuclear separations that is due to an avoided crossing of the two $^1\Pi$ states arising from the $S^+(^2D)$ and $S^+(^2P)$ separated atom limits.

Finally, a series of bands labelled III in Figure 11, having a structure characteristic of a $^3\Pi \leftarrow {}^3\Sigma$ absorption, is observed to predissociate into S^+ + H with a kinetic energy release in the range of 0.9 - 1.5 eV. The rotational structure of these bands is too dense to be assigned in the moderate resolution spectra thus far obtained. However, the bands almost certainly reflect absorptions from high (v<11) vibrational levels of the X state into a number of vibrational levels of the A state, and these levels are predissociated by the $^5\Sigma^-$ state arising from the $S^+(^4S)$ separated atom limit.

Despite the accurate photofragment kinetic energy releases measured in the present work, we cannot as yet confirm the bond dissociation energy of SH. All the bands observed in the present wavelength region originate in high vibrational levels whose energetic locations are not well characterized. Further progress on the study of the SH^+ ion will require the measurement of its photofragment spectrum in the region of 3000 Å.

G. CH_3I^+

1. Introduction

The X^2E ground electronic state of CH_3I^+, produced by removing a nonbonding electron centered on the iodine atom in the neutral molecule, exhibits a large spin-orbit splitting into $\widetilde{X}^2E_{3/2}$ and $\widetilde{X}^2E_{1/2}$ components. These states appear in the photoelectron spectrum[21] of CH_3I as two sharp peaks of roughly equal intensities, with adiabatic ionization potentials[22] of 9.5382 and 10.1642 ~ 0.0001 eV, respectively. Weak features that accompany the photoionization of methyl iodide have been assigned[21] to excitation of the ν_1, ν_2, ν_3, ν_4, and ν_6 vibrational modes in the ground state of the ion with frequencies comparable to those in the neutral molecule.

The removal of a bonding electron from methyl iodide centered on the C - I bond produces the first excited electronic state of CH_3I^+, the $\widetilde{A}^2A_1$ (in the C_{3v} point group) or $\widetilde{A}^2E_{1/2}$ (in the C_{3v}^* point group where account is taken of the strong spin-orbit coupling). This state appears in the high resolution photoelectron spectrum as a very broad peak on which weak vibrational structure spaced by ~ 300 cm^{-1} is superimposed. The adiabatic ionization potential of this state is fixed at 11.949 < 0.007 eV, and the vibrational structure is assigned to excitation of its ν_3 (C-I stretching) mode. This state has been studied using photoelectron-photoion coincidence spectroscopy by Eland et al.,[23] Mintz and Baer,[24] and Powis[25], and it is found to dissociate into CH_3^+ + I. Comparing the distribution of fragment kinetic energies produced in the dissociation with those predicted by various statistical theories of unimolecular dissociation, they found poor agreement except for very low values (< 50 meV) of kinetic energy release. This led them to suggest that internal conversion to the ground electronic state of the ion and its subsequent dissociation proceeded too rapidly to allow the equilibration of internal energy assumed by statistical theory. We show in our present work that this explanation is clearly not valid.

Photodissociation of CH_3I^+ has been studied by four laboratories, including the present work. Morrison and coworkers[26] first observed photodissociation of CH_3I^+ into CH_3^+ + I over the wavelength region of 6500 - 4500 Å. With a nominal resolution of 3 cm^{-1}, they identified two extensive series of vibrational bands, which they assigned to absorptions into the $\widetilde{A}$ state from the two spin-orbit components of the $\widetilde{X}$ state. They were

further able to assign the vibrational structure observed in these bands to progressions in the ν_3 mode of the $\tilde{A}$ state.[27] More recently, they have examined two of the vibrational bands with a resolution of 0.1 cm^{-1} and found extensive rotational structure.[28]

Tadjeddine et al.[29] have examined the kinetic energy release distributions of CH_3^+ photofragments produced with a spectral resolution of 30 cm^{-1}. For their investigation they chose three wavelengths corresponding to transitions into the first three photodissociating vibrational levels of the $\tilde{A}$ state. They were able to measure the anisotropy in the angular distribution of the photofragments, establishing that the $\tilde{A}$ state predissociated by internal conversion to the $^2E_{1/2}$ component of the $\tilde{X}$ state. They further found that for kinetic energy releases of < 10 meV, the statistical theory of Klots[30] gave a reasonable account of the dissociation process.

Chupka et al.[31] have recently prepared rotationally cold CH_3I^+ by resonant two-photon ionization in a supersonic beam of CH_3I and observed its photodissociation over the wavelength region of 6000 - 5730 Å. By eliminating hot bands from the photodissociation spectrum and greatly reducing rotational congestion, they were able to confirm the vibrational assignments of Morrison. From their more accurate bandhead spacings and comparison with the photoelectron spectrum, Chupka et al. conclude that Morrison's[27] vibrational numbering in the ν_3 progressions may be in error by two quanta. Unfortunately, the spectral resolution used in their work was not sufficient to resolve individual rotational lines in the vibrational bands.

2. Photodissociation of CH_3I^+ at Moderate Resolution

Under this contract, we have examined the photodissociation spectrum of CH_3I^+ at subtantially higher spectral resolution than in previous studies. Figure 12 shows the current of CH_3^+ photofragments observed at a spectral resolution of 0.5 cm^{-1} over the wavelength region of 6100 - 5750 Å. The four spectra shown in this figure were obtained by setting the energy analyzer to transmit those photofragments produced with center-of-mass kinetic energies of 0, 6, 12, and 20 meV, respectively, for each scan of the dye laser wavelength. The five bands labeled A - E correspond to transitions from the $X^2E_{1/2}(0,0,0)$ level into the first five vibrational levels of the A state that lie above the dissociation threshold. These have been assigned by
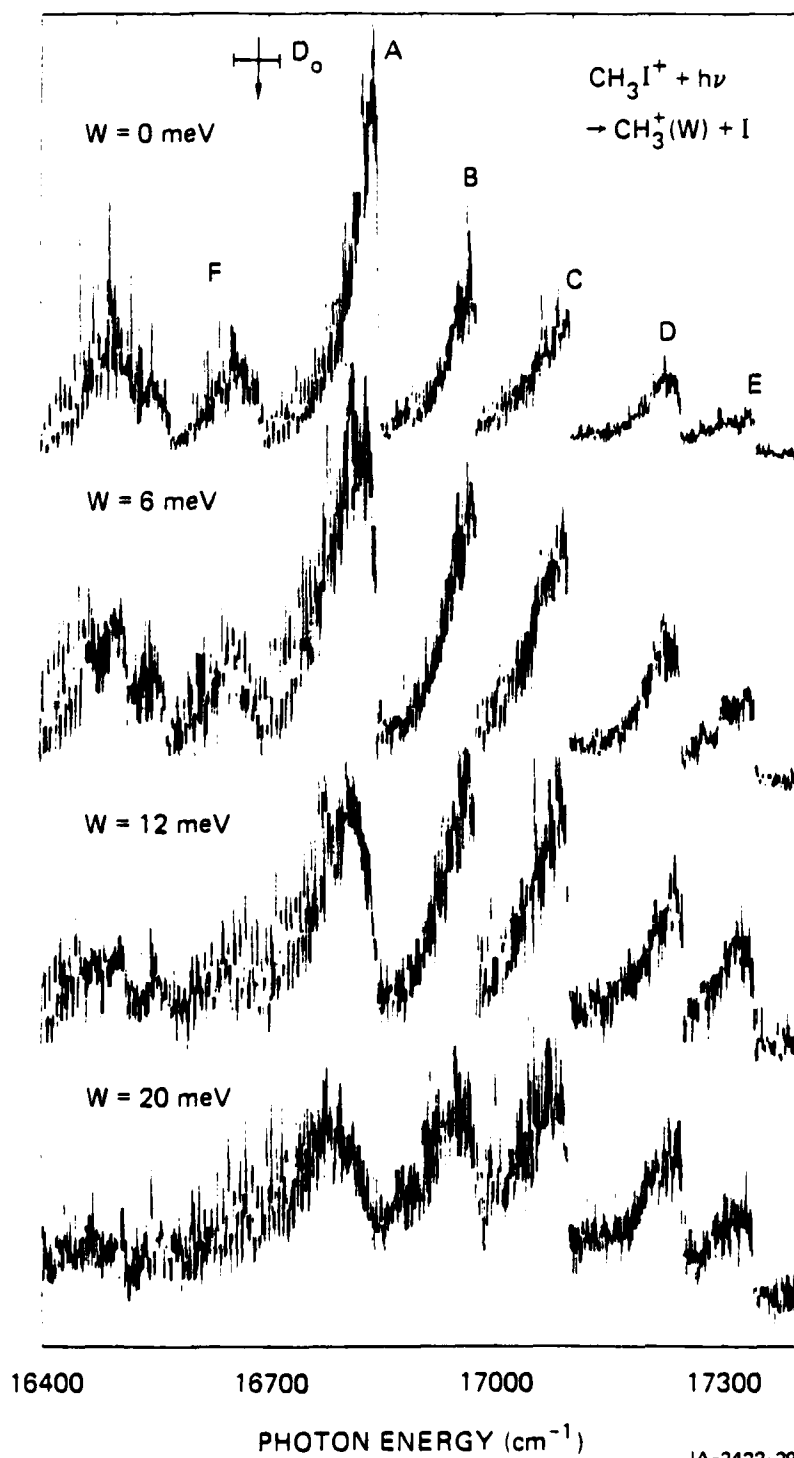
FIGURE 12 PHOTON ENERGY DEPENDENCE FOR THE PRODUCTION OF
CH_3^+ PHOTOFRAGMENTS FROM CH_3I^+ WITH CENTER-OF-MASS
KINETIC ENERGY RELEASES OF 0, 6, 12, AND 20 meV

The spectra were obtained with a laser resolution of 0.5 cm^{-1}.

Morrison as the $(\nu_1', \nu_2', \nu_3') = (0,0,11)$, $(0,1,7)$, $(0,0,12)$, $(0,1,8)$, and $(0,0,13)$ vibrational levels, respectively. Bands appearing at photon energies lower than 16700 cm^{-1} are attributed by Morrison[26] to hot bands, where the absorbing X state level is vibrationally excited. The rotational structure in each of these bands appears to be largely resolved, but we will later show that this is not the case.

It has been implied, but never demonstrated, in previous work that the onset of photodissociation in the $\tilde{A}$ state corresponds to the point where the energy of the dissociating $\tilde{A}$ state level exceeds the dissociation energy of CH_3I^+. We can calculate this energy $D(CH_3I^+)$ from the equation:

$$D(CH_3I^+) = D(CH_3I) + IP(CH_3) - IP(CH_3I),$$

where $D(CH_3I)$ is the dissociation energy of methyl iodide, $IP(CH_3)$ is the ionization potential of the methyl radical,[32] and $IP(CH_3I)$ is the ionization potential of methyl iodide.[22] The dissociation energy of methyl iodide is calculated from the accepted heats of formation[33] of CH_3, I, and CH_3I to be 2.387 ± 0.001 eV, which yields $D(CH_3I^+) = 2.063 \pm 0.005$ eV. However, a recent measurement of the photofragment kinetic energy spectrum of methyl iodide[34] has proposed a dissociation energy for this species of 2.294 ± 0.021 eV. This value yields $D(CH_3I^+) = 1.970 \pm 0.022$ eV. Notice that the difference between these two values of the dissociation energy greatly exceeds their combined error limits. The 2.063 eV value for the dissociation energy is given by the arrow and associated error bar in Figure 12; the 1.970 value is too small to appear in this figure.

We note that the rotational envelopes of the bands labeled A, B, and C exhibit sharp bandheads in the W = 0 spectrum since the photofragment kinetic energies produced in the predissociation of their lowest rotational levels fall within the 0 - 3 meV transmission window of the energy analyzer. The sharpness of the bandheads progressively decreases with increasing energy transmission setting of the energy analyzer. This is because the higher analyzer settings discriminate against photofragments produced by the lower rotational levels in each of these bands. The rate of bandhead disappearance is A > B > C since the energies at the rotational origins of the terminal A state vibrational levels corresponding to these transitions is $E_A < E_B < E_C$

33

relative to the dissociation limit. Photofragments produced in bands D and E exhibit a more complex dependence on analyzer transmission energy, and this relationship will be discussed later. Note that the shape of band A in the W = 20 meV spectrum corresponds closely to the shape of the weak band labelled F in the W = 0 spectrum. Band F lies at a photon energy where Morrison's[27] assignment predicts a transition into the (0,1,6) level of the A state would occur. It is clear from the shape of this band and the observed photo-dissociation at the rotational origin of the (0,0,11) level that the origin of the (0,1,6) level must lie 14 ± 2 meV below the dissociation threshold, such that only its highest rotational levels can predissociate. This predisso-ciation of high rotational levels in the (0,1,6) vibrational level demonstrates that the onset of photodissociation in the A state is governed by energy constraints in the dissociation channel rather than by any limitation imposed in the photon-absorption process; it also fixes the energy of the photodissociation threshold at 2.087 ± 0.002 eV above the $\tilde{X}^2E_{1/2}(0,0,0)$ level. This threshold is 24 ± 5 or 117 ± 22 meV above the two estimates for the dissociation energy of the $\tilde{X}^2E_{1/2}$ state.

We have also measured the kinetic energy spectra of the CH_3^+ photo-fragments produced near the origins of bands A - E. Since more than one rovibrational transition falls within the 0.5 cm^{-1} bandwidth of the laser, the observed spectra show distributions of kinetic energy release rather than the discrete kinetic energy releases that would be produced in the dissociation of a single excited state level. In Figure 13 we have plotted the most probable kinetic energy releases, W_{mp}, observed in the distributions measured for peaks A - E as a function of the exciting photon energy; with the exception of a small amount of rotational energy, this photon energy is equivalent to the energy of the dissociating levels above the $\tilde{X}^2E_{1/2}(0,0,0)$ level. The kinetic energy distributions obtained from bands D and E were found to be bimodal; the two values of W_{mp} obtained from each band are plotted in Figure 13. It can been seen from this figure that near the dissociation threshold, W_{mp} increases essentially linearly. Haney and Franklin[35] have found that the average release of kinetic energy in fragment ions produced by dissociative electron-impact ionization can be described by the equation $W_{mp} = E^*/0.44N$, where E^* is the excess energy of the molecule above its dissociation threshold and N is the number of vibrational modes in the parent ion, and 0.44 is an empirical factor. This equation is consistent with that predicted by more

34
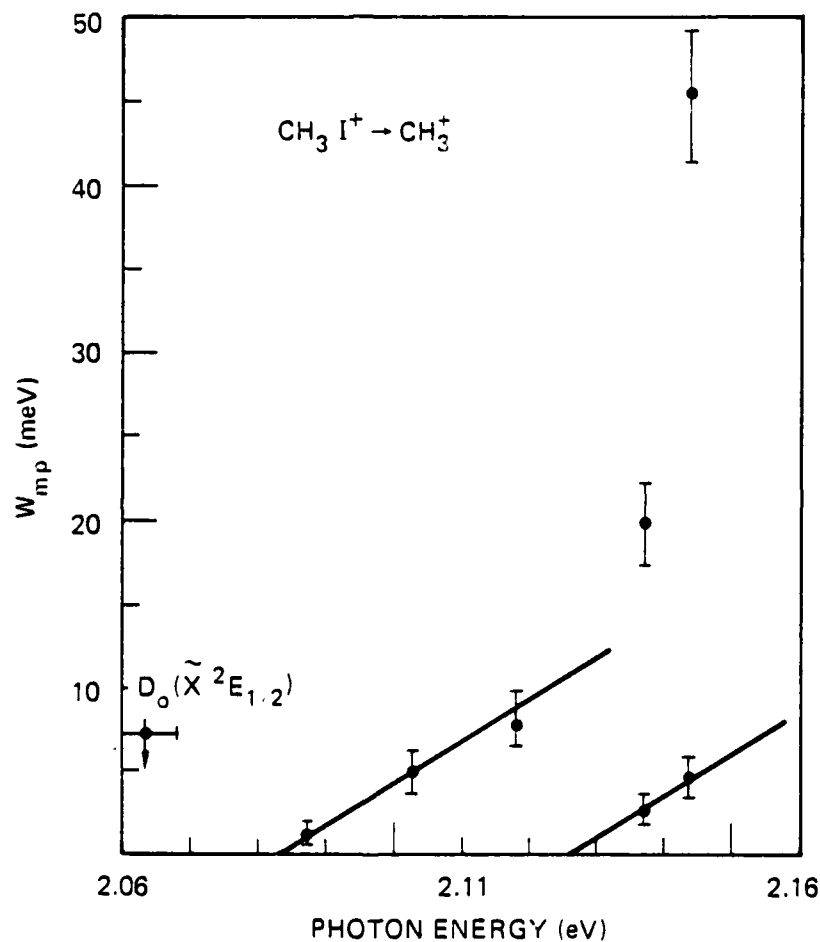
JA-2422-30

FIGURE 13 AVERAGE PHOTOFRAGMENT CENTER-OF-MASS KINETIC
ENERGY RELEASE (W_{mp}) FROM THE PHOTODISSOCIATION
OF CH_3I^+ AS A FUNCTION OF PHOTON ENERGY

The five photon energies shown correspond to absorptions in bands
A-E of Figure 12. Bands D and E yield bimodal kinetic energy
distributions; both average values are plotted in this Figure. The
solid curves are drawn through the points with a slope of $E^* 0.44N =$
0.2525. The arrow at 2.063 eV shows the higher of two possible
values for the dissociation energy of $X^2E_{1,2}$.

elaborate statistical discriptions of unimolecular dissociation. For CH_3I^+, this equation predicts W_{mp} should vary linearly with excess energy with a slope of 0.2525, as shown by the solid line in Figure 13. The values of W_{mp} observed in bands A, B, and C are consistent with this equation, but the higher values of W_{mp} obtained from bands D and E represent increases much more rapidly than linear. Rather, the lower values of W_{mp} obtained from bands D and E can be described by a second straight line of slope 0.2525.

The intercept of the lower energy straight line in Figure 13 indicates a photodissociation threshold of 2.083 eV, which is consistent with the value obtained from the spectra in Figure 12. The difference in the intercepts of the two lines is approximately 378 cm^{-1}. Qualitatively, one expects the occurence of a second, lower kinetic energy distrubution in bands D and E to indicate the production of the CH_3^+ fragment with one additional quantum of vibrational energy, and this quantum of energy should be 378 cm^{-1}. However, the smallest fundamental frequency calculated[36] for CH_3^+ is 1080 cm^{-1}. The actual vibrational frequencies in CH_3^+ may indeed be smaller than the theoretical values. Dyke et al.[32] have assigned a feature in the photo-electron spectrum of the methyl radical to the v_2 fundamental of the ion with a value of 700 cm^{-1}. However, it should also be remembered that the photodissociation threshold is between 19 and 139 meV (or 153 - 1121 cm^{-1}) above the range of possible values for dissociation of the $\widetilde{X}^2E_{1/2}$ into ground state products; thus, a significant barrier exists in the dissociation channel. The energy required to surmount this barrier must appear in the various degrees of freedom of the products. Figure 13 shows clearly that this energy is not in product translation at threshold, and internal excitation of the I fragment requires substantially more energy than is available. Orbital angular momentum of the separating fragments will certainly account for some of the energy, but this cannot play a major role at the immediate threshold. Consequently, we can expect most of the excess energy at threshold to be absorbed by rotational and vibrational excitation of the CH_3^+ fragment. Vibrational excitation of the CH_3^+ is not surprising when one considers that this radical has a pyramidal structure in CH_3I^+, whereas the ground state free radical is believed to be planar. If the lower of the two possible values for the $\widetilde{X}^2E_{1/2}$ dissociation energy is correct, then the CH_3^+ fragment could be produced with one quantum of vibrational excitation. The 378 cm^{-1} difference

in photodissociation thresholds could then represent a difference frequency in the CH_3^+ fragment, rather than a fundamental frequency.

3. Photodissociation of CH_3I^+ at High Resolution

We have also studied the photodissociation of CH_3I^+ at very high resolution (0.003 cm^{-1}). Figure 14 shows a 1.4 cm^{-1}-wide segment of band A obtained with a single mode dye laser having a linewidth of 0.0004 cm^{-1} (15 MHz). An enormous number of absorption lines appear in this small segment of the spectrum and similar line densities are observed in other bands. It is immediately clear that the 0.1 cm^{-1} laser bandwidth being used by Morrison[28] to investigate the rotational structure of CH_3I^+ will yield only absorption features representing the superposition of a number of rotational lines rather than the rotational lines themselves. Each of the absorption lines in Figure 14 is found to have a linewidth of ~ 80 MHz. Most, if not all, of this linewidth can be attributed to the residual Doppler width associated with the kinetic energy and angular spreads in the CH_3I^+ beam and with the laser linewidth. Consequently, the lifetime of the absorbing levels in the $\tilde{A}$ state must be > 2 ns. Dissociation of the $\tilde{A}$ state levels is believed to be a two-step process: internal conversion to the $\tilde{X}$ state is required for the ions to dissociate. The lower limit of > 2 ns is on the time required for the internal conversion; dissociation of the $\tilde{X}$ state could occur at a substantially faster or slower rate. Yet, we also know that the CH_3I^+ ions both absorb a photon and dissociate within the laser interaction region. No evidence was found for dissociation of the ions in the region between Q2 and the energy analyzer after a photon was absorbed in the region between Q1 and Q2 (see Fig. 1). This places an upper limit on the predissociation lifetime of < 1 μs, the magnitude of which is the minimum time required for photo-excited CH_3I^+ to traverse Q2. These very long lifetimes imply that the internal energy of the CH_3I^+ ion is not statistically randomized in the slow internal conversion process and that the slow internal conversion is followed by a very rapid predissociation of the $\tilde{X}^2E_{1/2}$ state.

We have measured the photofragment kinetic energy spectra of a large number of the individual rotational lines appearing in the high resolution absorption spectra. Rather than finding the distribution of kinetic energy releases that accompanied photoexcitation of the CH_3I^+ ions with a 0.5 cm^{-1}

$$CH_3 I^+ \rightarrow CH_3^+ + I$$

$W_\alpha = 2.7 \pm 0.1$ meV
$W_\beta = 3.4 \pm 0.2$ meV
$W_\gamma = 5.2 \pm 0.3$ meV

CH$_3^+$ CURRENT

16834.0   16834.5   16835.0
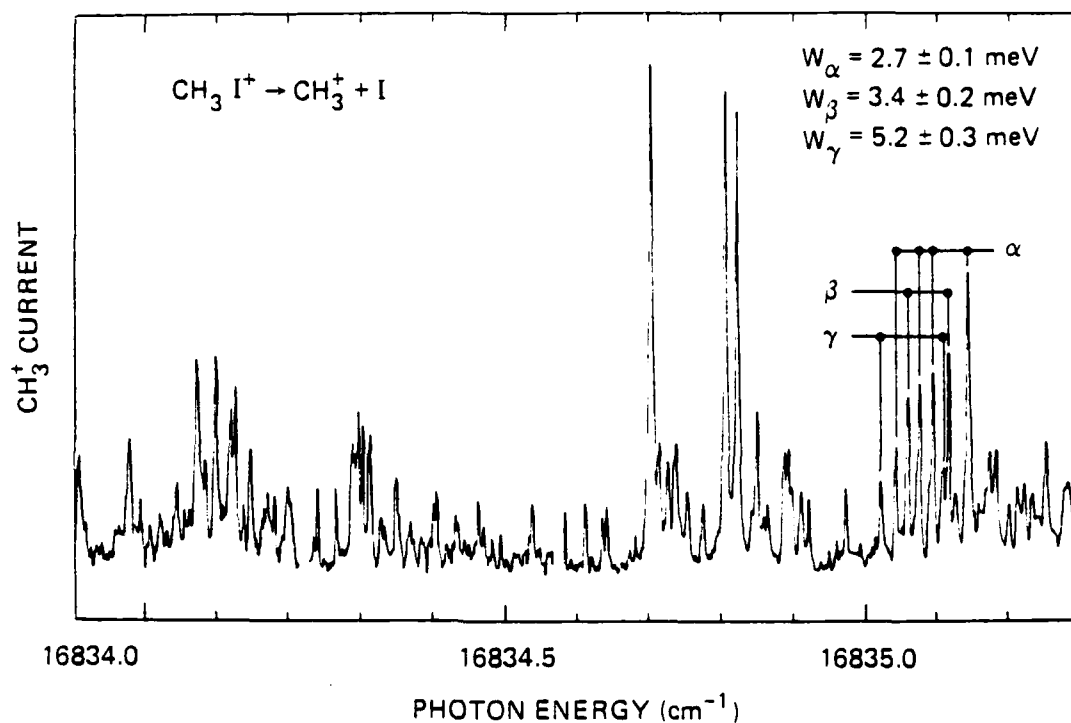
PHOTON ENERGY (cm^{-1})

JA-2422-31

FIGURE 14 PHOTON ENERGY DEPENDENCE FOR THE PRODUCTION OF CH$_3$I$^+$ PHOTOFRAGMENTS
FROM THE PHOTODISSOCIATION OF CH$_3$I$^+$ WITH A LASER RESOLUTION OF 0.00067 cm^{-1}
(20 MHz)

The spectrum was obtained in Band A of Figure 12. Observed linewidths of 80 MHz place an upper
limit on the predissociation lifetime of > 2 ns. Lines labeled α, β, and γ produce discrete photo-
fragment kinetic energy releases (W) given in the figure.

bandwidth laser, we found that the individual lines yield discrete releases of translational energy in the center of mass frame. In fact, the magnitude of the energy releases appears to be quantized. For example, the seven lines in the region of 16835.1 cm^{-1}, labelled α, β, and γ in Figure 14, produce only three different releases of kinetic energy: W_α = 2.7 ± 0.1 meV, W_β = 3.4 ± 0.2 meV, and W_γ = 5.2 ± 0.2 meV. Similar values extending as low as 2.0 meV at the bandhead are found for the prominent lines in other regions of band A. These energies are very close to the expected spacing of rotational levels in the CH_3^+ fragment. Using the calculated[36] rotational constants for this ion, the (J,K) = $(1,0) - (0,0)$ spacing is predicted to be 2.6 meV, $(2,0) - (1,0)$ is 5.3 meV, $(1,1) - (0,0)$ is 2.0 meV, and $(2,2) - (1,1)$ is 3.4 meV.

4. Conclusions

The observed production of a discrete CH_3^+ internal energy state from a discrete excited state of the parent CH_3I^+ molecule shows the possible dangers of applying a statistical description to unimolecular dissociation or bimolecular reaction dynamics in a collision-free environment without a very detailed knowledge of the intermolecular energy transfer rates in the molecule. In the present case of CH_3I^+, the observed energy width of individual $\tilde{A}$ state levels is so small that no significant overlap with other levels in the molecule can occur. In the absence of a thermal collision bath, this appears to prevent significant randomization of excess energy either within the parent ion or in the population of fragment molecule quantum states. However, when a sufficient number of initial states are simultaneously probed by a wide bandwidth laser, kinetic energy release distributions are obtained that appear to be consistent with the molecule dissociating statistically. In fact, we are only relying on a sufficient number of absorption lines to fall within the laser bandwidth to produce a pseudo-statistical distribution of excited levels in the molecule, and these energies then individually dissociate to produce a quasi-continuous distribution of fragment kinetic energies. This process has nothing to do with energy randomization in the molecule, but relies only on a fortuitous distribution of rotational lines in the absorption band.

Statistical theory has traditionally been applied to describe unimolecular dissociation processes in molecular ions. This theory has been

used extensively because it requires very little knowledge of the potential energy surfaces of the molecule, in contrast to the concept of nonadiabatic processes[37] controlling the unimolecular dissociation. Statistical theory, generally termed RRKM or quasi-equilibrium theory (QET), relies on the energy deposited in the reacting molecule to be uniformly distributed over its phase space prior to dissociation.[38] Thus, RRKM-QET predicts that the distribution of products from an unimolecular reaction will be independent of how a given energy content is produced within the reacting molecule. It is recognized[38] that if the rate of reaction exceeds the rate of randomization for the energy deposited in a given mode of the molecule, deviations will be observed in the distribution of dissociation lifetimes from that predicted by statistical theory. It is far more common for this diagnosis to be made on the basis of the translational energy distribution observed for the dissociation products.[30,39] However, we find that excitation bandwidth can yield a pseudo-continuous spectrum of kinetic energy release. Hase[40] has shown that excited molecules with non-RRKM-QET lifetime distributions can dissociate to products with apparent RRKM-QET translational energy distributions. It is generally believed that very rapid dissociations, occurring on time-scales < 1 ps,[38] are required to prevent statistical redistribution of the excitation energy. However, we find that this process does not occur in CH_3I^+ where the dissociation rate is 1000 times slower.

It thus appears that the basic assumptions of statistical theory will be satisfied only in those molecular ions that dissociate within a time window of approximately 1 ns < τ_{diss} < 1 ps. Moreover, it appears that the kinetic energy distribution observed for the dissociation products does not provide a reliable diagnostic for the application of statistical theory to a specific molecule. Direct measurement of the dissociation lifetime is clearly preferred, but has thus far been attempted for very few species. Nevertheless, it is clear that CH_3I^+ is not an isolated example of a polyatomic ion with a long dissociation lifetime. Goss et al.[28] have investigated the photodissociation of larger alkyl iodide cations and find evidence of rotational structure in the spectrum of $n-C_3H_7I^+$, although their 3 cm^{-1} bandwidth is much too large to determine whether individual rotational levels participate in the dissociation. Substantial high resolution work remains to be done in this area.

IV PROFESSIONAL PERSONNEL ASSOCIATED WITH THIS RESEARCH

(1) Coprincipal Investigator and Project Leader:

    Dr. P. C. Cosby, Senior Chemical Physicist

(2) Coprincipal Investigator and Project Supervisor:

    Dr. J. R. Peterson, Program Manager, Photochemistry

(3) Other SRI Professional Research Personnel:

    Dr. H. Helm, Research Physicist

    Dr. D. L. Huestis, Program Manager, Energy Transfer and Kinetics

    Dr. R. P. Saxon, Senior Chemical Physicist

V INTERACTIONS

Invited Presentations

1. P. C. Cosby, "The Half-Collision Approach to Low-Energy Ion-Atom Interactions," presented at the 12th International Conference on the Physics of Electronic and Atomic Collisions, Gatlinburg, TN, 21 July 81.

2. H. Helm, "Shape Resonances Studied by Ion Photofragment Spectroscopy," presented at the Symposium on Dynamics of Molecular Collisions, Williamsburg, VA, 23 July 81.

3. P. C. Cosby, "Photofragment Spectroscopy of Molecular Ions," presented at the Reaction Dynamics Seminar, Materials and Molecular Research Division, Lawrence Berkeley Laboratory, Berkeley, CA, 24 August 1981.

4. P. C. Cosby, "Photofragment Spectroscopy of Molecular Ions," presented to the Department of Chemistry, University of Alberta, Edmonton, Alberta, Canada, 27 Jan 83.

5. P. C. Cosby, "Spectroscopy and Photodissociation Dynamics of Molecular Ions," presented to the Chemical Physics Institute, University of Oregon, Eugene, OR, 23 Apr 84.

Contributed Presentations

1. P. C. Cosby, H. Helm, and D. L. Huestis, "Photofragment Spectroscopy of Molecular Ions," AFOSR Molecular Dynamics Conference, Hanscom AFB, MA, 8 Oct 80.

2. H. Helm and P. C. Cosby, "Experimental Study of the $NO^+ 2^3\Pi$ State," 12th Annual Meeting of the Division of Electron and Atomic Physics, Los Angeles, CA, 1 December 1980.

3. D. L. Huestis, H. Helm, and P. C. Cosby, "Spectroscopic Determination of a Barrier in a Diatomic Potential Curve," 12th Annual Meeting of the Division of Electron and Atomic Physics, Los Angeles, CA, 1 December 1980.

4. P. C. Cosby, H. Helm, and D. L. Huestis, "Photofragment Spectroscopy as a Tool for the Study of Low-Energy Ion-Atom Interactions," 12th Annual Meeting of the Division of Electron and Atomic Physics, Los Angeles, CA, 1 December 1980.

5. P. C. Cosby, D. L. Huestis, H. Helm, C. Pernot, J. A. Beswick, and J. Durup, "Predissociation of Quasibound Levels in $O_2^+ \underline{f}^4\Pi_g$," 12th International Conference on the Physics of Electronic and Atomic Collisions, Gatlinburg, TN, 21 July 1981.

6. P. C. Cosby, H. Helm, and D. L. Huestis, "Spectroscopy and Predissociation of $O_2^+ \underline{f}^4\Pi_g$," 37th Symposium on Molecular Spectroscopy, Ohio State University, Columbus, Ohio, 14 June 1982.

7. P. C. Cosby, H. Helm, and D. L. Huestis, "Photofragment Spectroscopy of Molecular Ions," AFOSR/FJSRL Molecular Dynamics and Surface Chemistry Conference, USAF Academy, CO, 1 December 1982.

8. P. C. Cosby, R. Möller, and H. Helm, "Photofragment Spectroscopy of N_2^{++}," 14th Annual Meeting of the Division of Electron and Atomic Physics, Boulder, CO, 23 May 1983.

9. P. C. Cosby, R. Möller, and H. Helm, "Photodissociation of N_2^{++}," 13th International Conference on the Physics of Electronic and Atomic Collisions, Berlin, FRG, 27 July 1983.

10. H. Helm and P. C. Cosby, "Laser Excitation of Shape Resonances in $OH^+ A^3\Pi$," Symposium on Atomic and Surface Physics, Hintermoos, Austria, 29 January 1984.

VI CUMULATIVE LIST OF PUBLICATIONS UNDER
THIS CONTRACT

1. J. T. Moseley, R. P. Saxon, B. A. Huber, P. C. Cosby, R. Abouaf, and M. Tadjeddine, "Photofragment Spectroscopy and Potential Curves of AR_2^+," J. Chem. Phys. <u>67</u>, 1659 (1977).

2. B. A. Huber, T. M. Miller, P. C. Cosby, H. D. Zeman, R. L. Leon, J. T. Moseley, and J. R. Peterson, "A Laser-Ion Coaxial Beams Spectrometer," Rev. Sci. Instrum. <u>48</u>, 1306 (1977).

3. P. C. Cosby, J. T. Moseley, J. R. Peterson, and J. H. Ling, "Photodissociation Spectroscopy of O_3^-," J. Chem. Phys. <u>69</u>, 2771 (1978).

4. R. Abouaf, B. A. Huber, P. C. Cosby, R. P. Saxon, and J. T. Moseley, "Photofragment Spectroscopy and Potential Curves of Kr_2^+," J. Chem. Phys. <u>68</u>, 2406 (1978).

5. D. L. Albritton, J. T. Moseley, P. C. Cosby, and M. Tadjeddine, "The Dissociation Energy of $O_2(X^3\Sigma_g^-)$," J. Mol. Spectros. <u>70</u>, 326 (1978).

6. L. C. Lee and G. P. Smith, "Photodissociation Cross Sections of Ne_2^+, Ar_2^+, Kr_2^+, and Xe_2^+ from 3500 to 5400 Å," Phys. Rev. A <u>19</u>, 2329 (1979).

7. P. C. Cosby, J. B. Ozenne, J. T. Moseley, and D. L. Albritton, "High Resolution Spectroscopy of $O_2^+(b^4\Sigma_g^-, v;=3,4,5 \leftarrow a^4\Pi_u, v'=3,4,5)$ Using Coaxial Laser and Ion Beams," J. Mol. Spectros. <u>79</u>, 203 (1980).

8. P. C. Cosby, H. Helm, and J. T. Moseley, "Observation of Predissociated Levels of CH^+, Astrophys. J. <u>235</u>, 52 (1980).

9. H. Helm, P. C. Cosby, and D. L. Huestis, "Laser Predissociation Spectroscopy of the $f^4\Pi_g$ State of O_2^+," J. Chem. Phys. <u>73</u>, 2629 (1980).

10. J. T. Moseley, J. B. Ozenne, and P. C. Cosby, "Photofragment Spectroscopy of O_3^+," J. Chem. Phys. <u>74</u>, 337 (1981).

11. P. C. Cosby and H. Helm, "Laser Photofragment Spectroscopy of NO^+ I. Predissociation of the $2^3\Pi$ State," J. Chem. Phys. <u>75</u>, 3882 (1981).

12. P. C. Cosby, R. Möller, and H. Helm, "Photofragment Spectroscopy of N_2^{++}," Phys. Rev. A <u>28</u>, 766 (1983).

13. P. C. Cosby, "Photofragment Spectroscopy of SO^+," J. Chem. Phys. <u>80</u>,xxxx (1984).

14. H. Helm, P. C. Cosby, and D. L. Huestis, "Photofragment Spectroscopy of Shape Resonances in OH^+," Phys. Rev. A. (accepted for publication).

15. P. C. Cosby, "Photofragment Spectroscopy of CH^3I^+: Observation of Bimodal CH_3^+ Product Kinetic Energy Distributions," Chem. Phys. Letter (in preparation).

16. P. C. Cosby, "High Resolution Photofragment Spectroscopy of CH_3I^+," Chem. Phys. Letter (in preparation).

17. P. C. Cosby, D. L. Huestis, and H. Helm, "Photofragment Spectroscopy of O_2^+: Molecular Constants and Potential Energy Curve of the $f^4\Pi_g$ State," J. Mol. Spectrosc. (in preparation).

18. H. Helm, D. L. Huestis, and P. C. Cosby, "Photofragment Spectroscopy of O_2^+: Predissociation Lifetimes of $f^4\Pi_g$ and Product State Distributions," J. Chem. Phys. (in preparation).

REFERENCES

1. B. A. Huber, T. M. Miller, P. C. Cosby, H. D. Zeman, R. L. Leon, J. T. Moseley, and J. R. Peterson, Rev. Sci. Instrum. 48, 1306 (1977).

2. P. K. Carroll, Can. J. Phys. 36, 1585 (1958).

3. G. Chambaud, J. M. Launay, B. Levy, P. Millie, E. Roueff, and F. Tran Minh, J. Phys. B 13, 4205 (1980).

4. M. Tsuji, C. Yamagiwa, M. Endoh, and Y. Nishimura, Chem. Phys. Letters 73, 407 (1980); I. Murakami, M. Tsuji, and Y. Nishi-mura, ibid. 92, 131 (1982).

5. D. Cossart, H. Lavendy, and J. M. Robbe, J. Molec. Spectrosc. 99, 369 (1983).

6. A. Tabche-Fouhaille, J. Durup, J. T. Moseley, J. B. Ozenne, C. Pernot, and M. Tadjeddine, Chem. Phys. 17, 81 (1976).

7. F. J. Grieman, J. T. Moseley, R. P. Saxon, and P. C. Cosby, Chem. Phys. 51, 169 (1980).

8. P. C. Cosby, J. B. Ozenne, J. T. Moseley, and D. L. Albritton, J. Mol. Spectrosc. 79, 203 (1980).

9. D. L. Albritton, J. T. Moseley, P. C. Cosby, and M. Tadjeddine, J. Mol. Spectrosc. 70, 326 (1978).

10. J. C. Hansen, M. M. Graff, J. T. Moseley, and P. C. Cosby, J. Chem. Phys. 74, 2195 (1981).

11. J. C. Hansen, J. T. Moseley, and P. C. Cosby, J. Mol. Spectrosc. 98, 48 (1983).

12. J. C. Hansen, J. T. Moseley, A. L. Roche, and P. C. Cosby, J. Chem. Phys. 77, 1206 (1982).

13. H. Helm, P. C. Cosby, and D. L. Huestis, J. Chem. Phys. 73, 2629 (1980).

14. P. C. Cosby and H. Helm, J. Chem. Phys. 76, 4720 (1982).

15. C. M. Marian, R. Marian, S. D. Peyerimhoff, B. A. Hess, R. J. Buenker, and G. Seger, Mol. Phys. 46, 779 (1982).

16. R. N. Zare, Ph.D. thesis, Harvard University, 1964.

17. J. Durup, Chem. Phys. 59, 351 (1981).

18. S. J. Dunlavey, J. M. Dyke, N. K. Fayad, N. Jonathan, and A. Morris, Mol. Phys. 38, 729 (1979).

19. M. Horani, S. Leach, and J. Rostas, J. Mol. Spectrosc. 23, 115 (1967); J. Rostas, private communication (1980).

20. C. P. Edwards, C. S. Maclean, and P. J. Sarre, J. Chem. Phys. 76, 3829 (1982).

21. L. Karlsson, R. Jadrny, L. Mattsson, F. T. Chau, and K. Siegbahn, Physica Scripta 16, 225 (1977).

22. M. A. Baig, J. P. Connerade, J. Dagata, and S. P. McGlynn, J. Phys. B 14, L25 (1981).

23. J. H. D. Eland, R. Frey, A. Kuestler, H. Schulte, and B. Brehm, Int. J. Mass Spectrom. Ion Phys. 22, 155 (1976).

24. D. M. Mintz and T. Baer, J. Chem. Phys. 65, 2407 (1976).

25. I. Powis, Chem. Phys. 74, 421 (1983).

26. D. C. McGilvery and J. D. Morrison, J. Chem. Phys. 67, 368 (1977); Int. J. Mass Spectrom. Ion Phys. 28, 81 (1978).

27. S. P. Goss, D. C. McGilvery, J. D. Morrison, and D. L. Smith, J. Chem. Phys. 75, 1820 (1981).

28. S. P. Goss, J. D. Morrison, and D. L. Smith, J. Chem. Phys. 75, 757 (1981).

29. M. Tadjeddine, G. Bouchoux, L. Malegat, J. Durup, C. Pernot, and J. Weiner, Chem. Phys. 69, 229 (1982).

30. C. E. Klots, J. Chem. Phys. 64, 4269 (1976).

31. W. A. Chupka, S. D. Colson, M. S. Seaver, and A. M. Woodward, Chem. Phys. Letters 95, 171 (1983).

32. J. Dyke, N. Jonathan, E. Lee, and A. Morris, J.C.S. Faraday II 8, 1385 (1976).

33. H. M. Rosenstock, K. Draxl, B. W. Steiner, and J. T. Herron, J. Phys. Chem. Ref. Data 6, Suppl. 1 (1977).

34. K. Shobatake, R. K. Sparks, L. R. Carlson, and Y. T. Lee, XI ICPEAC, Abstracts of Papers (Kyoto, 1979), p. 60.

35. M. A. Haney and J. L. Franklin, J. Chem. Phys. 48, 4093 (1968).

36. R. J. Blint, R. F. Marshall, and W. D. Watson, Astrophys. J. 206, 627 (1976).

37. A. J. Lorquet, J. C. Lorquet, and W. Forst, Chem. Phys. 51, 241 (1980).

38. W. J. Chesnavich and M. T. Bowers, in <u>Gas Phase Ion Chemistry</u>, edited by M. T. Bowers (Academic Press, New York, 1979), p. 119.

39. T. Baer, ibid., p. 153.

40. W. L. Hase, Chem. Phys. Letters <u>67</u>, 263 (1979).

APPENDIX   A

PHOTOFRAGMENT SPECTROSCOPY OF N_2^{2+}

Photofragment spectroscopy of N_2^{2+}

P. C. Cosby, R. Möller,* and H. Helm

Molecular Physics Laboratory, SRI International, Menlo Park, California 94025

(Received 21 March 1983)

N_2^{2+} ions, produced by electron impact of N_2, are observed to predissociate into $N^+ + N^+$ when irradiated by a dye laser at photon energies between 14 900 and 19 500 cm^{-1}. Five structured bands in the spectrum are associated with absorptions from $X\,^1\Sigma_g^+$ ($v=0,1,2$) into three predissociated levels of the $1\,^1\Pi_u$ state. The two highest levels of the $1\,^1\Pi_u$ are believed to dissociate by tunneling through the Coulombic barrier in its potential-energy curve, whereas the lowest level is predissociated by the $1\,^1\Sigma_u^-$ state. Kinetic-energy analysis of the N^+ photofragments establishes the energy of $X\,^1\Sigma_g^+$ ($v=0$) at 4.8 ± 0.2 eV above the $N^+ + N^+$ dissociation asymptote and yields an adiabatic appearance potential of 43.6 ± 0.2 eV. Molecular constants for the $X\,^1\Sigma_g^+$ and $1\,^1\Pi_u$ states are determined.

I. INTRODUCTION

Electronic states of doubly charged diatomic molecules dissociating to the single-charged atoms are mainly characterized by Coulomb repulsion of the atomic ions. However, at small internuclear distances, the chemical forces can lead to a local minimum in the potential-energy curve behind the Coulombic barrier. Although the potential curves in general lie entirely above the dissociation limit, there may exist quasibound states with nearly infinite lifetime if the potential barrier has a sufficient height and width. Experimental evidence for such long-lived metastable states has been found in electron-impact,[1-10] ion-bombardment,[11] and Auger electron[12-14] experiments, which provide the approximate position of the electronic states. The lower electronic states of such common species as N_2^{2+}, O_2^{2+}, and NO^{2+} are expected to have sufficiently long lifetimes[15] to permit detailed study of their molecular properties by optical spectroscopy. But so far there has been only one observation of discrete vibrational and rotational levels in any doubly charged molecule: Carroll[16] observed a single vibrational band in the vuv emission spectrum of a N_2-He discharge and assigned it to the $D\,^1\Sigma_u^+ \rightarrow X\,^1\Sigma_g^+$ transition in N_2^{2+}.

We report here the first application of photofragment spectroscopy to a doubly charged diatomic molecule. Discrete structure appears in the wavelength dependence of the photofragment spectrum of N_2^{2+} which allows the determination of the rotational and vibrational constants of two electronic states of this ion. In addition, the observed kinetic energies of the photofragments establish the absolute energy of these levels with respect to the $N^+ + N^+$ dissociation limit.

II. EXPERIMENTAL

The laser-ion coaxial beams photofragment spectrometer used in the experiment has been described in detail previously.[17] The $^{14,14}N_2^{2+}$ ions are produced by electron-impact ionization (~100 eV) of N_2 gas, accelerated to typically 5000 eV, mass selected, and collimated. The ion beam is then merged coaxially using an electrostatic quadrupole ($Q1$) with a laser beam over a length of 60 cm, corresponding to an interaction time of typically 3 μs. The

fragment ions produced in the interaction region are separated from the primary ion beam by a second quadrupole field ($Q2$) and then either detected on an open electron multiplier ($M1$) or passed through a hemispherical electrostatic energy analyzer and detected by a second multiplier ($M2$).

Dissociation of a homonuclear diatomic ion which releases a kinetic energy W in its center-of-mass frame leads to a maximum (or minimum) translational energy of the fragments in the laboratory frame of

$$T_{\mathrm{max,min}} = E_0/2 + W/2 \pm (E_0 W)^{1/2} , \qquad (1)$$

where E_0 is the kinetic energy of the N_2^{2+} beam. If no kinetic energy were released in the dissociation ($W=0$), then the fragment ions N^+ would appear at one-half the energy and at the same laboratory velocity as the N_2^{2+} ions. Since the deflection in $Q2$ (or in the energy analyzer) depends on the ratio $T/Z = mv^2/2Z$, where Z is the charge number, both N_2^{2+} primary ions and N^+ fragment ions would follow the same flight paths and be indistinguishable. Fortunately, the metastable nature of the N_2^{2+} molecule assures that the photodissociation process $N_2^{2+} + h\nu \rightarrow N^+ + N^+ + W$ leads to an energy release W of several eV in the center-of-mass system of the dissociating molecule. This high value of W produces a considerable difference between T/Z of the photofragments N^+ and the primary N_2^{2+} ions, which permits their separation using only electrostatic fields. The kinetic energy of the photofragments also leads to high transverse-velocity components of the fragment ions due to their angular distribution. This decreases the efficiency of a detector collecting only fragments which dissociate into a cone of center-of-mass solid angle $\phi \sim \sin^{-1}[\alpha(E/W)^{1/2}]$, where α is the acceptance angle of the detector. Therefore, the open multiplier with its relatively large α of about 20 mrad, corresponding to $\phi = 30°$, has mainly been used. Only when determining the kinetic energy of the fragments was the energy analyzer with $\alpha = 2$ mrad or $\phi = 2°$ applied.

Transitions which lead to the dissociation of N_2^{2+} into $N^+ + N^+$ were observed at a resolution of ~ 2 cm^{-1} in the spectral range of 14 900–19 500 cm^{-1} using a multimode cw dye laser. As the interaction with the ion beam lies in
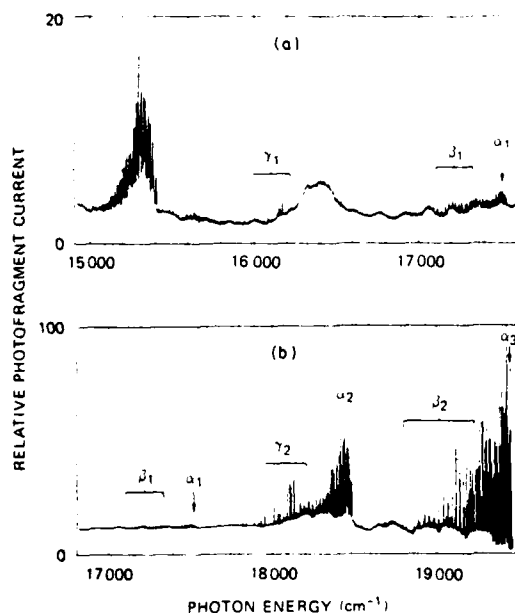
FIG. 1. Photon-energy dependence for the production of N^+ photofragments from N_2^{2+}. Spectrum was taken within the dye-laser cavity at an approximate resolution of 1.5 cm^{-1}. Both Doppler components, separated by 18.9–24.7 cm^{-1}, appear in the spectrum for each transition. Origins of the α bands are indicated by arrows. Range over which rotational lines are observed is shown for the β and γ bands.
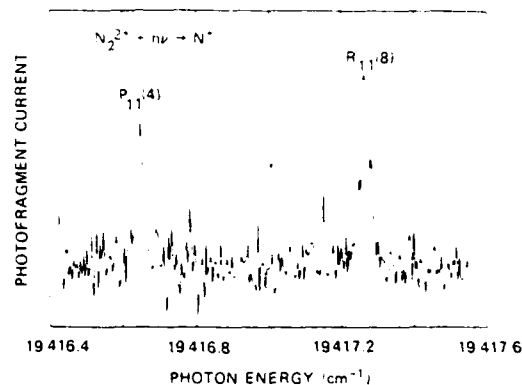

FIG. 2. High-resolution spectrum of a portion of the α_1 band. Laser was operated single mode at 19 429.79 cm^{-1} while the N_2^{2+} ion-beam energy was varied from 6120 to 4920 eV to obtain this spectrum. Assigned transitions in the α_3 band are labeled.

the cavity of the laser, every line appears twice in the spectra due to the opposite Doppler shifts for the parallel and the antiparallel traveling electromagnetic waves. Nine lines were also measured at high resolution (0.003 cm^{-1}) by an experimental arrangement where the ion beam interacts extracavity with the beam of a single-mode Ar$^+$ laser. By varying the kinetic energy of the N_2^{2+} beam in the interaction region, the Doppler-shifted frequency of the laser could be scanned continuously over two regions of ~6 cm^{-1} with the laser copropagating or counterpropagating with respect to the ion-beam velocity.

III. OBSERVED SPECTRA

The photofragment spectrum displayed in Fig. 1 shows the photon-energy dependence in the range of 14 900–19 500 cm^{-1} for the production of N^+ fragment ions from N_2^{2+} with center-of-mass kinetic energies between 3–10 eV. Three red-shaded bands labeled α_1, α_2, and α_3, each containing complete P, Q, and R branches could be identified. Partially overlapping with the α_1 and α_3 bands were two bands labeled β_1 and β_2 which consisted only of Q branches similar to those contained in the α bands. In addition, two irregular patterns of discrete lines having very similar structures were found near 17 200 and 19 200 cm^{-1}. These are labeled γ_1 and γ_2, respectively. The photodissociation continuum which extends over the entire observed range and the structured band at the red end of the spectrum in Fig. 1 have not yet been identified.

A region of approximately 10 cm^{-1} near the head of the α_1 band was investigated at high resolution using the 5145-Å line of a single-mode Ar$^+$ laser. Figure 2 shows a 1.1-cm^{-1} portion of the spectrum which was obtained by scanning the energy of the N_2^{2+} beam from 6120 to 4920 eV with the laser beam copropagating with the ion beam. Two of the observed transitions appear in this segment of the spectrum. A total of nine lines belonging to this band were identified, each having a linewidth of 1.0±0.2 GHz. The measured positions of these lines are listed in Table I.

Kinetic-energy spectra were obtained for three N_2^{2+} dissociation processes: Photon-independent spontaneous dissociation of N_2^{2+} into N^+ was observed to occur with a release of $W = 6.8 \pm 0.3$ eV. This process was monitored following a flight time of order 13 μs after formation of the N_2^{2+} ions in the source and had an intensity of approximately 10% that of the photon-induced continuum background in Fig. 1. Kinetic-energy releases from the continuum process were found to vary from 8.1 eV at 6490 Å to 8.6 eV at 5421 Å. Subtracting the energy of the photon from W locates the absorbing N_2^{2+} levels at 6.26±0.4 eV above the $N^+ + N^+$ dissociation limit. Finally, the kinetic-energy release found for the α_3 band was 7.3±0.2 eV, thus placing the absorbing level 5.06±0.2 eV above the $N^+ + N^+$ dissociation limit.

TABLE I. Lines measured at high resolution in the α_1 band.

Branch	J''	Observed (cm^{-1})[a]	Calculated (cm^{-1})[b]
Q	6	19 413.237	19 413.289
P	4	19 416.720	19 416.767
R	8	19 417.342	19 417.381
Q	5	19 420.626	19 420.601
R	0	19 441.305	19 441.346
R	3	19 441.468	19 441.524
R	1	19 442.584	19 441.621
R	2	19 442.641	19 442.681
R	4	19 439.063	19 439.147

[a]Uncertainty is ±0.03 cm^{-1}.
[b]Calculated using the merged constants in Table II.

TABLE II. Molecular constants of N_2^{2+}.

	Level	T^a	B	D (10^{-5})	q (10^{-3})	Bands
$1^1\Pi_u$	v'	21 405.7(1.4)[b]	1.243 37(14)	3.38(5)	1.30(5)	α_1 and α_3
	$v'-1$	20 436.3(2.6)	1.287 5(107)	$-3(6)$		α_2
	$v'-2$	19 382.6(1.5)	1.329 3(53)	0.2(4)		β_1 and β_2
	$(v'-3)$	(18 192)				γ_1 and γ_2
$X^1\Sigma_g^+$	2	3882.2(1.4)	1.805(5)	$-1.6(2.2)$		α_1
	1	1965.6(6)	1.851 33(12)	1.31(16)		α_2, α_3, β_1, and γ_2
	0	0	1.880 0(6)	0.68(4)		$(D\rightarrow X)$, β_2, and γ_2

[a] All units are cm^{-1}.

[b] 1-s.d. uncertainty in the final digits of the quoted value.

IV. ROTATIONAL ANALYSIS

The low-lying electronic states expected for N_2^{2+} are Σ, Π, and Δ in the multiplicities singlet, triplet, and quintet.[18] For the α bands, single P, Q, and R branches could be identified. In addition, no indication for fine-structure splitting could be found even at high resolution. Hence, we conclude that these bands arise from a singlet-singlet transition. The relative intensities of the branches in these bands further indicate that the transition must be $\Delta\Lambda = \pm 1$. An additional aid to the identification of the bands is obtained from the intensity alternation of the rotational lines within each branch. Lines originating in even- and odd-J'' values appear in the spectra with an intensity ratio of 2:1. This alternation arises from the nuclear spin $(I=1)$ of ^{14}N and is expected to be observed only in $\Sigma\leftarrow\Pi$, $\Sigma\leftarrow\Sigma$, and $\Pi\leftarrow\Sigma$ systems, where only one Λ component is pumped for a specific P, Q, or R transition. Since $\Sigma\leftarrow\Sigma$ is excluded due to the observed presence of the strong Q branches in the bands, we conclude that the α bands are due to either a $\Sigma\leftarrow\Pi$ or a $\Pi\leftarrow\Sigma$ transition. Furthermore, the fact that the P, Q, and R lines are strong for even J'' restricts the choice to $^1\Pi_g\leftarrow{}^1\Sigma_u^-$ or $^1\Pi_u\leftarrow{}^1\Sigma_g^+$, because only in these two cases will the P, Q, and R lines originate in the same weak or strong level of the Σ state. As will be discussed later, we assign the observed transitions to a $^1\Pi_u\leftarrow{}^1\Sigma_g^+$ system.

A. α bands

Approximately 35 rotational lines were unambiguously assigned in each of the three α bands. A direct nonlinear least-squares fit of these lines to the $^1\Pi_u$ and $^1\Sigma_g^+$ Hamiltonians[19] yielded the molecular constants listed in Table II. Only in the α_1 band, where high-resolution measurements were made, was the Λ-doubling coefficient of the $^1\Pi_u$ state statistically significant and included in the fit. As can be seen from this table, the α_1 and α_3 bands yielded the same upper-state rotational constants, whereas the α_2 and α_3 bands yielded the same lower-state rotational constants. We therefore conclude that the α_2 and α_3 bands terminate in the same upper-state vibrational level (v'). Hence, the α_1, α_2, and α_3 transitions can be labeled $(v',v''+1)$, $(v'-1,v'')$, and (v',v''), respectively.

Carroll[16] has observed a $^1\Sigma_u^+\rightarrow{}^1\Sigma_g^+$ emission band of N_2^{2+} which is believed to terminate in the lowest vibrational level of the $X^1\Sigma_g^+$ ground state. The rotational constant for this level obtained from this band is $B_0 = 1.8800$.

In a state described by a Morse potential, the variation in the rotational constant with vibrational level is given[18] by the equation

$$B_v = B_e - \alpha_e(v + \tfrac{1}{2}) \ . \tag{2}$$

Hence, the difference in B_v between any two adjacent vibrational levels is α_e. From the two lower-state rotational constants obtained from the α bands $B_{v''}$ and $B_{v''+1}$, one expects $\alpha_e \sim 0.0463 \pm 0.005$. Thus, the rotational constant for the next lower vibrational level in the absorbing electronic state should be approximately $B_{v''-1} = 1.851\,33 + 0.0463$ or 1.898 ± 0.005. This value compares very favorably with Carroll's value for B_0 in the $X^1\Sigma_g^+$ state, suggesting that the α bands arise from $v=1$ and 2 of this same state. As a check of this assignment, we can also compare the lower-state vibrational frequencies. From the relationship between the rotational constant B_0 and its centrifugal distortion correction D_0 in an harmonic oscillator, Carroll estimated the equilibrium vibrational frequency of the X state to be $\omega_e \sim 1960$ cm^{-1}. Using this value together with our observed value of α_e and Carroll's value of B_0, the anharmonicity of the X state is estimated from the Pekeris relation[18] to be $\omega_e x_e \sim 51$ cm^{-1}. Hence the estimated vibrational spacing of $v=1$ and 2 in the X state would be of order 1756 cm^{-1}. This, too, is consistent with the observed spacing of 1916.6 cm^{-1}. We can therefore be reasonably confident that the assignment of $X^1\Sigma_g^+$ $(v=1,2)$ to the two observed lower-state levels is correct.

The transitions assigned to the α bands are shown schematically as a function of energy by the solid vertical lines in Fig. 3. Since the $v=0$ level of the X state is likely also populated in the ion beam, one would expect absorptions from it into the two completely predissociated upper-state levels. However, these transitions, would occur at photon energies higher than 20 000 cm^{-1}, outside the energy range covered in the photofragment spectra. Finally, one would also expect the transition $(v'-1,2)$, shown as the dotted vertical line in Fig. 3, to occur with its origin at 16 554.1 cm^{-1}. Indeed, weak structure does appear in this region superimposed on the continuum background, but is much too indistinct to attempt a rotational assignment.

B. β bands

The β_1 and β_2 bands appear as additional structure within the rotational manifolds of the α_1 and α_3 bands.

A-3
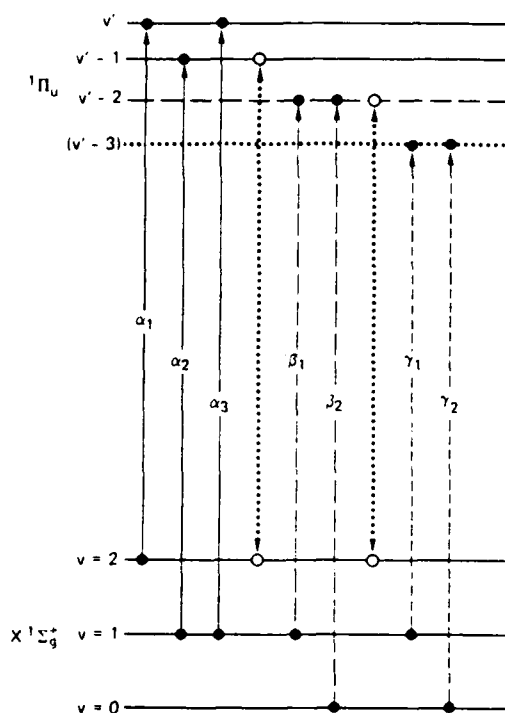
FIG. 3. Schematic of the levels involved in the α, β, and γ bands. Dotted vertical lines represent unobserved transitions. Assignment of the upper state of the γ bands is not supported by a rotational analysis; hence the existence of a $v' - 3$ level in the $^1\Pi_u$ state is speculative.
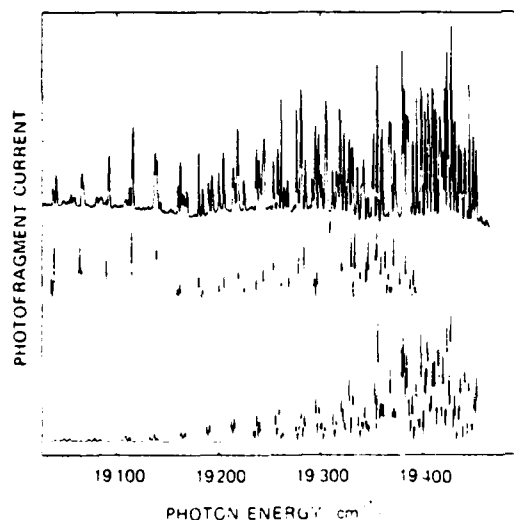

FIG. 4. A portion of the photofragment spectrum from Fig. 1 shown on an expanded photon-energy scale. Upper curve is the experimental spectrum. Center and bottom curves are synthetic spectra of the β_2 and α_3 bands, respectively, generated from the constants in Table II assuming a rotational temperature of 400 K and a laser resolution of 1.5 cm^{-1}.

The upper portion of Fig. 4 shows the photofragment spectrum observed within the spectral range of 19 027–19 491 cm^{-1}. In the lower portion of this figure is a synthetic spectrum of the α_3 band. As can be seen by comparing the synthetic and observed spectra, significant additional structure appears among the higher rotational transitions of the α_3 band. Similar additional structure is found within the α_1 band. These additional lines are named the β_1 and β_2 bands. They are each found to consist only of a single Q branch. Consequently only the band origins and the difference between the upper- and lower-state origins can be uniquely determined from the line positions. For the β_2 band, the band origin v_0 was found to be 19 360 cm^{-1} and $\Delta B = 0.615 \pm 0.010$ cm^{-1}, whereas for β_1, $v_0 = 17\,405$ cm^{-1} and $\Delta B = 0.631 \pm 0.019$ cm^{-1}. A simulation of the β_2 band is shown in the center of Fig. 4.

The intensities within the Q branches of the β bands are very similar at higher J to those of the α bands. However, the intensity at $J'' < 10$ is substantially less than would be expected and very low-J transitions may indeed not be present at all. Moreover, there is no evidence of the corresponding P and R branches in the spectra. The absence of these branches implies that only the f components of the $^1\Pi$ state are predissociated, in contrast to the upper-state vibrational levels accessed in the α bands, where both e and f components of all rotational levels are predissociated. As discussed later, the upper-state vibrational levels of the α bands are likely to predissociate by tunneling through the Coulombic barrier in the $^1\Pi$ potential well. Predissociation of only the f components in the β bands suggests that the upper-state levels must lie deeper in the $^1\Pi$ potential well such that the barrier width prevents efficient tunneling, thus requiring it to be predissociated by the continuum of another state. Since assignment of the α bands fixes the relative energies of the higher, completely predissociated vibrational levels and the bottom of the $X\,^1\Sigma_g^+$ potential well, the observed band origins of the β_1 and β_2 bands require that they originate from $v = 1$ and 0, respectively, of the X state and terminate in a single, partially predissociated level $v' - 2$ of the $^1\Pi$ state. These transitions are shown schematically by the long-dashed lines in Fig. 3. Fixing the values of the lower-state rotational constants to those listed in Table II, a least-squares fit of the β_1 and β_2 bands to the $^1\Pi$ and $^1\Sigma$ Hamiltonians yielded the molecular constants and energy separation of the $v'' = 0$ and 1 levels of the $^1\Sigma_g^+$ state. These are also shown in Table II.

C. γ bands

Finally, two groups of lines labeled γ_1 and γ_2 appear in the photofragment spectrum near 17 200 and 19 200 cm^{-1}. Their line positions are listed in Table III. The spacing of the lines within each group is irregular; they apparently do not represent transitions into contiguous rotational levels. However, the spacings within each group are quite similar, with the separation of the corresponding lines varying from 1947.3 to 1956.2 cm^{-1}. This separation is quite close to the spacing of $v = 1$ and 0 of the $X\,^1\Sigma_g^-$ state, suggesting that γ_1 and γ_2 originate from these levels and terminate in a fourth predissociated level $v' - 3$ of the $^1\Pi_u$ state, as shown by the short-dashed lines in Fig. 3. The

TABLE III. Observed lines in the γ bands.

γ_1 (cm^{-1})[a]	γ_2 (cm^{-1})[a]	Difference (cm^{-1})
15 992.0	17 940.2	1948.2
16 074.5	18 021.8	1947.3
16 150.9	18 101.5	1950.6
16 162.3	18 118.0	1955.7
16 222.3	18 178.5	1956.2

[a]Uncertainty in the line positions is ± 2 cm^{-1}.

expected energy of this level, extrapolated from the spacings of the higher vibrational levels in this state, is 18 192 cm^{-1}. Thus, the transitions lie in the correct general location for a red-shaded band. We have not yet been able, however, to assign the lines to specific rotational transitions, possibly due to level shifts or extra lines produced by the predissociating state. Consequently, we consider our attribution of γ_1 and γ_2 to the $(v'-3,1)$ and $(v'-3,0)$ bands in the $^1\Pi_u \leftarrow ^1\Sigma_g^+$ system to be only speculative.

V. VIBRATIONAL ANALYSIS

Rotational analysis of the α and β bands strongly suggests that they arise from the three lowest vibrational levels of the $X^1\Sigma_g^+$ state. The spacing of the band origins yields the vibrational constants for this state: $\omega_e = 2014.6 \pm 1.7$ cm^{-1} and $\omega_e x_e = 24.5 \pm 0.8$ cm^{-1}. Similarly, B_e and r_e can be estimated from the constants for these three levels as 1.899 ± 0.004 cm^{-1} and 1.126 ± 0.001 Å, respectively.

An upper limit for the energy of the lowest electronic state of N_2^{2+} relative to the $N^+ + N^+$ dissociation limit is given by the relation (in eV)

$$U_0 = V_{AP}(N_2^{2+}) - D_0(N_2) - 2V_{IP}(N)$$
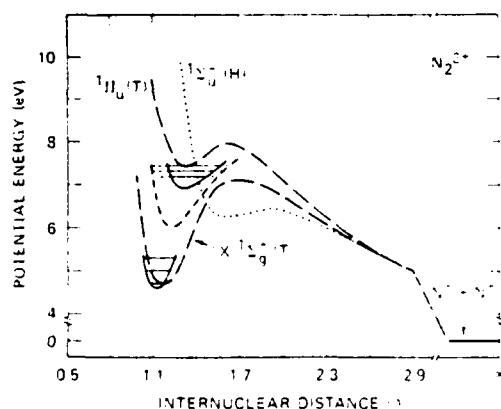
$$= 4.2 \pm 0.4 , \tag{3}$$

FIG. 5. Potential-energy curves of N_2^{2+}. Lower solid curve is the RKR potential of the $X^1\Sigma_g^+$ state derived in this work. Upper solid and short-dashed curves are the RKR potentials of the $^1\Pi_u$ state obtained assuming the vibrational numbering of the observed levels was 1,2,3 and 6,7,8, respectively. Long-dashed curves are the theoretical curves for these states from Ref. 24. Dotted curve is the theoretical $^1\Sigma_u^-$ curve for C given by Ref. 27 transformed to N_2^{2+} using the method of Ref. 15.

where $V_{AP}(N_2^{2+})$ is the appearance potential of N_2^{2+} from N_2 determined by Auger spectroscopy[13] $(43.0 \pm 0.4$ eV), $D_0(N_2)$ is the dissociation energy of $N_2(9.7594$ eV),[20] and $V_{IP}(N)$ is the ionization potential of the nitrogen atom[21] (14.5342 eV). The energy of $X^1\Sigma_g^+$ $(v=0)$ can be independently determined from the present measurements. Photodissociation in the α_2 band produced photofragments with center-of-mass kinetic energies of 7.3 ± 0.2 eV. Since, from Table II, the predissociated level lies 2.5338 eV above $X^1\Sigma_g^+$ $(v=0)$, the energy of $X^1\Sigma_g^+$ $(v=0)$ relative to the $N^+ + N^+$ limit must be the difference between these two energies, or $U_0 = 4.8 \pm 0.2$ eV. Inversion of Eq. (3) using this value of U_0 yields the appearance potential for $N_2^{2+} X^1\Sigma_g^+$ $(v=0)$ to be 43.6 ± 0.2 eV.

Agreement between these two values for U_0 is only marginally good, they fall together just within the range of each set of error limits. This may suggest that the lowest energy state appearing in the Auger spectrum (or formed by electron impact) is not the $X^1\Sigma_g^+$ state, but another state which lies 0.0 to 1.2 eV lower in energy. Indeed, the self-consistent-field (SCF) calculations of Cobb et al.[22] show the $^3\Sigma_g^-$ state to lie 0.6 eV below the $^1\Sigma_g^+$. Unfortunately, the errors associated with the observations are too large to provide definitive information on the actual location of the N_2^{2+} triplet states. Nevertheless, we retain the currently accepted[20] label X, for the lowest singlet state of N_2^{2+} $^1\Sigma_g^+$.

Using our value for U_0 together with the vibrational and rotational constants, the Rydberg-Klein-Rees (RKR) potential curve for the $^1\Sigma_g^+$ state was constructed[23] and is shown by the lower solid curve in Fig. 5. The energies of the three observed vibrational levels of the $^1\Pi_u$ state relative to $X^1\Sigma_g^+$ $(v=0)$ are listed in Table II. The second difference of these energies yields an anharmonicity for these levels of $\omega_e x_e = 40.8 \pm 1.9$ cm^{-1}. The vibrational numbering of the levels cannot be established from these data alone; hence ω_e and the potential curve cannot be directly determined.

VI. IDENTIFICATION OF THE ELECTRONIC STATES

Assignment of the observed absorption bands to specific states of N_2^{2+} requires the use of theoretical calculations of this structure of the ion. Experimentally, we know that the transitions in the α bands must be either $^1\Pi_u \leftarrow ^1\Sigma_g^+$ or $^1\Pi_g \leftarrow ^1\Sigma_u^-$. We further know that the absorbing levels of the $^1\Sigma$ lower state lie 4.8 ± 0.2 eV above the $N^+ + N^+$ dissociation limit.

There have been two detailed ab initio calculations of the lower electronic states of N_2^{2+}. The configuration-interaction calculations of Thulstrup and Andersen[24] (TA) encompassed all of the bound singlet states lying within 10 eV of the ground state and the six lowest bound triplet states. They predict the ground state to be the $^1\Sigma_g^+$ and that no bound $^1\Sigma_u^-$ states lie within this energy range. Their calculations extend only to about $6a_0$; hence, the energy of these states relative to the dissociation limit is not given directly. However, at these large internuclear distances, the force between the two N^+ ions is almost purely Coulombic. Hence, using the expression for Coulomb repulsion between two point charges $V(r) = 14.40$ eV/r(Å), we can normalize their curves to an absolute en-

ergy scale at a single large internuclear distance. These normalized curves for the $^1\Sigma_g^+$ and $^1\Pi_u$ states are shown by the lower and upper dashed curves, respectively, in Fig. 5.

We can also compare with the unrestricted SCF calculations of Cobb, Moran, Borkman, and Childs (CMBC).[22] They too predict the $^1\Sigma_g^+$ state to be the lowest singlet state, but find this state to lie 3.0 eV above the $N^+ + N^+$ dissocation limit with an equilibrium internuclear separation of 1.259 Å and vibrational constants $\omega_e = 1674$ cm^{-1}, $\omega_e x_e = 20.1$ cm^{-1}. Finally, comparison can be made with the semiempirical calculations of Hurley and Maslen (HM).[15] Their technique uses an integral form of the quantum-mechanical virial theorem to deduce potential curves of doubly charged ions from those of the isoelectronic neutral molecule, in this case, C_2. Using the most recent constants for this molecule,[20] we find that the minimum of the $^1\Sigma_g^+$ curve predicted by HM lies 3.8 eV above the $N^+ + N^+$ limit with an equilibrium internuclear distance of 1.017 Å and the vibrational constants $\omega_e = 1787$ cm^{-1}, $\omega_e x_e = 35.5$ cm^{-1} for the lowest vibrational levels.

Thus both the CMBC and HM calculations predict the $^1\Sigma_g^+$ state to lie lower in energy with somewhat wider potential wells than is experimentally observed. On the other hand, agreement between the TA potential curve and the experimental $^1\Sigma_g^+$ curve is remarkably good. The two curves have nearly the same energies and potential-well shapes, although the theoretical curve lies at slightly larger internuclear distances.

Agreement between the theoretical potential curves for the $^1\Pi_u$ state and the observed upper-state levels is less favorable. The TA $^1\Pi_u$ curve is shown as the upper long-dashed curve in Fig. 5. Numerical solution of the Schrödinger equation using the program of LeRoy[25] yielded four vibrational levels for this potential curve with the highest level lying 7.94 eV above the $N^+ + N^+$ dissociation limit. The three highest levels were found to predissociate efficiently by tunneling through the Coulombic barrier with lifetimes ranging from 10^{-7} to 10^{-13} s. The calculated spacing of the levels was $\Delta G_{0.5} = 1347$, $\Delta G_{1.5} = 1190$, and $\Delta G_{2.5} = 920$ cm^{-1}, giving an apparent anharmonicity constant for the highest levels of $\omega_e x_e = 135$ cm^{-1}. If we assume the observed levels correspond to $v = 1, 2, 3$, an RKR potential curve for the $^1\Pi_u$ state can be generated and is shown as the upper solid curve in Fig. 5.

The $^1\Pi_u$ curve predicted by the HM calculation is substantially deeper than the TA curve with an $R_e = 1.095$ Å. Numerical solution of the Schrödinger equation for this curve yields ten vibrational levels with the highest level 6.20 eV above $N^+ + N^+$. Only the two highest levels are found to predissociate efficiently with lifetimes of $\tau_8 = 1.5 \times 10^{-7}$ and $\tau_9 = 2.1 \times 10^{-11}$ s. The calculated spacings of the levels is $\Delta G_{7.5} = 823$ cm^{-1} and $\Delta G_{8.5} = 709$ cm^{-1}, yielding an apparent anharmonicity of $\omega_e x_e = 57$ cm^{-1}. The CMBC $^1\Pi_u$ curve is deeper yet, with its minimum only 3.5 eV above the dissociation asymptote and an $r_e = 1.1906$ Å. The calculated curve does not extend over sufficient range of internuclear distance to calculate the maximum number of vibrational levels supported in the well or their predissociation lifetimes. The well depth implies, however, that the number

of levels is substantially greater than ten.

For comparison, we have calculated the RKR potential well for the $^1\Pi_u$ state assuming that the vibrational quantum numbers of the observed levels is $v = 6, 7, 8$. This is shown as the short-dashed curve in Fig. 5. As can be seen from the figure, the predicted potential well changes dramatically with the choice of vibrational numbering. Unfortunately, there is yet no clear choice of which vibrational numbering scheme to select for the $^1\Pi_u$. The energies, level spacings, and rotational constants of the observed levels agree best with those of the TA potential curve, suggesting the solid RKR curve is the better representation of this state. However, the $^1\Pi_u - {}^1\Sigma_g^+$ Franck-Condon factors obtained using this curve would predict the α bands to have nearly equal intensities, whereas they actually differ by more than an order of magnitude. This is more consistent with what is predicted from the dashed RKR curve. Consequently, we cannot determine the vibrational numbering of the observed levels lacking additional observations on an isotopic molecule. We can, however, conclude that our identification of the upper state as the $^1\Pi_u$ is fully consistent with theoretical predictions.

VII. PREDISSOCIATION MECHANISM

We know from the difference in the number of branches appearing in the α and β bands that the $^1\Pi_u$ state is predissociated by at least two mechanisms. Numerical calculations for the theoretical potential curves for this state show that the two or three highest vibrational levels in this state can predissociate efficiently by tunneling through the Coulombic barrier. This mechanism most likely produces the photodissociation arising from the α bands, which access the two highest of the three observed vibrational levels and results in predissociation of all rotational levels. The linewidths measured for transitions into the lower rotational levels of the highest vibrational level set a lower limit on the lifetimes of this level of greater than 1.6×10^{-10} s. This compares favorably with the expected lifetimes of the highest level in the $^1\Pi_u$ state predicted by the HM calculation of 2.1×10^{-11} s. The calculated lifetime of $v = 3$ in the TA potential curve is only 1.0×10^{-13} s; transitions into such a level would have linewidths of 52 cm^{-1}, hence they would appear only as a continuum in the photofragment spectrum. The next lower vibrational level $v = 2$, however, has a calculated lifetime of 2.9×10^{-10} s, which is more consistent with the experimental limit.

The $v = 0$ level in the TA potential and the $v = 7$ level in the HM potential, have lifetimes much too long $(1.3 \times 10^{-2}$ and 5.4×10^{-3} s, respectively) to dissociate by tunneling. Hence, another mechanism must be responsible for predissociation of this level. Indeed, only Q-branch transitions are observed in the β bands, which access this level. These transitions populate only the f components in the $^1\Pi_u$ state, whereas the unobserved P- and R-branch transitions would populate the e component. Thus, a mechanism which selectively predissociates only the f components must be found. Of the 18 electronic states arising from the $N^+ \, {}^3P + N^+ \, {}^3P$ asymptote, only rotational coupling to the $^1\Sigma_u^-$ state could selectively predissociate[26] the f components of the $^1\Pi_u$. The potential curve for this state has not been calculated for N_2^{2+}, nor has it been ex-

perimentally observed in C_2. However, using the theoretical C_2 curve from Fougere and Nesbet,[27] the curve can be transformed using the method of Hurley and Maslen[15] and is shown as the dotted curve in Fig. 5. It can be seen that the continuum of this state passes directly through the observed level, hence efficient coupling between the $^1\Pi_u$ and $^1\Sigma_u^-$ states should be feasible. Further, since the magnitude of the coupling scales with rotation of the molecule, this could account for the apparent lack of low-J transitions in the β bands.

Finally, we must consider the γ bands which consist of only a few isolated rotational levels. If these bands accessed the $(v'-3)$ level of the $^1\Pi_u$ state, predissociation might result from perturbations of this level by other bound states, which are themselves predissociated. In that case, only those levels would appear in the spectra which accidentally have energies similar to the corresponding rotational levels of the perturbing state. Assignment of these bands to the $^1\Pi_u$ state is only speculative, since we would expect the $^1\Sigma_u^-$ to also predissociate this level unless its vibrational overlap were accidentally very small.

this ion, establish the absorptions as occurring from $X\,^1\Sigma_g^+$ ($v=0,1,2$) into three predissociated levels of the $1\,^1\Pi_u$ state. The two highest levels of this state are believed to predissociate by tunneling through the Coulombic barrier in its potential energy curve. In contrast, the lowest of the three levels is found to be predissociated by the $1\,^1\Sigma_u^-$ state. Molecular constants are determined for both the $X\,^1\Sigma_g^+$ and $1\,^1\Pi_u$ states and the potential-energy curve of the X state is constructed. The lack of vibrational identification of the $^1\Pi_u$ levels prevents a unique construction of its potential energy curve. Comparison is made for both states with the potential energy-curves calculated by two ab initio methods and one semiempirical method. Best agreement is observed with the calculations of Thulstrup and Andersen.[24] Kinetic-energy analysis of the N^+ photofragments places the $X\,^1\Sigma_g^-$ state and the predissociated levels of the $1\,^1\Pi_u$ state on an absolute energy scale. Comparison with the accepted experimental values of the N_2^{2+} appearance potential suggests that the $X\,^1\Sigma_g^+$ may not be the lowest energy state of this ion.

VIII. SUMMARY

Photodissociation of N_2^{2+} yields a series of structured bands in the photon-energy dependence for the production of N^+ fragments. Rotational analysis of five of the bands, and comparison with both electronic structure calculations and lines previously observed in the emission spectrum of

ACKNOWLEDGMENTS

*Present address: Fakultät für Physik der Universität Freiburg, Herman Herderstrasse 3, D-7800 Freiburg, West Germany.

[1]F. H. Dorman and J. D. Morrison, J. Chem. Phys. 35, 575 (1961).

[2]S. E. Kupriyanov, Zh. Tekh. Fiz. 34, 861 (1964) [Sov. Phys.–Tech. Phys. 9, 659 (1964)].

[3]A. S. Newton and A. F. Sciamanna, J. Chem. Phys. 50, 4868 (1969).

[4]J. H. Beynon, R. M. Caprioli, and J. W. Richardson, J. Am. Chem. Soc. 93, 1852 (1971).

[5]L. Deleanu and J. A. D. Stockdale, J. Chem. Phys. 63, 3898 (1975).

[6]T. D. Märk, J. Chem. Phys. 63, 3731 (1975).

[7]J. A. D. Stockdale, J. Chem. Phys. 66, 1792 (1977).

[8]B. Brehm and G. DeFrenes, Int. J. Mass Spectrom. Ion Phys. 26, 251 (1978).

[9]R. Locht and J. Momigny, Chem. Phys. Lett. 66, 574 (1979).

[10]J. H. Agee, J. B. Wilcox, L. E. Abbey, and T. F. Moran, Chem. Phys. 61, 171 (1981).

[11]A. K. Edwards and R. M. Wood, J. Chem. Phys. 76, 2938 (1982).

[12]D. Stalherm, B. Cleff, H. Hillig, and W. Mehlhorn, Z. Naturforsch. 24a, 1728 (1969).

[13]K. Siegbahn, C. Nordling, G. Johansson, J. Hedman, P. F. Heden, K. Hamrin, U. Gelius, T. Bergmark, L. O. Werme, R. Manne, and Y. Baer, ESCA Applied to Free Molecules (North-Holland, Amsterdam, 1971), pp. 62–69.

[14]W. E. Moddeman, T. A. Carlson, M. O. Krause, B. P. Pullen, W. E. Bull, and G. K. Schweitzer, J. Chem. Phys. 55, 2317

(1971).

[15]A. C. Hurley and V. W. Maslen, J. Chem. Phys. 34, 1919 (1961); A. C. Hurley, J. Mol. Spectrosc. 9, 18 (1962).

[16]P. K. Carroll, Can. J. Phys. 36, 1585 (1958); P. K. Carroll and A. C. Hurley, J. Chem. Phys. 35, 2247 (1961).

[17]B. A. Huber, T. M. Miller, P. C. Cosby, H. D. Zeman, R. L. Leon, J. T. Moseley, and J. R. Peterson, Rev. Sci. Instrum. 48, 1306 (1977).

[18]G. Herzberg, Molecular Spectra and Molecular Structure I. Spectra of Diatomic Molecules (Van Nostrand Reinhold, New York, 1950).

[19]R. N. Zare, A. L. Schmeltekopf, W. J. Harrop, and D. L. Albritton, J. Mol. Spectrosc. 46, 37 (1973).

[20]K. P. Huber and G. Herzberg, Molecular Spectra and Molecular Structure IV. Constants of Diatomic Molecules (Van Nostrand Reinhold, New York, 1979).

[21]C. E. Moore, Ionization Potentials and Ionization Limits Derived from the Analysis of Optical Spectra, Natl. Stand. Ref. Data Ser., Natl. Bur. Stand. U. S. Circ. No. 34 (1970).

[22]M. Cobb, T. F. Moran, R. F. Borkman, and R. Childs, J. Chem. Phys. 72, 4463 (1980).

[23]R. N. Zare, J. Chem. Phys. 40, 1934 (1964).

[24]E. W. Thulstrup and A. Andersen, J. Phys. B 8, 965 (1975).

[25]R. J. LeRoy, University of Waterloo Chemical Physics Research Report No. CP-110 (unpublished).

[26]I. Kovacs, Rotational Structure in the Spectra of Diatomic Molecules (American Elsevier, New York, 1969), p. 253.

[27]P. F. Fougere and R. K. Nesbet, J. Chem. Phys. 44, 285 (1966).

APPENDIX   B

LASER PHOTOFRAGMENT SPECTROSCOPY OF NO⁺. I.   PREDISSOCIATION OF

THE $2^3\Pi$ STATE[a])

Laser photofragment spectroscopy of NO^+. I. Predissociation of the 2 $^3\Pi$ state[a]

P. C. Cosby and H. Helm

Molecular Physics Laboratory, SRI International, Menlo Park, California 94025
(Received 3 April 1981; accepted 2 July 1981)

NO^+ ions, produced by electron impact on NO, are observed to predissociate into $O^+(^4S^0) + N(^4S^0)$ when irradiated by a dye laser at wavelengths between 6600–5650 Å. The highly structured wavelength dependence of the photofragments reflects absorptions from three vibrational levels in a long-lived NO^+ electronic state to 20 vibrational levels of a predissociated electronic state. The transitions are tentatively identified as $2\,^3\Pi(v' = 0$–$19)$—$b'\,^3\Sigma^-(v'' = 8$–$10)$. The weakly bound $2\,^3\Pi$ state is found to lie 0.698–0.925 eV above the lowest separated atom limit of NO^+ and to adiabatically correlate to the $N^+(^3P) + O(^3P)$ limit. This state is also found to be homogeneously perturbed, most likely by the $^3\Pi$ state arising from the $O^+(^4S^0) + N(^2D^0)$ limit, and to be predissociated by the $\alpha\,^3\Sigma^+$ state. The predissociation lifetimes for all rotational levels in $v' = 0$–8 are ≥ 1.6 ns. Perturbations in $b'\,^3\Sigma^-(v = 9)$ are discussed.

I. INTRODUCTION

Because of its exceptionally low heat of formation, NO^+ is the most abundant chemical species in the thermosphere and is a key reactant at lower altitudes.[1-3] Yet, in contrast to its isoelectronic neutral analog N_2, very little spectroscopic information has been obtained on the electronic structure of NO^+. Only the $A\,^1\Pi - X\,^1\Sigma^+$ Miescher–Baer bands[4] have been identified in a nitric oxide gas discharge. They are also the only emission bands that have been rotationally analyzed.[5-7] Two additional band systems attributed to $b'\,^3\Sigma^- - X\,^1\Sigma^+$ and $b\,^3\Pi - X\,^1\Sigma^+$ have been observed at low resolution in the fluorescence from an NO^+ ion beam.[7,8] Nevertheless, a relatively complete description of eight low-lying electronic states of NO^+ has emerged from the combination of these measurements with electronic structure calculations[9-11] and the photoelectron spectroscopy of NO.[12] Current knowledge of these states has recently been reviewed by Albritton, Schmeltekopf, and Zare[13] who derived the NO^+ potential energy curves shown in Fig. 1.

Experimental information on electronic states above the lowest dissociation limit $O^+(^4S^0) + N(^4S^0)$ is only fragmentary. Theoretical calculations by Michels[11] predict twelve additional bound states to lie within 24 eV of the $NO X\,^2\Pi$ ground state. Only two prominent features are observed by photoelectron spectroscopy above the lowest dissociation limit.[12] They refer to bound states at 21.72 and 22.7 eV. Photoabsorption,[14,15] photodissociative ionization,[15,16] and photoelectron-photoion coincidence[17] spectroscopy of NO, together with studies of spontaneous[18-20] and collisional dissociation[20-22] of NO^+, have also probed the NO^+ electronic states in this region, but *none of these techniques* has achieved sufficient resolution to permit state identifications.

We report here the initial application of predissociation photofragment spectroscopy to the investigation of NO^+ excited states. This technique allows the first observation of bound–bound absorption transitions in NO^+. The transitions are pumped by a laser and are detected

by observing the subsequent predissociation of the upper electronic state to $O^+(^4S^0) + N(^4S^0)$ products. Measurement of the kinetic energies of these photofragments establishes the absolute energy locations of both the (lower) absorbing and (upper) predissociating states with respect to this lowest separated atom limit of NO^+. The transitions are attributed to $2\,^3\Pi(v' = 0$–$19) - b'\,^3(v''= 8, 9, 10)$. Vibrational analysis of the absorption bands indicates the $2\,^3\Pi$ state correlates to the $N^+(^3P) + O(^3P)$ separated atom limit and exhibits a shallow well ($D_0 \geq 0.21$ eV) at an internuclear distance near 1.7 Å. Abrupt changes observed in the vibrational spacings suggest this state is homogeneously perturbed. Portions of the spectra are observed with sub-Doppler resolution allowing complete resolution of a complex rotational structure which could not yet be assigned. The absorption linewidths yield a predissociation lifetime of $\geq 1.6 \times 10^{-9}$ s for the lower vibrational levels of the $2\,^3\Pi$ state.

II. EXPERIMENTAL METHOD

The apparatus used in the present study has been described in detail elsewhere,[23] as has its application to the high resolution spectroscopy of molecular ions.[24] Briefly, the beam from a tunable cw dye laser is made coaxial with a fast ion beam of NO^+ over an interaction length of about 60 cm. The NO^+ ions are produced by electron impact ionization of NO in a high pressure ion source (0.5 Torr, ~100 eV electron energy). The ions are accelerated to typically 4000 eV, mass selected, collimated, and merged with the laser beam. If an absorption of photons occurs which results in photodissociation, the photofragments N^+ or O^+ which are ejected perpendicular to the direction of laser polarization are detected after kinetic energy analysis. The time interval between formation of the NO^+ ions in the source and their irradiation by the laser is estimated to be between 12–30 μs, the principal uncertainty in this estimate being the residence time of the ions in the source.

Most of the spectra reported here were obtained with the dye laser operating multimode at a bandwidth of approximately 1 cm^{-1} and irradiating the NO^+ ion beam within the cavity of the laser. The advantage of high photon flux obtained using this technique is partially off-
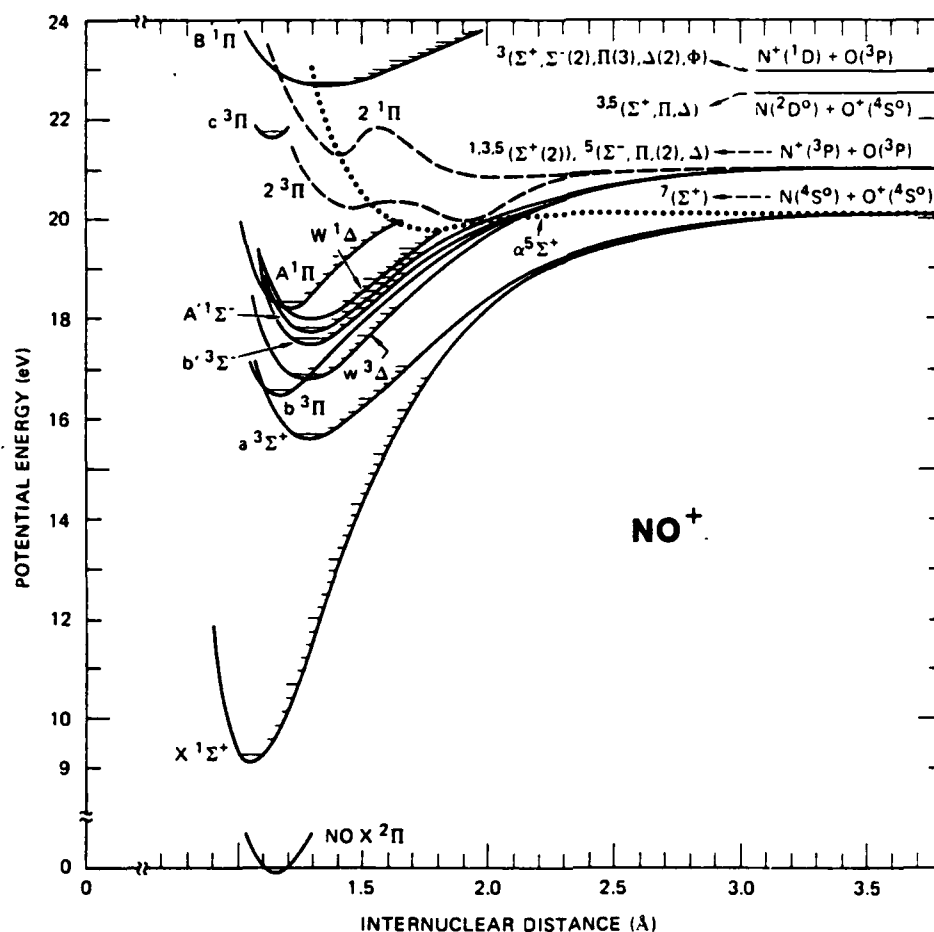
FIG. 1. Potential energy curves for the experimentally observed electronic states of NO⁺ given by Ref. 13. The accuracy of the individual curves varies—see Ref. 13. Unobserved states are listed at their expected separated atom limits. The potential curves for the $2\,^1\Pi$ and $2\,^3\Pi$ states are the adiabatic curves calculated by Ref. 10; the $\alpha\,^5\Sigma^+$ is that of Ref. 11.

set by the doubling of each absorption transition by the opposite Doppler shifts produced by photons propagating parallel and antiparallel to the ion beam velocity. Scans of the dye laser wavelength were made over the range of 6600–5650 Å for various settings of the energy analyzer to detect either N⁺ or O⁺ photofragments produced with center-of-mass separation energies (W) between 0 and 1 eV. More limited scans were made using the extra-cavity beam of the laser to irradiate the ion beam. In this case only a single Doppler component is observed, but at a substantially reduced signal to noise ratio.

Portions of the spectra were obtained using the extra-cavity beam of a single-mode ring dye laser having a bandwidth of ±25 MHz (0.0008 cm⁻¹). The laser was scanned over wave number ranges of ~1.5 cm⁻¹ by piezo-electrically tuning an intracavity etalon while modulating the laser cavity length to obtain a pseudohomogeneous distribution of laser frequencies between its 100 MHz cavity mode spacing. The procedure increased the effective bandwidth of the laser to between 50–100 MHz. A substantially smaller bandwidth could be achieved by fixing the laser frequency and velocity tuning the ion beam. However, this necessitated a more limited wavelength coverage than was required in the present study. The total apparatus produced linewidth of an absorption is the convolution of the laser bandwidth with the Doppler

width of the transition due to the finite velocity spread in the NO⁺ ion beam. The coaxial arrangement of the laser and ion beams together with the use of relatively high ion beam kinetic energies reduces this Doppler contribution to < 100 MHz.

During the course of these measurements, the previously reported[18–20] metastable decomposition (spontaneous predissociation) of NO⁺ was observed to produce O⁺ fragments with $W = 50$, 140, 220, 300, and 370 meV. This fragmentation is not influenced by laser irradiation at wavelengths between 6600–5650 Å. No higher energy O⁺ fragments and no N⁺ fragments arising from metastable decomposition were detected. It should be noted that the weak features observed at $W = 95$ and 181 meV in the kinetic energy spectra of Govers and Schopman[19] did not appear in the present measurements, probably reflecting the difference in ion sources and flight times between the two experiments.

In addition, no direct photodissociation processes (bound-free transitions), arising from perpendicular transitions to repulsive NO⁺ states were observed between 6600–5650 Å. The direct dissociation of NO⁺ to N⁺, which has been observed[25] in a parallel transition at an unspecified argon ion laser wavelength, was not investigated here.
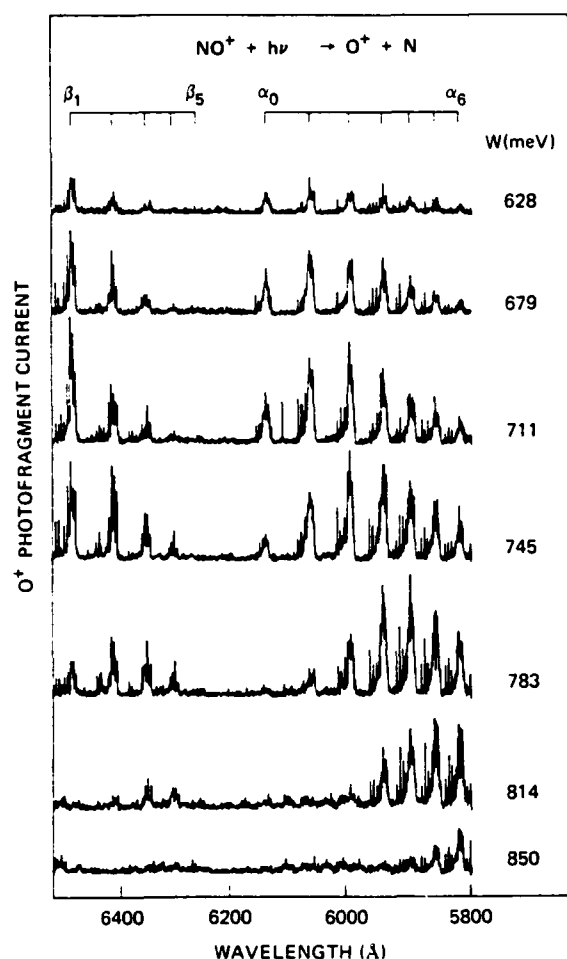
FIG. 2. Low resolution (~ 1 Å) wavelength dependence for the production of O$^+$ photofragments with various center-of-mass kinetic energies (W). The NO$^+$ ions were irradiated in the laser cavity; each absorption appears as a Doppler doublet separated by ~ 5 Å.

III. OBSERVED SPECTRA

More than 40 NO$^+$ absorption bands are observed between 6600–5650 Å which produce O$^+$ photofragments with W in the range of 0–900 meV and N$^+$ photofragments with W in the range of 0–600 meV. The most prominent band system produced O$^+$ photofragments with W between 698–925 meV. Only this predissociation band system will be discussed in the present paper.

The wavelength dependence for the production of O$^+$ photofragments between 6500–5750 Å with various center-of-mass separation energies (W) is shown in Fig. 2. The data were obtained intracavity; the Doppler doublets are separated by ~ 5 Å at 6000 Å. Two prominent vibrational progressions appear in this wavelength range. For the purpose of discussion, the members of these progressions are labeled $\alpha_0 - \alpha_6$ and $\beta_1 - \beta_5$. The reason for this choice of subscripts will become apparent.

The variation of photofragment separation energy with

wavelength is an important factor for the identification of the spectra. If we follow any given band in Fig. 2, we observe a maximum intensity at a particular setting of the energy analyzer. For example, bands α_1 and β_1 are observed with maximum intensity in the $W \sim 711$ meV spectrum. A composite spectrum of the two band progressions which reflects the absorption strengths of the transitions rather than the kinetic energy distributions of the resulting photofragments may be constructed by piecing together wavelength scans at the optimum energy analyzer setting of each band. Such a spectrum is shown in Fig. 3 for the wavelength range of 6600–5650 Å.

More detailed information on the photofragment separation energies is obtained by setting the laser to a fixed wavelength within each band and scanning the energy analyzer. The value of W observed in each of the bands is given in Table I together with the photon energy of the transitions ($G_{v',v''}$). It can be seen that within each of the progressions α and β, the variation in W from one band to the next corresponds directly to the photon energy difference of the bands $\Delta G_{v'}$. We may therefore conclude that progression α involves transitions from one vibrational level of the absorbing state to 11 closely-spaced vibrational levels in the upper electronic state which predissociate. In addition, bands $\beta_0 - \beta_5$ have the same values of W and $\Delta G_{v'}$ as bands $\alpha_0 - \alpha_5$ in the progression at higher photon energy. This demonstrates that both progressions share the same upper state vibrational levels. The relative numbering of these levels is given by the subscripts in the band designations.

The energies of the absorbing levels in the lower electronic state, relative to the O$^+$ + N limit produced by the photodissociation, are obtained by subtracting the transition energy $G_{v',v''}$ for each band from the photofragment kinetic energy W observed in the band. These values are listed in the last column of Table I. It can be seen that the α bands arise from a vibrational level of 1.323 eV below the separated atom limit whereas the β bands originate in a higher vibrational level located 1.187 eV below this limit. The similarity in the rotational structure of the α and β bands suggests that each progression originates from the same lower electronic state.

In addition to these two strong progressions, two weaker progressions produce O$^+$ photofragments with center-of-mass kinetic energies between 830–925 meV. These transitions, labeled γ and δ, in Fig. 4 appear at wavelengths between 6134–5914 Å and 6379–6268 Å, respectively. It is clear from the $W - G_{v',v''}$ values in Table I that the γ bands originate from the same lower vibrational level as the β bands, but access higher vibrational levels in the predissociated upper state. The δ bands, on the other hand, originate from a third, higher vibrational level in the absorbing electronic state. The values of W, together with the upper state vibrational spacings, show that the pairs of bands α_8 and γ_8, α_9 and γ_9, as well as α_{10} and γ_{10} each share the same upper state vibrational levels. Similarly, the four pairs of bands $\gamma_{13} - \delta_{13}$ through $\gamma_{16} - \delta_{16}$ also share common upper state vibrational levels. Thus, three absorbing vibrational levels in an upper electronic state are ob-
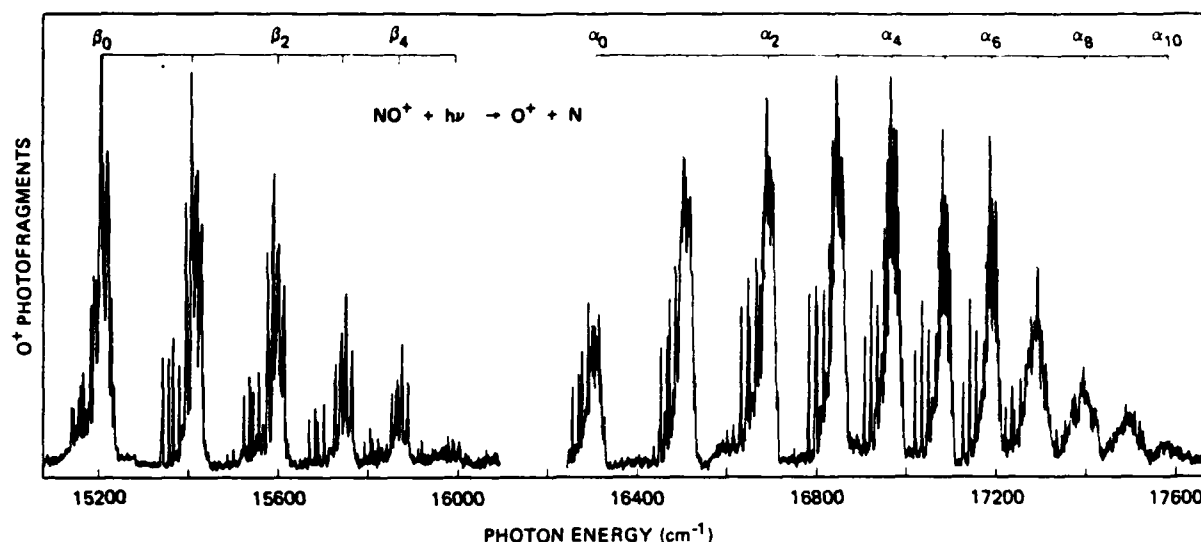
B-3

FIG. 3. Moderate resolution (~ 1 cm^{-1}), composite spectrum for the production of O$^+$ photofragments. The center-of-mass kinetic energy of the collected photofragments linearly increases with photon energy from 0.68 eV at 15 100 cm^{-1} to 0.81 eV at 16 150 cm^{-1} and from 0.67 eV at 16 250 cm^{-1} to 0.85 eV at 17 670 cm^{-1}. The NO$^+$ ions were irradiated in the laser cavity; each absorption appears as a Doppler doublet separated by ~ 14 cm^{-1}.

TABLE I. Observed transitions and photofragment kinetic energies.

Band	v''	v'	$G_{v',v''}$ (cm^{-1})[a]	$\Delta G_{v'}$ (cm^{-1})[b]	$\Delta G_{v''}$ (cm^{-1})[c]	W (eV)[d]	$W - G_{v',v''}$ (eV)[e]
α_0	8	0	16 306	203	1103	0.698	−1.324
α_1	8	1	16 509	182	1100	0.724	−1.323
α_2	8	2	16 691	155	1099	0.748	−1.321
α_3	8	3	16 846	120	1102	0.765	−1.324
α_4	8	4	16 966	118	1097	0.781	−1.323
α_5	8	5	17 084	107	$\cdots$	0.793	−1.325
α_6	8	6	17 191	100	$\cdots$	0.808	−1.323
α_7	8	7	17 291	106	$\cdots$	0.823	−1.321
α_8	8	8	17 396	97	1095	0.832	−1.325
α_9	8	9	17 493	88	1097	$\cdots$	$\cdots$
α_{10}	8	10	17 581	$\cdots$	1094	$\cdots$	$\cdots$
β_0	9	0	15 203	206	$\cdots$	$\cdots$	$\cdots$
β_1	9	1	15 409	183	$\cdots$	0.723	−1.188
β_2	9	2	15 592	152	$\cdots$	0.745	−1.188
β_3	9	3	15 744	125	$\cdots$	0.771	−1.181
β_4	9	4	15 869	124	$\cdots$	0.780	−1.188
β_5	9	5	(15 993)[f]	$\cdots$	$\cdots$	0.794	−1.189
γ_8	9	8	16 301	95	$\cdots$	0.828	−1.193
γ_9	9	9	16 396	91	$\cdots$	0.847	−1.186
γ_{10}	9	10	16 487	90	$\cdots$	$\cdots$	$\cdots$
γ_{11}	9	11	16 577	78	$\cdots$	0.869	−1.186
γ_{12}	9	12	16 655	68	$\cdots$	0.882	−1.183
γ_{13}	9	13	16 723	67	1035	0.893	−1.180
γ_{14}	9	14	(16 790)	59	1036	0.899	−1.183
γ_{15}	9	15	(16 849)	54	1039	$\cdots$	$\cdots$
γ_{16}	9	16	(16 903)	$\cdots$	1035	$\cdots$	$\cdots$
δ_{13}	10	13	15 688	66	$\cdots$	$\cdots$	$\cdots$
δ_{14}	10	14	15 754	56	$\cdots$	0.900	−1.053
δ_{15}	10	15	15 810	58	$\cdots$	$\cdots$	$\cdots$
δ_{16}	10	16	15 868	52	$\cdots$	0.915	−1.052
δ_{17}	10	17	15 920	43	$\cdots$	$\cdots$	$\cdots$
δ_{18}	10	18	15 963	(36)	$\cdots$	$\cdots$	$\cdots$
δ_{19}	10	19	(15 999)	$\cdots$	$\cdots$	0.925	−1.059

[a] Photon energy measured at band center.   [b] $G_{v'+1,v''} - G_{v',v''}$.   [c] $G_{v',v''} - G_{v',v''+1}$.

[d] Translational energy released in the photodissociation. The absolute uncertainties in these values are $^{+0.005}_{-0.010}$ eV. The relative uncertainty between measurements is about a factor of two smaller.

[e] 1 eV $\cong$ 8065.479 cm^{-1}.

[f] Parentheses denote values especially uncertain because spectral features were weak or poorly defined.
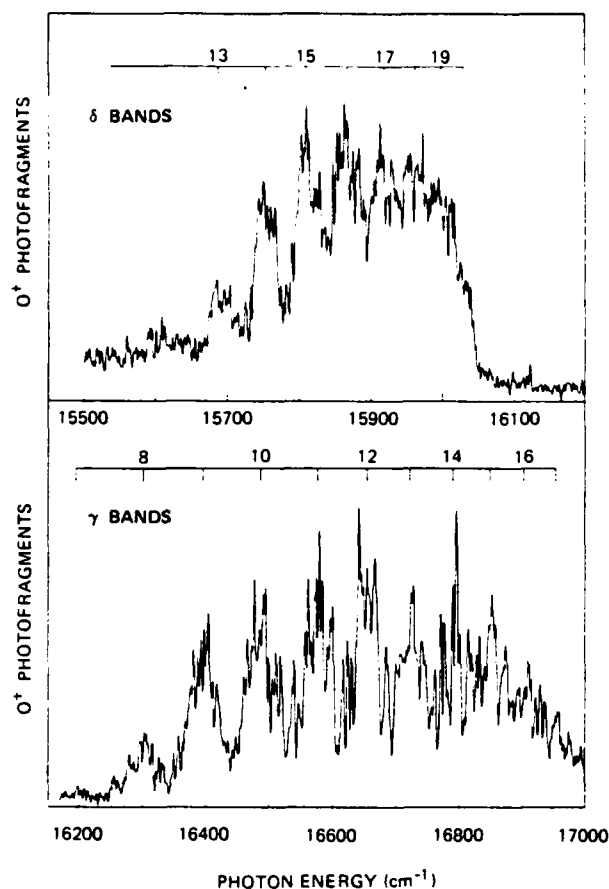
J. Chem. Phys., Vol. 75, No. 8, 15 October 1981

B-4

FIG. 4. Moderate resolution (~1 cm⁻¹), intracavity spectra of the γ and δ bands. The center-of-mass kinetic energies of the collected O⁺ photofragments increases linearly with photon energy from 0.85 to 0.94 eV in the upper spectrum and from 0.81 to 0.92 eV in the lower spectrum.

IV. DISCUSSION

A. Identification of the lower electronic state

The locations of the three absorbing vibrational levels in the lower electronic state below the O⁺ + N separated atom limit are directly given by the $W - G_{v',v'}$ values listed in Table I. The energies of these levels averaged over the α, β, γ, and δ bands are -1.323 ± 0.002, -1.187 ± 0.005, and -1.055 ± 0.005 eV. The error limits here refer only to the relative uncertainties in the measurement of W. An absolute uncertainty of $^{+0.005}_{-0.010}$ eV in the W measurement is the actual accuracy with which the absolute energy of this group of three levels can be established.[27]

The separation of the lower state vibrational levels can be more precisely determined from the photon energy difference of bands terminating in the same upper state vibrational levels. These separations are given as $\Delta G_{v'}$ in Table I. Average values of $\Delta G_{v''} = 1098 \pm 6$ cm⁻¹ and $\Delta G_{v''+1} = 1036 \pm 6$ cm⁻¹ from the four progressions each contain an unknown error due to our use of band centers rather than band origins, in the absence of a rotational analysis. This error is manifested by the small, but statistically significant, decrease in $\Delta G_{v'}$ with increasing upper state vibrational level. The magnitude of the error introduced by the use of band centers, however, is not likely to exceed 6 cm⁻¹; measurements of these band separations from other locations within the rotational envelopes of the bands give values for the lower state vibrational spacings which agree with the band-center values to within the stated precisions.

Although the measurement of photofragment kinetic energies establishes the location of the lower state vibrational levels with respect to O⁺ + N, the electronic states of the photofragments must be deduced indirectly. If the predissociation leads to the lowest separated atom limit O⁺(⁴S⁰) + N(⁴S⁰), the lowest of the three vibrational

served in the 6600–5650 Å wavelength region.

Band α_2 and portions of bands α_0–α_3 were investigated at high resolution. A 0.5 Å segment of band α_2 is shown in Fig. 5. The transition linewidths observed here, as well as in the other bands, are ~100 MHz, corresponding to the apparatus-induced linewidth. This places a lower limit on the predissociation lifetime of the upper electronic state of $\tau_d \geq 1.6 \times 10^{-9}$ s. The high resolution spectrum of band α_2 was found to consist of more than 280 resolved transitions having no discernible pattern other than an apparent clustering of rotational lines into three groups separated by approximately 10–12 cm⁻¹. It should be noted that the intensity of the transitions detected is dependent on the photofragment angular distributions, which vary[26] with both J and ΔJ. Rotational analysis of this spectrum has not yet been possible, but even without it we are able to identify the observed transitions primarily on the basis of the measured photofragment separation energies, as discussed in the following sections.

FIG. 5. High resolution (~0.003 cm⁻¹) spectrum of a portion of the α_2 band.

B-5

TABLE II. Lower state vibrational levels.[a]

State	v''	$\Delta G_{v''}$ (cm^{-1})[b]	$\Delta G_{v''+1}$ (cm^{-1})[c]	$D_{v''}$ (eV)[d]
$b'^3\Sigma^-$	8	1089 ± 13	1068 ± 14	-1.338 ± 0.015
$A'^1\Sigma^-$	7	1069 ± 6	1042 ± 6	-1.277 ± 0.010
$W^1\Delta$	5	1079 ± 18	1056 ± 20	-1.326 ± 0.058
This work	v''	1098 ± 3	1036 ± 10	$-1.323^{+0.005}_{-0.010}$

[a]Values for the b', A', and W states are calculated from the molecular constants in Table I of Ref. 13.
[b]$G_{v''} - G_{v''+1}$.
[c]$G_{v''+1} - G_{v''+2}$.
[d]Energy of v'' with respect to the $O^+(^4S^0) + N(^4S^0)$ separated atom limit. The b', A', and W states actually correlate to the $N^+(^3P) + O(^3P)$ limit, which is higher in energy by 0.916 eV.

levels would lie 18.80 eV above NO $X^2\Pi$ ($v = 0$). Dissociation to the next higher O^+ limits: $O^+(^4S^0) + N(^2D^0)$, $O^+(^2D^0) + N(^4S^0)$, or $O^+(^4S^0) + N(^2P^0)$ would place this vibrational level at 21.17, 22.12, or 22.37 eV, respectively. However, it is unlikely that bound states at the energies required for the production of electronically excited photofragments would be present in the ion beam. No features appear in the NO photoelectron spectrum[12] at these energies, which indicates such levels would not be populated by direct ionization of NO in the ion source. Nevertheless, electronic states not observed in the photoelectron spectrum are predicted by theory[10,11] to lie in this general energy range. These states are bound at internuclear distances too large to permit their production in a direct ionization process or involve multiple electron excitations but could conceivably be produced by radiative cascade from higher states. Such higher states would, however, be metastable with respect to predissociation by the manifold of states arising from the two lowest separated atom limits. Indeed, production of O^+ and N^+ is observed in the photodissociative ionization spectrum[15,16] of NO at all photon energies above these respective thresholds. In addition, no production of N^+ of O^+ from the unimolecular decomposition of NO$^+$ in a beam is observed from states above 20.5 eV, indicating the predissociation lifetimes of such states, if formed, is much shorter than the $\sim 10^{-5}$ s transit time between the ion source and the photon interaction region in the present experiment. We therefore conclude that the observed photon-induced predissociations produce photofragments in their ground electronic states. Further support for this conclusion is presented in Sec. IV B.

Eight of the 22 electronic states which arise from the two lowest dissociation limits have been defined experimentally. Using the molecular constants[13] for these eight states, we may calculate the locations of their vibrational levels in the energy region of our observed lower state levels. Only three of these states, the $A'^1\Sigma^-$, $b'^3\Sigma^-$, and $W^1\Delta$, have vibrational spacings in the vicinity of the measured values of 1098 and 1036 cm^{-1}. The calculated positions of their vibrational levels with respect to the $O^+(^4S^0) + N(^4S^0)$ separated atom limit are given in Table II. It can be seen from this table that the A' state must be excluded from the list of candidate lower states because the locations of its rele-

vant vibrational levels are 0.05 eV away from the observed levels, which is well beyond the combined uncertainties in these locations.

The $W^1\Delta(v'' = 5, 6, 7)$ level separations are in good agreement with the lower state energies of the predissociation bands. However, an important consideration argues against the selection of a singlet state as the candidate lower state: the large number of rotational lines observed would require the lower state in even the most complex singlet–singlet absorption system to have a rotational temperature of > 800 K. In contrast, the rotational temperature of O_2^+ ions produced by electron impact on O_2 in our source is found[28] to be 400 ± 50 K. The formation of NO$^+$ from NO is completely analogous; hence we expect a similar rotational temperature. Consequently, the most likely candidate lower electronic state is $b'^3\Sigma^-(v'' = 8, 9, 10)$. Observation of a perturbation in $v'' = 9$ of this state (Sec. IV C) lends additional support for its selection.

B. The upper electronic state

The lowest vibrational level of the upper electronic state which predissociates in the wavelength region of 6600–5650 Å lies $0.698^{+0.005}_{-0.010}$ eV above the $O^+(^4S^0) + N(^4S^0)$ separated atom limit. This level is accessed by bands α_0 and β_0 in Fig. 3. A detailed search of this spectral region gave no indication of lower energy vibrational levels in this electronic state (see, e.g., the $W = 628$ meV spectrum in Fig. 2). The relative intensities of transitions to the upper state levels from each of the three vibrational levels in the b' state are given in Fig. 6. It can be seen that the intensities from $v'' = 8$ and 9, which otherwise exhibit a periodic variation with upper state level, abruptly terminate at our lowest observed level. This suggests assignment of the $W = 0.698$ eV level to $v' = 0$. We note that the long predissociation
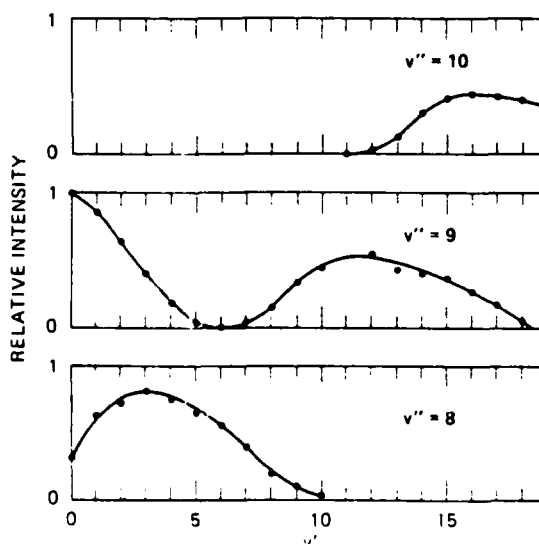

FIG. 6. Relative intensities of transitions to the predissociated vibrational levels (v') of the upper electronic state from $b'^3\Sigma^-$ $(v'' = 8, 9, 10)$. The intensities (points) are connected by arbitrary, smooth curves.

J. Chem. Phys., Vol. 75, No. 8, 15 October 1981

B-6

lifetimes of these levels, as evidenced by their narrow absorption linewidths, demonstrates a predissociation caused by a weak interaction. It is unlikely that the onset of this interaction would begin abruptly at other than the lowest upper state vibrational level. Thus, we adopt, for the sake of discussion, the assignment of the lowest observed level to $v' = 0$ while awaiting future work on the isotopically substituted ion to confirm the assignment. Thus, bands $\alpha_0-\alpha_{10}$ correspond to (v', v'') $= (0, 8)-(10, 8)$, bands $\beta_0-\beta_5$ correspond to $(0, 9)-(5, 9)$, bands $\gamma_8-\gamma_{16}$ correspond to $(8, 9)-(16, 9)$, and bands $\delta_{13}-\delta_{19}$ correspond to $(13, 10)-(19, 10)$.

The upper state vibrational spacings $\Delta G_{v'}$, determined from the centers of the observed bands, are shown as a function of mean upper state vibrational quantum number $(v' + 1/2)$, in Fig. 7(a). The squares, circles, open triangles, and closed triangles are the values determined from bands α, β, γ, and δ, respectively. The error bars for $(v' + \frac{1}{2}) = 0.5 - 6.5$ reflect the variation in $\Delta G_{v'}$ values obtained using the separations of bandheads, isolated rotational lines, and band centers. Thus, the magnitude of this variation gives some measure of the influence of changes in the upper state rotational constants with vibrational level on the apparent upper state vibrational separations determined from the band centers alone. The error bars for points at $(v' + \frac{1}{2}) \geq 7.5$ reflect only the uncertainty in locating the band centers.

The slope of $\Delta G_{v'}$ in Fig. 7(a) exhibits a strong discontinuity at $v' \sim 4$. The magnitude of this discontinuity far exceeds any possible uncertainty in the upper state vibrational spacing arising from the use of band center separations rather than band origins. Its presence suggests[29,30] that a homogeneous perturbation occurs in the upper electronic state. This will be discussed in Sec. IV D.

The observed values of $\Delta G_{v'}$ are replotted in Fig. 7(b) as a function of the energy of the upper state vibrational levels with respect to the $O^*(^4S^0) + N(^4S^0)$ separated atom limit $(W_{v' \cdot 1})$. The functional dependence of the energy eigenvalue separations of a Morse oscillator on such a plot is that of a parabola with its apex near the dissociation energy of the oscillator.[30] Also shown in Fig. 7(b) are the corresponding energies of the nine fine-structure combinations possible for the $N^*(^3P) + O(^3P)$ separated atom limit.

It is clear from Fig. 7(b) that the upper electronic state correlates to an atomic limit 0.94 ± 0.001 eV above the separated atom limit populated in the predissociation. This energy difference is quite independent of any presumption of photofragment atomic state. The fact that the observed difference directly corresponds to the energy separation of the two lowest separated atom limits of NO$^+$: $O^*(^4S^0) + N(^4S^0)$ and $N^*(^3P) + O(^3P)$, rather than to any pair of higher energy limits, confirms the arguments made in Sec. IV A that only ground electronic state photofragments are produced in the photodissociation.

The selection of candidate upper states can be restricted to those correlating to the $N^*(^3P) + O(^3P)$ limit which can reasonably be expected to exhibit the vibra-
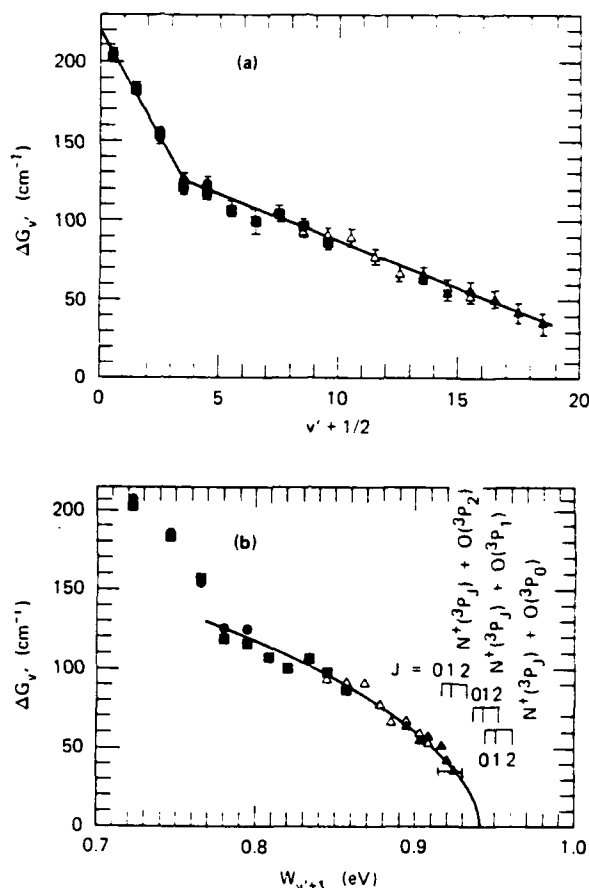

FIG. 7. Vibrational spacing in the predissociated upper electronic state as a function of (a) mean upper state vibrational quantum number $(v' - \frac{1}{2})$ and (b) upper state energy with respect to $O^*(^4S^0) - N(^4S^0)$. The energies of the nine fine-structure combinations of $N^*(^3P) + O(^3P)$ are also shown in (b). The squares, circles, open triangles, and closed triangles are the spacings derived from the α, β, γ, and δ bands, respectively. The dashed curves are least-squares fits of $\Delta G_{v'}$ to a linear functional dependence on $(v' - \frac{1}{2})$ in (a) and a quadratic functional dependence on $W_{v' \cdot 1}$ in (b). The horizontal error bar in (b) shows the absolute uncertainty in the energy scale.

tional frequencies and homogeneous perturbation discussed in the preceding section. In addition, we require an upper state that is optically connected to the $b'^3\Sigma^-$ state by a dipole-allowed transition. This reduces the candidate upper states to either the $b^3\Pi$ or the $2^3\Pi$ states (see Fig. 1).

Only the first two vibrational levels of the b state have been observed by photoelectron spectroscopy. Extrapolation of the constants for this state 14 vibrational levels into the energy region of the observed upper state yields vibrational spacings more than a factor of five larger than those of the predissociating levels. Moreover, it is clear from Fig. 1 that the vibrational overlap between the high vibrational levels of the b state and $b'^3\Sigma^-(v'' = 8, 9, 10)$ will be extremely poor.

In contrast, the properties of the $2^3\Pi$ state are quali-

J. Chem. Phys., Vol. 75, No. 8, 15 October 1981

B-7

tatively in agreement with those expected from the ob-
served transitions. The potential curve of this $2\,^3\Pi$ state
calculated by Thulstrup et al.[10] is shown as the lower
dashed curve in Fig. 1. The curve calculated by
Michels[11] for this state has an outer minimum of ~0.5
eV at ~1.95 Å and no inner minimum. Each of these
calculations yields a $2\,^3\Pi$ potential curve which allows
vertical transitions to this state from the $b'\,^3\Sigma^-$ (v''
$=8-10$) and has the shallow potential well necessary to
explain the small upper state vibrational spacings ob-
served in the predissociation spectra. In addition, both
calculations predict one or more avoided crossings be-
tween the $2\,^3\Pi$ state and other curves arising from higher
NO⁺ dissociation limits. In the calculations of Thul-
strup et al., one of these perturbations occurs within
the bound region of the potential, leading to the forma-
tion of a second minimum at shorter internuclear dis-
tances. Such a feature would qualitatively account for
the abrupt change in vibrational spacings observed in the
predissociation spectra.

No significant structure appears in the NO photoelec-
tron spectrum[12] which could be associated with the
predissociated levels of the $2\,^3\Pi$ state. However, an in-
tense peak is observed in the spectrum at 21.722 eV.
Four Rydberg series involving excitation of the NO $\sigma^*\,2s$
orbital have been identified which converge to this same
energy.[14] These observations have suggested that the
origin of an NO⁺ state lies at this energy with an equi-
librium internuclear distance close to that of NO($X\,^2\Pi$)
and an electron configuration of

$$\sigma 1s^2\,\sigma^*1s^2\,\sigma 2s^2\,\sigma^*2s^1\,\sigma 2p^2\,\pi 2p^4\,\pi^*2p^1 \ . \tag{1}$$

Lefebvre-Brion[31] has calculated the properties of the
NO⁺ states arising from this configuration and found that
the assignment of this feature to a $^3\Pi$ state is in best
agreement with the experimental observations. This
state has been named[12,31] $c\,^3\Pi$ by analogy with the N₂
state having the same configuration,[11] $C\,^3\Pi_u$, which
adiabatically correlates to very highly excited atomic
products.[32] The approximate location[13] of this state is
shown in Fig. 1.

The configuration of the $2\,^3\Pi$ state has not been re-
ported; however, we know that it must correlate to the
N⁺(^3P) + O(^3P) separated atom limit. Only two $^3\Pi$ states
are possible from this limit. One of these is known[11] to
be the $b\,^3\Pi$ state. We therefore attribute either of the
configurations:

$$\sigma 1s^2\,\sigma^*1s^2\,\sigma 2s^2\,\sigma^*2s^2\,\sigma 2p^2\,\pi 2p^3\,\sigma^*2p^1 \tag{2}$$

or

$$\sigma 1s^2\,\sigma^*1s^2\,\sigma 2s^2\,\sigma^*2s^2\,\sigma 2p^1\,\pi 2p^3\,\pi^*2p^2 \tag{3}$$

to the $2\,^3\Pi$ state. Configuration (3) is equivalent to the
major configuration[11] of the $C'\,^3\Pi_u$ state in N₂. Thus
this state may be the isoelectronic analog of the $2\,^3\Pi$ in
NO⁺. Figure 1 does suggest that the repulsive wall of
the $2\,^3\Pi$ state will pass close to the potential well of the
$c\,^3\Pi$ state. Even the weak coupling expected between
(1)-(2) or (1)-(3) would predissociate the c state. In-
deed photoelectron-photoion coincidence studies[15] have
found that the c state is completely predissociated to
N⁺(^3P) + O(^3P).

The theoretical calculations which are presently avail-
able do not accurately describe the NO⁺ potential curves
above the first separated atom limit. This is particu-
larly unfortunate in the present investigation since the
states in this region are expected to have strongly mixed
configurations, particularly at the larger internuclear
separations observed here. Thus existing calculations
are of little assistance in identifying the true form of
the $2\,^3\Pi$ potential curve. We are currently analyzing the
numerous other predissociation bands, apparently un-
related to the present band systems, which terminate in
levels above and below those discussed here. Hopefully,
some of these bands will provide additional information
on the location of the perturbing $^3\Pi$ state.

In summary, the following arguments have led us to
identify the main features of the observed band systems
as $2\,^3\Pi - b'\,^3\Sigma^-$ transitions: (a) The energy locations and
vibrational spacing of $v=8$, 9, and 10 of the b' state
agree with the lower state vibrational levels measured
in this experiment; (b) the complexity of the band struc-
ture, coupled with the apparent clustering of rotational
lines into three groups,[33] is consistent with a $^3\Pi - ^3\Sigma^-$
combination; (c) the predicted position of the $2\,^3\Pi$ state
allows good vibrational overlap with the relevant b'
levels; and (d) the homogeneous perturbation predicted
for the $2\,^3\Pi$ state is consistent with the perturbed vibra-
tional spacings observed in the upper state. Additional
confirmation for this identification comes from the ob-
servation of a rotational perturbation in the $v=9$ level
of the $b'\,^3\Sigma^-$ state, which is discussed in the next section.

C. Rotational features in the bands

Detailed comparison of the low resolution spectra of
the α and β band systems shown in Fig. 3 reveals
marked differences in their rotational envelopes. These
differences are shown more clearly in Fig. 8 where the
(3,8) and (3,9) bands are given on an expanded wave-
length scale. Although both bands have the same gen-
eral shape, the rotational structure in the (3,9) band is
decidedly less congested. This suggests that $v''=9$ of
the $b'\,^3\Sigma^-$ state has fewer rotational levels populated
among the NO⁺ ions in the beam than does $v''=8$.

The $b'\,^3\Sigma^-$ state is not the lowest triplet state in the
NO⁺ manifold (see Fig. 1). It may radiate in allowed
transitions to the $b\,^3\Pi$ [the (9,0) band origin would be
at 5272 Å]. However, transitions in the $b'-b$ system
have never been observed despite intensive searches in
spectra emitted from discharge lamps. This is un-
doubtedly because, as Field[3] suggests, the triplet states
of NO⁺ are quenched in the discharge faster than they
can radiate. Consequently, the only experimental evi-
dence for a long radiative lifetime for the b' state comes
from the ion beam emission studies of Maier and Hol-
land.[3] Several features in their spectra have been at-
tributed to transitions in the $b'\,^3\Sigma^- - X\,^1\Sigma^+$ system, in-
duced by spin-orbit interaction between the $A\,^1\Pi$ and
$b'\,^3\Sigma^-$ states.[3] Their measurements indicate lifetimes
of order 10 μs for several vibrational levels in the b'
state. The corresponding system $e'\,^3\Sigma^- - X\,^1\Sigma^+$ in the iso-
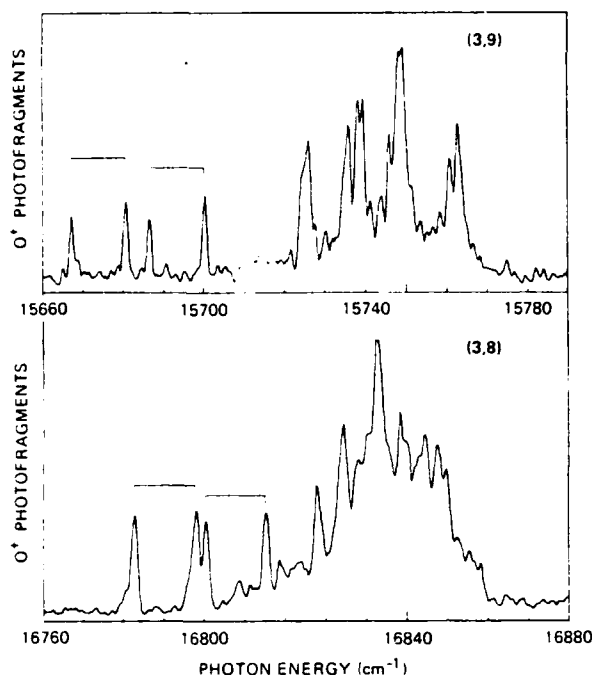electronic CO molecule is also known[34] to be long-lived
($\tau=3$ μs).

FIG. 3. Moderate resolution (~ 1 cm^{-1}), intracavity spectra of predissociations in $2\,^3\Pi(v' = 3)$ when accessed by absorptions from $v'' = 9$ (upper spectrum) and $v'' = 8$ (lower spectrum) of the $b'\,^3\Sigma^-$ state. Each absorption appears as a Doppler doublet separated by ~ 14.6 cm^{-1} in the upper spectrum and ~ 13.9 cm^{-1} in the lower spectrum. The Doppler doublets corresponding to the isolated rotational features discussed in the text are indicated in each spectrum.

The time required for NO+ ions in our experiment to reach the laser from the ion source is about 20 μs. Therefore, an appreciable fraction of the b' state levels that are populated during the ionization process will be lost due to radiation. This direct radiative loss should be essentially uniform among the rotational levels, hence the Boltzmann distribution of rotational levels in the ion source will be retained during the transit time of the beam and will be similar within each of the vibrational levels in the b' state. However, $v'' = 9$ of the b' state is locally perturbed by the $v = 3$ level of the $A\,^1\Pi$ state, whereas the $v'' = 8$ and 10 levels are not. This perturbation was first predicted by Field[7] and has more recently been observed by Alberti and Douglas[6] in the $A\,^1\Pi \to X\,^1\Sigma^+$ emission spectrum. Figure 9(a) shows the deviation of the rotational term positions measured by Alberti and Douglas for the e levels in $v = 3$ of the A state from the term values that are expected in the absence of the perturbation. The discontinuities in this figure arise from the near-degeneracy of several rotational levels in $A\,^1\Pi(v = 3)$ with the corresponding levels in the F_1 ($N = J - 1$) and F_3 ($N = J + 1$) components (e levels) of $b'\,^3\Sigma^-(v'' = 9)$. Perturbation of the f levels by the F_2 ($N = J$) component is also observed.

The A state is short-lived (56 ns)[35]; hence, the radiative lifetime of the perturbed rotational levels in the b' state will decrease to a degree dependent on the strength of the perturbation. In order to assess this effect on

the rotational distribution of NO+ ion arriving at the laser, we have analyzed[36] these perturbations using a nonlinear least-squares fitting procedure employing the rotational energy expressions given by Herzberg[37] and Kovacs[38] for the $^3\Sigma^-$ and $^1\Pi$ states, respectively. The resulting deperturbed molecular constants obtained for $A\,^1\Pi(v = 3)$ and $b'\,^3\Sigma^-(v = 9)$ are given in Table III. Also given in this table is the value obtained for the spin–orbit matrix element (H_{so}) that couples these states. We note that it differs by less than 10% from the estimate given by Field.[7] Using these constants, together with the measured lifetimes of 56 ns for the A state and 10 μs for the b' state, we have calculated the lifetime of individual rotational levels in $b'\,^3\Sigma^-(v = 9)$. The pre-
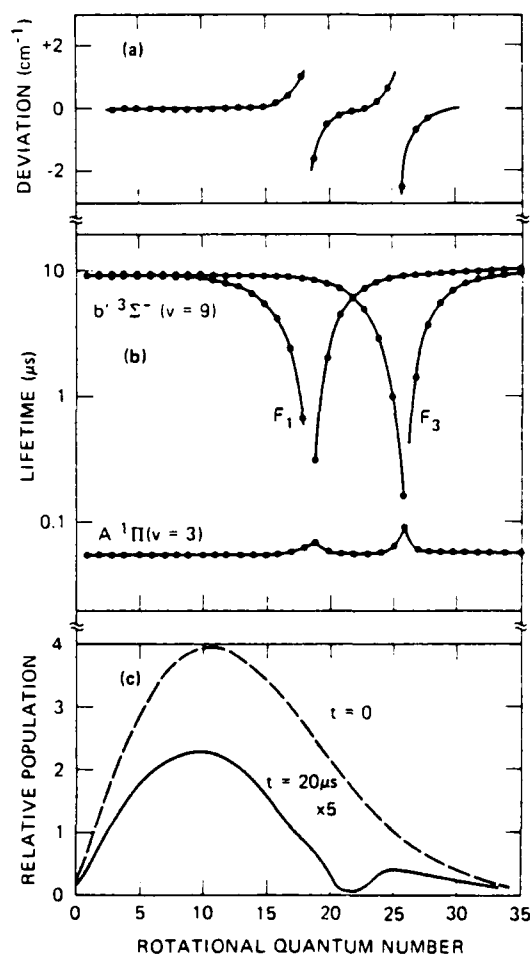

FIG. 9. Effects of the $A\,^1\Pi(v = 3)$, $b'\,^3\Sigma^-(v = 9)$ perturbation as a function of rotational quantum number. The upper figure (a) shows the deviation of the term energies of e levels in $A\,^1\Pi(v = 3)$ reported by Ref. 6 from the energies expected in the absence of perturbation by $b'\,^3\Sigma^-(v = 9, F = 1, 3)$. The center figure (b) gives the expected radiative lifetimes of these levels as a result of the perturbation and the lifetimes of the perturbing $b'\,^3\Sigma^-(v = 9)$ levels. The bottom figure (c) shows the expected 400 K Boltzmann population distribution in the rotational levels of the $b'\,^3\Sigma^-$ state produced by electron impact in the ion source (dashed curve) and the population distribution in $b'\,^3\Sigma^-(v = 9)$ upon arrival at the laser 20 μs later (solid curve).

J. Chem. Phys., Vol. 75, No. 8, 15 October 1981

B-9

TABLE III. Molecular constants from the $A^1\Pi$ ($v=3$), $b'^3\Sigma^-$ ($v=9$) perturbation.[a]

$A^1\Pi$ ($v=3$)	$b'^3\Sigma^-$ ($v=9$)[b]
$T_v = 77\,638.399$	$T_v = 77\,306.8$
$B_e = 1.500\,95$	$B = 1.159\,97$
$B_f = 1.501\,09$	$\gamma = -0.141$
$D = 6.7931 \times 10^{-6}$	$\lambda = 1.01$
	$H_{so} = 4.649$[c]

[a] Units are cm^{-1}.
[b] See Ref. 37.
[c] $H_{so} = \langle A^1\Pi, v=3 |H_{so}|^3\Sigma^-_1, v=9\rangle$.

dicted lifetimes of the F_1 and F_3 components of this state together with those of the e levels of $A^1\Pi(v=3)$ are shown in Fig. 10(b). A similar dependence is found for the F_2 component and the f levels with their respective lifetime extrema occurring at $J=22$. The resulting effect of this perturbation on the rotational distribution in $b'^3\Sigma^-(v=9)$ after a 20 μs beam transit time is shown by the solid curve in Fig. 10(c). In comparison with the 400 K Boltzmann distribution that should characterize the $b'^3\Sigma^-(v=8)$ levels, which is shown by the dashed curve in this figure, an appreciable fraction of the higher rotational levels of $v=9$ will not be present in the beam at the time of photoabsorption. The loss of these levels likely accounts for the different rotational envelopes in the $v''=8$ and $v''=9$ progressions.

A second prominent feature in the band structure of the $2^3\Pi - b'^3\Sigma^-$ transitions is the two isolated lines which appear in the low resolution spectra, Figs. 3 and 9, on the long-wavelength side of each band terminating in $v' \leqslant 7$. Above $v'=7$, the lines appear to be blended with adjacent band structures due to the decreasing vibrational spacing in the $2^3\Pi$ state. The spacing within each pair of lines is weakly dependent on upper state vibrational quantum number, varying from 22 cm^{-1} at $v'=0$ to 15 cm^{-1} at $v'=7$, and is comparable in both the $v''=8$ and 9 progressions. The isolated line which appears in Fig. 9 with Doppler components at 16 654 and 16 669 cm^{-1} was examined at high resolution. It was found to consist predominately of two strong transitions separated by 3.00 cm^{-1}, each having linewidths $\leqslant 100$ Mhz. A number of other, weaker features also appear in this wavelength region as well as in the interval between this "line" and the main band.

The sudden onset of the isolated lines at $v'=0$ in both the $v''=8$ and 9 progressions, their intensity pattern, their photofragment kinetic energies, as well as the upper state vibrational spacings derived from their spacings are all consistent with the bands which we have attributed to the $2^3\Pi - b'^3\Sigma^-$ transitions. This strongly suggests that these lines also terminate in the $2^3\Pi$ state. However, the substantial separation of the lines from the main body of each band makes it difficult to associate them with the same rotational envelopes. In addition, the lower state separation derived from the isolated lines (1110.1 cm^{-1} at $v'=0$ increasing to 1114.4 at v'

$=4$) is significantly different from that derived from the main band features (1101.7 cm^{-1} at $v'=0$ decreasing to 1098.9 at $v'=4$). It is likely that these lines arise from transitions into $2^3\Pi$ from perturbed levels of a singlet state.

D. Predissociation mechanism

The high resolution spectra of the bands terminating in $v''=0-8$ show no measurable variation in transition linewidths. Rather, the observed linewidths are apparatus limited demonstrating that predissociation of the $2^3\Pi$ state occurs only slowly (predissociation lifetimes $\geqslant 1.6$ ns). Because only O⁺ photofragments are produced, the state responsible for the predissociation must be one of the four states ($^{1,3,5,7}\Sigma^+$) arising from the N($^4S^0$) + O⁺($^4S^0$) limit. The $X^1\Sigma^+$ and $a^3\Sigma^+$ states are too strongly bound to interact effectively with bound levels of the $2^3\Pi$ state and the $^7\Sigma^+$ state is not directly coupled to the $2^3\Pi$ state ($\Delta S = 2$). This leaves the $\alpha^5\Sigma^+$ as the best candidate for the predissociating state.

The $\alpha^5\Sigma^+$ state is coupled to the $2^3\Pi$ state through the spin–orbit operator. The general effects of this interaction on the linewidths (Γ_n) of the predissociating transitions may be investigated using the Fermi golden rule[39]

$$\Gamma_n = 2\pi \,|\langle\Psi_n(r,R)\,|\,V(R)\,|\,\Psi_E(r,R)\rangle|^2 \;. \qquad (4)$$

Here $\Psi_n(r,R)$ and $\Psi_E(r,R)$ denote the rovibronic wave function of the predissociated level n and the continuum wave function at energy E above the dissociation limit, respectively, and $V(R)$ is the operator that couples the bound and continuum states. The use of Eq. (4) to predict the linewidths of the transitions neglects any linewidth contributions from the properties of the lower state involved in the transitions, $b'^3\Sigma^-$. This neglect is justified on the basis of the long lifetimes[2,3] of the b' levels.

For the ($2^3\Pi$, $\alpha^5\Sigma^+$) interaction, Eq. (4) reduces to

$$\Gamma_\Omega = 2\pi \sum_j |H(2^3\Pi_\Omega; \alpha^5\Sigma^+_j)|^2 \;. \qquad (5)$$

The summation over the components j of the Σ^+ state which interact with a particular fine-structure level Ω of the $^3\Pi$ state is based on the assumption that only insignificant phase differences among the j components are accumulated from the point of interaction to the dissociation limit. This is expected to be valid for a Σ state because its fine-structure levels lie close in energy. We have evaluated the matrix elements for the $H(2^3\Pi_\Omega; \alpha^5\Sigma^+_j)$ using the $^5\Sigma^+$ transformation matrix elements given by Kovacs[40] and Hund's case (a) elements for spin–orbit coupling given by Freed[41]:

$$\langle J\Omega S'\Lambda'\Sigma'|H_{so}|J\Omega S\Lambda\Sigma\rangle = (-1)^E \begin{pmatrix} 1 & 1 & 2 \\ \Sigma-1 & 1 & -\Sigma \end{pmatrix} A_{10}, \qquad (6)$$

where A_{10} is the intercombination analog of the spin-orbit parameter. The resulting linewidths for the three substates of $2^3\Pi$ are $\Gamma_0 \approx A_{10}$, $\Gamma_1 \approx 3A_{10}$, and $\Gamma_2 \approx 6A_{10}$. On the other hand, when both states are described by case (b) coupling, the ratio of expected linewidths among the three components is $0.67:0.77:1$.

Neither case would be distinguishable if A_{10} were so small ($< 10^{-3}$ cm^{-1}) that the expected linewidth variations fall below the limit of our experimental resolution. We should therefore consider the possible magnitude of this matrix element. The dominant electron configuration for the $\alpha\,{}^5\Sigma^+$ state is[11]

$$\sigma 1s^2\,\sigma^*1s^2\,\sigma 2s^2\,\sigma^*2s^2\,\sigma 2p^2\,\sigma^*2p^2\,\pi 2p^2\,\pi^*2p^2 \ . \tag{7}$$

The probable configurations of the $2\,{}^3\Pi$ state were given by Eqs. (2) and (3) in Sec. IV B. Both of these configurations transform into (7) via single electron excitations. This suggests approximating A_{10} by single electron spin-orbit integrals. Thus

$$A_{10} \sim \langle v|\chi\rangle\langle\pi^*2p\,|al_+|\,\sigma^*2p\rangle \ , \tag{8}$$

if $2\,{}^3\Pi$ is described by configuration (2), or

$$A_{10} \sim \langle v|\chi\rangle\langle\pi 2p\,|al_+|\,\sigma 2p\rangle \tag{9}$$

for configuration (3), where $|v\rangle$ and $|\chi\rangle$ are the vibrational and continuum wave functions of the $2\,{}^3\Pi$ and $\alpha\,{}^5\Sigma^+$ states, respectively. The one-electron spin-orbit matrix element in Eq. (9) has been reported[7] to be 76.6 cm^{-1}. The value for the corresponding matrix element in Eq. (8) has not been measured, but is likely to be the same order of magnitude. Consequently, at this level of approximation, only a uniformly small ($\sim 10^{-4}$–10^{-5}) vibrational overlap between the $2\,{}^3\Pi$ and $\alpha\,{}^5\Sigma^+$ states would lead to the observed linewidths.

As can be seen in Fig. 1, the calculated potential energy curve for the α state passes directly through the potential well of the $2\,{}^3\Pi$ state. While this may certainly lead to the requisite small overlaps for specific vibrational levels of the $2\,{}^3\Pi$, it is unreasonable to expect accidentally small vibrational overlaps to account for the narrow linewidths observed in each of the first nine vibrational levels of the $2\,{}^3\Pi$ state.[42] This could indicate that the relative locations shown for these two curves in Fig. 1 are not accurate. However, we also note that the $(2\,{}^3\Pi,\ \alpha\,{}^5\Sigma^+)$ crossing occurs in the perturbed region of the $2\,{}^3\Pi$ state. Since the perturbing $^3\Pi$ state undoubtedly has a configuration different from either (2) or (3), the use of a single configuration description for the $2\,{}^3\Pi$ state is clearly inappropriate. Proper treatment of the $(2\,{}^3\Pi,\ \alpha\,{}^5\Sigma^+)$ interaction will therefore require explicit calculation of the complete spin-orbit matrix element taking full account of the configuration mixing when improved theoretical potential curves become available.

V. CONCLUSIONS

Twenty vibrational levels of a weakly bound NO⁺ electronic state correlating to N⁺(^3P) + O(^3P) are observed to predissociate to O⁺($^4S^0$) + N($^4S^0$). The levels are accessed by electronic transitions from three vibrational levels in a lower energy electronic state of NO⁺ which are sufficiently long-lived to be significantly populated 20 μs after their formation. The energies of the predissociated levels, together with the rotational and vibrational structure in the transitions, are most consistent with assignment of the upper and lower electronic states to $2\,{}^3\Pi$ and $b'\,{}^3\Sigma^-$, respectively. The predissociated vibrational levels in the $2\,{}^3\Pi$ state are tentatively identified as $v' = 0$–19.

A number of perturbations are observed in the predissociation spectra. The rotational population of the $b'\,{}^3\Sigma^-(v'' = 9)$ levels appears to be selectively depleted due to interaction with $A\,{}^1\Pi(v = 3)$. The $2\,{}^3\Pi$ state is believed to be predissociated by the $\alpha\,{}^5\Sigma^+$ state, but the long predissociation lifetime of $\geqslant 1.6$ ns has not allowed confirmation of this assignment. In addition, the $2\,{}^3\Pi$ state is found to be homogeneously perturbed. The perturbing state is likely not the $c\,{}^3\Pi$ state observed by photoelectron spectroscopy, but the $^3\Pi$ state arising from the O⁺($^4S^0$) + N($^2D^0$) limit. On the other hand, the location of the $2\,{}^3\Pi$ state makes it the likely candidate for causing the reported predissociation of the $c\,{}^3\Pi$ state.

Molecular constants are not given for the highly perturbed vibrational structure of the $2\,{}^3\Pi$ state nor has rotational assignment of the spectra been possible. However, this study has suggested a number of experimental investigations which may lead to a unique description of the $2\,{}^3\Pi$ state. Zeeman splitting of the rotational lines in the $2\,{}^3\Pi - b'\,{}^3\Sigma^-$ transitions would greatly assist in their assignment. Extension of the wavelength region covered in the predissociation spectra to include transitions originating in lower vibrational levels of the b' state would also more precisely establish the $2\,{}^3\Pi$ state location. Isotope shifts in the vibrational structure would confirm the vibrational numbering in the bands and identify those bands which may arise from the perturbing $^3\Pi$ state. Finally, assignment of the other band systems in the NO⁺ predissociation spectra may locate the perturbing $^3\Pi$ state. These will be the subject of future investigations on NO⁺.

ACKNOWLEDGMENTS

[1]M. Oppenheimer, A. Dalgarno, E. P. Trebino, L. H. Brace, H. C. Brinton, and J. H. Hoffman, J. Geophys. Res. 82, 191 (1977).

[2]D. G. Torr and M. R. Torr, J. Atmos. Terr. Phys. 41, 797 (1979).

[3]E. E. Ferguson, in *Kinetics of Ion-Molecule Reactions*, edited by P. Ausloos (Plenum, New York, 1979), p. 377.

[4]P. Baer and E. Miescher, Helv. Phys. Acta 26, 91 (1953).

[5]E. Miescher, Helv. Phys. Acta 29, 135 (1956).

[6]F. Alberti and A. E. Douglas, Can. J. Phys. 53, 1179 (1975).

[7]R. W. Field, J. Mol. Spectrosc. 47, 194 (1973).

[8]W. B. Maier and R. F. Holland, J. Chem. Phys. 54, 2693 (1971).

[9]H. Lefebvre-Brion and C. M. Moser, J. Chem. Phys. 44, 2951 (1966).

[10]P. W. Thulstrup, E. W. Thulstrup, A. Anderson, and Y. Ohrn, J. Chem. Phys. 60, 3975 (1974).

[11]H. H. Michels, in *The Excited State in Chemical Physics,*

edited by J. W. McGowan (Wiley, New York, 1980), Vol. II.

[12]O. Edqvist, L. Åsbrink, and E. Lindholm, Z. Naturforsch. A 26, 1407 (1971).

[13]D. L. Albritton, A. L. Schmeltekopf, and R. N. Zare, J. Chem. Phys. 71, 3271 (1979).

[14]M. Sasanuma, Y. Morioka, E. Ishiguro, and M. Nakamura, J. Chem. Phys. 60, 327 (1974).

[15]H. Hertz, H. W. Jochims, H. Schenk, and W. Sroka, Chem. Phys. Lett. 29, 572 (1974).

[16]P. L. Kronebusch and J. Berkowitz, Int. J. Mass Spectrom. Ion Phys. 22, 283 (1976).

[17]J. H. Eland, J. Chem. Phys. 70, 2926 (1979).

[18]A. S. Newton and A. F. Sciamanna, J. Chem. Phys. 50, 4868 (1969).

[19]T. R. Govers and J. Schopman, Chem. Phys. Lett. 12, 414 (1971).

[20]Pham D. and M. Bizot, Int. J. Mass Spectrom. Ion Phys. 10, 227 (1972/73).

[21]T. F. Moran, F. C. Petty, and A. F. Hedrick, J. Chem. Phys. 51, 2112 (1969).

[22]T. O. Tiernan and R. E. Marcotte, J. Chem. Phys. 53, 2107 (1970).

[23]B. A. Huber, T. M. Miller, P. C. Cosby, H. D. Zeman, R. L. Leon, J. T. Moseley, and J. R. Peterson, Rev. Sci. Instrum. 48, 1306 (1977).

[24]P. C. Cosby, J. B. Ozenne, J. T. Moseley, and D. L. Albritton, J. Mol. Spectrosc. 79, 203 (1980).

[25]A. Carrington, D. R. Milverton, and P. J. Sarre, Mol. Phys. 32, 297 (1976).

[26]C. Pernot, J. Durup, J. B. Ozenne, J. A. Berwick, P. C. Cosby, and J. T. Moseley, J. Chem. Phys. 71, 2387 (1979).

[27]The angular distribution of the photofragments, which establishes the exact shape of the kinetic energy spectrum in the laboratory frame for a given W value, is dependent on rotational quantum number. See Ref. 26.

[28]F. J. Grieman, J. T. Moseley, R. P. Saxon, and P. C. Cosby, Chem. Phys. 51, 169 (1980).

[29]G. Herzberg, *Molecular Spectra and Molecular Structure I. Spectra of Diatomic Molecules* (Van Nostrand Reinhold, New York, 1950), p. 295.

[30]A. G. Gaydon, *Dissociation Energies and Spectra of Diatomic Molecules*, 3rd ed. (Chapman and Hall, London, 1968), p. 96.

[31]H. Lefebvre-Brion, Chem. Phys. Lett. 9, 463 (1971).

[32]R. S. Mulliken, in *The Threshold of Space*, edited by M. Zelikoff (Pergamon, New York, 1957), p. 169.

[33]The clustering of rotational lines into three groups separated by approximately 10 cm^{-1} suggests the spin–orbit parameter for the $2\,^3\Pi$ state is of this magnitude.

[34]W. C. Paske, A. W. Garrett, and D. E. Golden, Bull. Am. Phys. Soc. 25, 1119 (1980).

[35]J. H. Hesser, J. Chem. Phys. 48, 2518 (1968).

[36]H. Helm (to be published).

[37]Reference 29, p. 223. A constant term of $-5.05\times10^{-5}\,[N(N+1)]^2$ was included in Eqs. (V.17) to correct for centrifugal distortion.

[38]I. Kovács, *Rotational Structure in Spectra of Diatomic Molecules* (American Elsevier, New York, 1968), p. 58.

[39]L. I. Schiff, *Quantum Mechanics* (McGraw-Hill, New York, 1968), p. 285.

[40]Reference 38, p. 150.

[41]K. F. Freed, J. Chem. Phys. 45, 4214 (1966).

[42]J. N. Murrell and J. M. Taylor, Mol. Phys. 16, 609 (1969).

J. Chem. Phys., Vol. 75, No. 8, 15 October 1981

B-12

PHOTOFRAGMENT SPECTROSCOPY OF SHAPE RESONANCES IN OH^+

H. Helm, P. C. Cosby, and D. L. Huestis
Molecular Physics Department,
SRI International, Menlo Park, Ca 94025

ABSTRACT

Discrete transitions are observed in an OH^+ ion beam which lead to predissociation into $O^+ + H$. The transitions are assigned to the $A^3\Pi \leftarrow X^3\Sigma^-$ system leading to quasibound levels supported by the $\Omega = 2$ and $\Omega = 1$ substates of $A^3\Pi$. The observed predissociation manifests the action of long range dynamic coupling in the $O^+ + H$, $O + H^+$ charge-transfer channels. Improved values for the bond energy of OH^+ and the ionization potential of OH are obtained.

INTRODUCTION

The charge-transfer reaction $O + H^+ \rightarrow O^+ + H$ is the first step in the interstellar chemical cycle leading to the formation of OH.[1] The reverse reaction represents the major ionization source for atomic hydrogen in the earth's ionosphere.[2] The high rate at which this reaction proceeds in either direction derives in part from the accidental coincidence between the dissociation limits $O(^3P_1) + H^+$ and $O^+(^4S^o) + H(^2S)$, which are degenerate within the current knowledge of the ionization potentials of atomic oxygen and hydrogen[3] (see Figure 1). The importance of the charge-exchange reaction has triggered a number of theoretical investigations, the most fundamental being the close-coupling calculations by Chambaud et al.[4] who explicitly included the fine-structure excitation in the charge-exchange channel. These authors showed that the charge transfer event arises from dynamical coupling among the OH^+ molecular states at large internuclear separations (4-6 Å), with enhancement in the cross section at specific energies corresponding to shape resonances in the $A^3\Pi$ state. Here we report a first experimental study of two such resonances, which in a molecular picture may be viewed as quasibound levels of the adiabatic fine-structure states of $A^3\Pi$ shown in Figure 1. The levels are excited from the $X^3\Sigma^-$ ground state in a mass selected OH^+ ion beam with a CW UV laser. The dissociative decay of these resonances into $O^+ + H$ is monitored by observation of the charged photofragments and measurement of their kinetic energy distribution. Analysis of the excitation spectrum, the photofragment separation energies and the excitation linewidths of the resonances allows the assignment of quantum numbers to the resonances and a first direct measurement of the dissociation energy of OH^+.

EXPERIMENTAL

The apparatus, a laser-ion coaxial beams photofragment spectrometer, has been described in detail previously,[5] as has its application to spectroscopic studies.[6] The OH^+ was produced by dissociative electron-impact ionization of water vapor and accelerated to a specified energy between 2 and 4 keV. The mass selected and collimated ion beam was merged with the laser beam over a distance of 50 cm. The argon-ion laser used in this work provided 6 discrete wavelengths in the UV: 3638, 3511, 3514, 3358, 3345, and 3336 Å. External prisms were used to select the wavelength, which was then calibrated against a stabilized HeNe laser. Transistions in OH^+ were velocity-tuned into resonance with the fixed laser frequency by varying the velocity of the OH^+ beam in the laser interaction region. By directing the laser both parallel and antiparallel to the ion beam, 10 spectral regions were investigated, each covering approximately 7-10 cm^{-1} in width. The O^+ photofragments produced in photodissociation of OH^+ were deflected into an energy analyzer and detected by a channeltron. Energy analysis of the photofragments allowed determination of the energy of the dissociated levels above the dissociation limit, called the separation energy W.

Seven discrete transitions and a weak continuous background were observed to lead to photodissociation into O^+ + H. Figure 2 shows a typical wavelength scan for W=0 obtained using the single frequency output of the Ar ion laser at 3514 Å and tuning the OH^+ beam energy from 2000 to 2500 eV. The inserts give the kinetic energy spectra of the O^+ photofragments obtained from the two transitions. The discrete separation energy of the photofragments in the center of mass frame is determined from the width of the kinetic energy dis-

tributions measured at half height. The experimental parameters determined
for the observed transitions are compiled in Table I.

The transition linewidths (Γ) are determined from the breadth of the
absorption peaks at half maximum. They are wider than the apparatus limited
width ($\sim$ 100 MHz) and hence reflect the predissociation lifetimes of the
excited levels involved.

An attempt was made to observe H^+ photofragments. To our surprise none
were found. We now understand that the failure to observe H^+ is due to the
greatly differing sensitivities of the photofragment spectrometer in detecting
O^+ and H^+ fragments. To discuss the detection sensitivity we must examine the
spatial distribution of photofragments, which is illustrated in Figure 3. The
primary ion beam is merged with the laser beam in the first electrostatic
quadrupole element, Q_1. In the region between the two quadrupoles, the laser
with its polarization perpendicular to the parent beam velocity excites pri-
mary beam molecules to predissociated levels. Emerging from this event, the
fragment velocity is a sum of the original beam velocity and a component from
the separation energy. This latter component causes a shift in the laboratory
energy and angle of each fragment, the laboratory distributions depending on
the center-of-mass angular distribution of the photofragments. Shown in
Figure 3 are two extremes of such distributions, $\sin^2\theta$ and $\cos^2\theta$, labelled
parallel and perpendicular respectively. The true distributions produced
depend upon the various angular momentum quantum numbers of the states
involved and their lifetimes and lie somewhere between these two extreme
values. In the second quadrupole one of the photofragments (H^+ or O^+) is
energy selected and thus separated from the remainder of the beam. The proton
fragments are centered around 1/17th of the primary beam energy, the oxygen
fragments around 16/17th of the primary beam energy. Due to the imparted

separation energy most of the fragments will spread around the original beam direction, preferentially collecting within a circle with a radius determined by the ratio of center of mass speed of the separating fragments to the primary beam speed and the distance from the dissociation region. The two spatial distributions shown in Figure 3 were obtained by a Monte Carlo calculation of actual apparatus trajectories accounting for realistic operating conditions such as a finite beam size, and interaction length, as well as dispersion effects in Q_2. To understand the greatly different sensitivity for proton and oxygen fragments we have to recall that only a small fraction of the spatial distribution of photofragments is accepted into the electrostatic energy analyzer which is situated about 170 cm downstream from the second quadrupole and has an acceptance aperture of 1 mm diameter. For an example we assume a primary beam energy of 3000 eV and a separation energy of W = 40 meV. A simple calculation for the spatial distribution of fragments after 200 cm of flight path shows that oxygen fragments will fall into a ring of ~ 2 mm diameter. By contrast proton fragments, which due to their lower mass carry most of the separation energy, will spread much farther around the beam, into a ring of ~ 30 mm. As a result the number of proton fragments falling into the aperture of the energy analyzer is order of magnitude below that of the oxygen fragments. We believe that this discrimination is the origin for our inability to date to detect proton fragments from the predissociating transitions given in Table I.

A more sensitive scheme for detecting the proton fragments is being developed. The current paper describes results and interpretation derived from the detection of the oxygen ion fragment alone.

A. $A^3\Pi \leftarrow X^3\Sigma^-$ Transitions

As can be seen in Table I the measured linewidths and separation energies are, within their experimental uncertainties, identical among the three transitions a,b, and c (group I), and the two transitions labeled d and e (group II), respectively. Both linewidth and separation energy are attributes of the upper electronic state involved and hence these results suggest that all transitions within each group access a similar (or the same) predissociated level in the upper state. If we assume that the dissociation occurs to the lowest dissociation limit, $O^+(^4S^o_{3/2}) + H(^2S)$, the lower electronic state involved in transitions observed in both groups I and II has, for energetic reasons, to be $X^3\Sigma^-$ (see Figure 4). The observed spacings of the transitions in both groups (0.61 and 4.80 cm^{-1} in group I and 4.60 cm^{-1} in group II) are consistent with the expected spin-splitting of levels in the $X^3\Sigma^-$ ground state of OH^+, but are much smaller than the rotational spacing in the ground state. This further suggests that within each group the transitions access a single quasibound level from the spin-split components of a single rotational level of the ground state $X^3\Sigma^-$. The energetic location of these rotational levels relative to the dissociation limit $O^+ + H$ may be obtained by subtracting the measured separation energies from the transition energies. The lower state levels involved in the group I transitions lie 28080 ± 30 cm^{-1} below the dissociation limit, whereas those of group II lie 29678 ± 30 cm^{-1} below this limit. The stated uncertainties arise from the uncertainty in the experimental measurement of W. Using the bond energy[8-10] of the OH^+ ground state, 40446 ± 90 cm^{-1}, the rovibrational energy of the rotational levels (relative to the lowest existing level in the ground state) are 12366 ± 120 (group I)

and 10768 ± 120 cm^{-1} (group II). The relative location of the lower state levels is shown in Figure 4.

Merer[11] et al. have studied the A – X system of OH$^+$ in emission, and have analyzed rovibrational levels of the ground state up to 9700 cm^{-1} excitation energy, covering the ground state vibrational levels v" = 0, 1, and 2. Extrapolation of their levels using their molecular constants into the energy range observed here shows that two rovibrational levels with the required lower state spacing fall into the range of dissociation energies for groups I and II. These levels are v"=2, N"=21 (12304 cm^{-1}), and v"=2, N"=18 (10677 cm^{-1}). Since it is unlikely that the extrapolated rotational spacing is in error by as much as 100 cm^{-1} the assignment of lower state levels to v"=2, N"=18 and 21 is firm, provided the bond energy of OH$^+$ is correct within the uncertainties stated in previous work.[9,10]

Assuming that an allowed electronic transition is observed, the upper electronic state accessed by the transitions in groups I and II has to be the $A^3\Pi$ state which correlates adiabatically to the $O(^3P) + H^+$ limit. Three pieces of experimental information are available which facilitate the assignment of quantum numbers to the predissociated levels. For one, the kinetic energy distributions (see as example Figure 2) identify[11] the transitions labeled b and d in Table I as Q-type transitions (J'-J" = 0), the remainder being of type R or P (J'-J" = ± 1). Secondly, the observed relative intensities show that in group I the Q transition is strong while in group II the strong transition is either type P or R (see Table I). A third source of information comes from the spin-splitting of the lower state levels involved. In Figure 5 we show the transitions of group I and group II on a molecular energy scale. Since the ordering of fine-structure levels in the $^3\Sigma^-$ ground state has been established by the work of Merer et al.,[12] we can

identify the lower fine-structure levels involved in the Q-type transitions of groups I and II as F_2'' ($N''=J''$). The similarities among the transition linewidths and among the separation energies observed for transitions in each group suggest that each group accesses a single predissociated level, thus requiring the assignment of the remaining transitions as P type (for transitions d and e) and R type (transition b), with the R-branch transition of group II being conspicuously absent in the experiment.

We have calculated the intensity distribution of the 27 possible branches in the OH^+ $A^3\Pi$ - $X^3\Sigma^-$ transition using Merer's molecular constants and the computer program "RLS" kindly provided by Albritton.[13] We find that, in order to reproduce the observed intensity distribution, the upper state fine-structure level for group I has to be assigned to F_1' [corresponding to $^3\Pi_2$ in Hund's case (a)] while it has to be F_2' ($^3\Pi_1$) for the transitions in group II. The calculated intensities and observed, normalized intensities for the assigned transitions are given in Table I. It may be seen that the third transition expected for group II, $R_{13}(17)$, has a predicted intensity 100 times smaller than that of transition $Q_{12}(18)$. Since the count rate for the latter transition amounted to as little as 30 counts/s, the $R_{13}(17)$ transition expected for group II remained undetected. We note from Table I that the predicted intensities for the strong transitions are higher than those observed by a factor of 2 and 3. One possible explanation for this disagreement is saturation of the transitions (the ions are illuminated with single frequency radiation at power levels of typically 50 W/cm^2 for several μs).

The vibrational assignments in the upper state can be made by extrapolating the known high-J' energy levels for the $A^3\Pi$ state (v'=0-2 for OH^+ and v'=0-3 for OD^+, from Reference 12) to the energetic dissociation limit. This led to assignment of v'=6 and 5 for Groups I and II respectively.

B.   Remaining Transitions

The two transitions observed in group III appear with separation energies too high to be supported by the $A^3\Pi$ state. A tentative assignment of these transitions to the $c^1\Pi - a^1\Delta$ system can be made on the basis of the following argument: Subtracting the separation energy from the transition energy we find the lower state levels involved in transitions g and h to lie 22100 ± 600 cm^{-1} below the dissociation limit. If this limit is assumed to be $O^+(^4S^o) + H(^2S)$ the lower state levels involved are calculated to lie 2.46 ± 0.07 eV above the bottom of the well of the OH$^+$ ground state (see Fig. 4). The OH photoelectron spectrum obtained by Katsumata and Lloyd[10] places the lowest vibrational level in the $a^1\Delta$ state at 2.19 eV. The deperturbation study in the A-X system of OD$^+$ by Merer et al.,[12] when combined with the photoelectron results, places this level in OH$^+$ at 2.175 eV. Thus rotational levels of $a^1\Delta(v=0)$ with $J = 11$ are expected to lie in the energy range required for the transitions g and h. The $c^1\Pi$ state in OH$^+$ has never been observed experimentally, however the calculations of Liu and Verhaegen[7] place the lowest vibrational level in this state ~ 800 meV above the lowest dissociation limit. The group III transitions are thus consistent with the expected energies for transitions in the $c^1\Pi \leftarrow a^1\Delta$ system of OH$^+$. However, the two transitions, g and h, do not provide sufficient information to uniquely assign the vibrational and rotational quantum numbers involved.

DISCUSSION

The assignment of the transitions in groups I and II warrants a further analysis of the bond energy of OH^+ and a discussion of the dissociation mechanism involved in the observed fragmentation into $O^+ + H$.

Based on our lower state assignment, an independent value of the bond energy of OH^+ can be derived from the current observations using the measured separation energies. In order to do so, the rotational constants for the ground state as obtained by Merer et al.[12] have to be used to extrapolate from the highest previously observed rotational levels (at 9700 cm^{-1}) to the levels involved here (at 10700 and 12300 cm^{-1}, respectively). A value of 40384 ± 45 cm^{-1} is obtained, where the stated error limits does not include a small, but unknown uncertainty arising from the extrapolation. Using this value for the bond energy in a thermodynamic cycle, an adiabatic ionization potential of OH of 104873 ± 60 cm^{-1} is obtained, the additional 15 cm^{-1} uncertainty arising from the uncertatinty in the bond energy[9] of neutral OH. The direct measurement of the vertical ionization potential by Katsumata and Lloyd[10] gave a value of 104931 cm^{-1}; the appearance potential measurement of OH^+ in the photoionization of H_2O provided an a upper limit[14] for the ionization potential of 104811 ± 75 cm^{-1}. Our value is consistent with both of these previous values for the OH ionization potential and thus our bond energy value represents an improvement over the previous, indirect values of the bond energy of OH^+. The combination of all of these values, assuming an uncertainty of ± 80 cm^{-1} in the dissociation energy derived from the work of Katsumata and Lloyd, yields a "best" value for the OH^+ dissociation energy of 104866 ± 20 cm^{-1}.

The potential energy curves shown in Figure 1 and 4 suggest that the observed quasibound levels are trapped behind the rotational barrier in the $A^3\Pi$ state, and that tunneling through the barrier may be a plausible predissociation mechanism. The potential energy curves shown in Figure 1 were constructed by diagonalizing the asymptotic rotationless model Hamiltonian for OH^+, following exactly the work of Gentry and Giese[15] and Chambaud et al.[3], including the known polarizabilities of O and H, quadrupole moment of O, and spin-orbit coupling in O, and assumed[3] charge-exchange matrix elements between the $^3\Sigma^-$ states arising from $O + H^+$ and $O^+ + H$, and exponential repulsion in the $^5\Sigma^-$ state. Inclusion of off-diagonal coriolis couplings is straight-forward in the atomic basis.[16] This allows us to set up the asymptotic spin-rotation Hamiltonian which we give in Tables II and III, and to calculate rotationally-adiabatic potential energy curves for both e- and f- parity levels.[17] Such calculations, which are illustrated in Figure 6 for $J = 18$ e-parity levels, show rotational barriers of 60 and 120 meV (above $O^+ + H$) for $^3\Pi_2$ ($J=18$) and $^3\Pi_1$($J=21$), respectively. These barriers are sufficiently high to support the levels observed here. By integrating $\sqrt{V(R)-E}$ we calculated semiclassical lifetimes against barrier penetration[18] and found that in the former case the barrier height and width are consistent with the observed linewidths (Group II of Table I). In Group I however, the barrier calculated for $^3\Pi_1$ is found to be too high for tunneling to be the only predissociation mechanism.

Having rationalized the existence of quasibound levels in the $A^3\Pi$ state of OH^+, we next seek to identify the mechanism by which these levels can dissociate to $O^+ + H$. Diabatically, all components of the $A^3\Pi$ state are derived from the neutral oxygen dissociation limit. The adiabatic correlations are more complicated. Given the assumed degeneracy of the $O(^3P_1) + H^+$

and $O^+(^4S) + H$ dissociation limits, and including all interactions, only two definite conclusions can be reached: the $\Omega = 2$ component must correlate to $O(^3P_2)$, while all other components must lead to either $O(^3P_1)$ or $O^+(^4S)$. Our observation of O^+ fragments from excitation of both the $^3\Pi_2$ and $^3\Pi_1$ states confirms the importance of both spin-orbit and rotational coupling between the Π and Σ states. For example, the $^3\Pi_2$ could yield O^+ by two mechanisms: (1) weak spin-orbit interaction with $^5\Sigma^-$ near 4 Å (which we have not included in Table II because there is no first-order matrix element) or (2) it could mix with $^3\Pi_1$ by rotational coupling near 4 Å and mix a second time with $^3\Sigma^-$ by spin-orbit and charge-transfer. We note that the rotational coupling matrix element between the two $^3\Pi$ states (labeled f in Table II) amounts to 40 cm^{-1} at 4 Å. With potential energy curves that are only qualitatively reasonable, and with only the limited experimental data, we can not make more quantitative statements at this time. By detecting both the O^+ and H^+ fragments we would be able to establish the branching between the four possible dissociation limits, which should reveal a more detailed view of the dynamics of predissociation, and of the reverse process, charge exchange.

CONCLUSION

The observation of predissociation of quasibound levels in the $A^3\Pi$ state now opens the possibility of an experimental study of the long-range interactions in OH^+, similar to our previous studies[19,20] in O_2^+ and N_2^+. Our observation of fragmentation into the O^+ channel is direct evidence for the action of nonadiabatic couplings between the $^3\Pi$ potential and the $^{3,5}\Sigma^-$ states which correlate to the $O^+(^4S^o) + H^2S$ limit. A first search for photofragments reaching the $H^+ + O(^3P)$ channel has been unsuccessful, due to the low sensitivity of the present configuration to detect a light photofragment from a heavy diatomic. We are currently working on an improved detection scheme to study the branching among the four dissociation channels.

REFERENCES

1. J. H. Black and A. Dalgarno, Astrophys. J. Suppl. 34, 405 (1977).

2. R. F. Stebbings, A. C. H. Smith, and H. Erhardt, J. Geophys. Res. 68, 2349 (1967).

3. G. Chambaud, J. M. Launay, B. Levy, P. Millie, E. Roueff, and F. Tran Minh, J. Phys. B 13, 4205 (1980).

4. C. E. Moore, "Ionization Potentials and Ionization Limits Derived from the Analysis of Optical Spectra," Natl. Stand. Ref. Data Ser., Natl. Bur. Stand. U. S. Circ. No 34 (1970).

5. B. A. Huber, T. M. Miller, P. C. Cosby, H. D. Zeman, R. L. Leon, J. T. Moseley, and J. R. Peterson, Rev. Sci. Instrum. 48, 1306 (1977).

6. P. C. Cosby, J. B. Ozenne, J. T. Moseley, and D. L. Albritton, J. Mol. Spectrosc. 79, 203 (1980).

7. M. P. D. Liu and G. Verhaegen, Int. J. Quantum Chem. 5, 103 (1971).

8. The bond energy is obtained from the spectroscopic bond energy of the OH ground state[9] and the spectroscopic measurement of the ionization potentials of OH[10] and of atomic oxygen[3].

9. C. Carlone and F. W. Dalby, Can. J. Phys. 47, 1945 (1969).

10. S. Katsumata and D. R. Lloyd, Chem. Phys. Lett. 45, 519 (1977).

11. H. Helm, P. C. Cosby, M. M. Graff, and J. T. Moseley, Phys. Rev. A 25, 304 (1982).

12. A. J. Merer, D. N. Malm, R. W. Martin, M. Horani, and J. Rostas, Can. J. Phys, 53, 251, (1975).

13. D. L. Albritton, private communication.

14. K. E. McCulloh, Int. J. Mass Spectr. Ion Phys. 21, 333 (1976).

15. W. R. Gentry and C. F. Giese, J. Chem. Phys. _67_, 2355 (1977).

16. V. Aquilanti and G. Grossi, J. Chem. Phys. _73_, 1165 (1980).

17. H. Helm, P. C. Cosby, R. P. Saxon, and D. L. Huestis, J. Chem. Phys. _76_, 2516 (1982).

18. R. J. LeRoy and W.-K. Liu, J. Chem. Phys. _69_, 3622 (1978).

19. H. Helm, P. C. Cosby, and D. L. Huestis, J. Chem. Phys. _73_, 2629 (1980).

20. H. Helm and P. C. Cosby, J. Chem. Phys. _76_, 4720 (1982).

TABLE I. Transitions To Discrete, Predissociated Levels
Observed in OH^+.

Label	$h\nu$ (cm^{-1})	W (meV)	Γ (MHz)	Observed Intensity	Calculated Intensity	Assignment	(v', v")
Group I						$A \leftarrow X$	
a	28432.01	40	550	1	1	$R_{23}(20)$	(5,2)
b	28432.62	40	550	15	41	$Q_{22}(21)$	(5,2)
c	28437.40	~ 40	~ 550	1	1.1	$P_{21}(22)$	(5,2)
Group II						$A \leftarrow X$	
d	29948.16	34	4500	1	1	$Q_{12}(18)$	(6,2)
e	29452.76	34	4500	5	9.9	$P_{11}(19)$	(6,2)
f	-	-	-	not observed	0.01	$R_{13}(17)$	(6,2)
Group III						$c \leftarrow a$	
g	28454.39	800	225	--	--	--	(0,0)*
h	28432.01	750	< 550	--	--	--	(0,0)*

---

* tentative assignment

Table 11. Model Spin-Rotation Hamiltonian for OH$^+$

	$\Omega=2^a$		$\Omega=1$				$\Omega=0^+$			$\Omega=0^-$	
	$^3P_2{}^2$	$^5\Sigma_2{}^-$	$^3P_2{}^1$	$^3P_1{}^1$	$^5\Sigma_1{}^-$	$^3\Sigma_1{}^-$	$^3P_2{}^0$	$^3P_U{}^0$	$^3\Sigma_0{}^-$	$^3P_1{}^0$	$^5\Sigma_U{}^-$
$\Omega=2$											
$^3P_2{}^2$	$a+b+P_2-2B$	0	f	0	0	0	0	0	0	0	0
$^5\Sigma_2{}^-$	0	$c+e+S-2B$	0	0	f	0	0	0	0	0	0
$\Omega=1$											
$^3P_2{}^1$	f	0	$a-\frac{b}{2}+P_2+4B$	$-\frac{3}{2}b$	0	$d/\sqrt{2}$	$\sqrt{3}\,g$	0	0	0	0
$^3P_1{}^1$	0	0	$-\frac{3}{2}b$	$a-\frac{b}{2}+P_1$	0	$d/\sqrt{2}$	0	0	0	g	0
$^5\Sigma_1{}^-$	0	f	0	0	$c+e+S+4B$	0	0	0	0	0	$\sqrt{3}\,g$
$^3\Sigma_1{}^-$	0	0	$d/\sqrt{2}$	$d/\sqrt{2}$	0	$c+s$	0	0	g	0	0
$\Omega=0^+$											
$^3P_2{}^0$	0	0	$\sqrt{3}\,g$	0	0	0	$a-b+P_2+6B$	$\sqrt{2}\,b$	$2d/\sqrt{6}$	—	—
$^3P_U{}^0$	0	0	0	0	0	0	$\sqrt{2}\,b$	$a+P_0$	$-d/\sqrt{3}$	—	—
$^5\Sigma_0{}^-$	0	0	0	0	0	g	$2d/\sqrt{6}$	$-d/\sqrt{3}$	$c+S+2B$	—	—
$\Omega=0^-$											
$^3P_1{}^0$	0	0	0	g	0	0	—	—	—	$a+b+P_1+2B$	0
$^5\Sigma_U{}^-$	0	0	0	0	$\sqrt{3}\,g$	0	—	—	—	0	$c+e+S+6B$

^{a}For e-levels include $\Omega = 2, 1, 0^+$. For f-levels include $\Omega = 2, 1, 0^-$. Parameter values are given in Table 3.
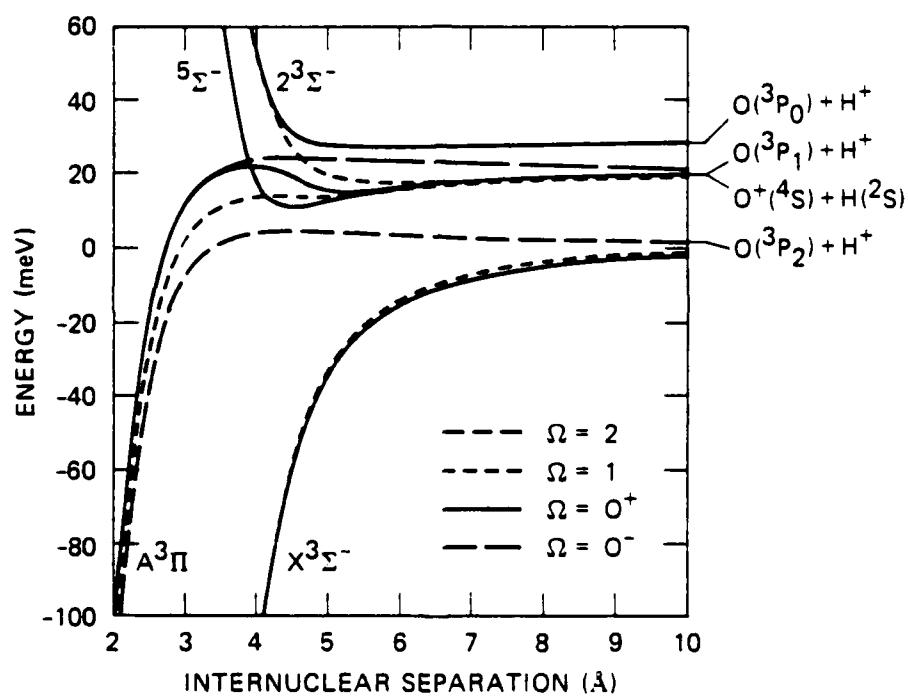
Table III. Hamiltonian Parameters for OH$^+$

Symbol	Expression[a]	Description
a(R)	$= -\dfrac{q^2}{6R^4}[2\,\alpha_\Pi^0 + \alpha_\Sigma^0] = -\dfrac{5.770}{R^4}$	O – atom spherical charge-induced dipole[b]
b(R)	$= -\dfrac{qQ^0}{4R^3} - \dfrac{q^2}{6R^4}[\alpha_\Pi^0 - \alpha_\Sigma^0] = \dfrac{1.612}{R^3} - \dfrac{0.0336}{R^4}$	O – atom charge-quadrupole plus anisotropic charge-induced dipole[b]
c(R)	$= -\dfrac{q^2}{2R^4}\alpha^H = -\dfrac{4.799}{R^4}$	H-atom charge-induced dipole[c]
d(R)	$= 69.3\ \exp\,(-1.70R)$	Charge-exchange[c]
e(R)	$= 16382\ \exp\,(-3.46R)$	Quintet repulsion[c]
g(R)	$= 2B(R)\ \sqrt{J(J+1)}$	Off-diagonal rotational coupling
f(R)	$= 2B(R)\ \sqrt{J(J+1)-2}$	
B(R)	$= \dfrac{\hbar^2}{2\mu R^2} = \dfrac{2.204 \times 10^{-3}}{R^2}$	Rotational constant
P_2	$= -19.62 \times 10^{-3}$	
P_1	$= 1.1 \times 10^{-6}$	Asymptotic energies[d] for O + H$^+$
P_0	$= 8.520 \times 10^{-3}$	
S	$= 0$	Asymptotic energy[d] for O$^+$ + H

---

[a]Energies in eV, distances in Å.

[b]Reference 15.

[c]Reference 3.

[d]Reference 4.

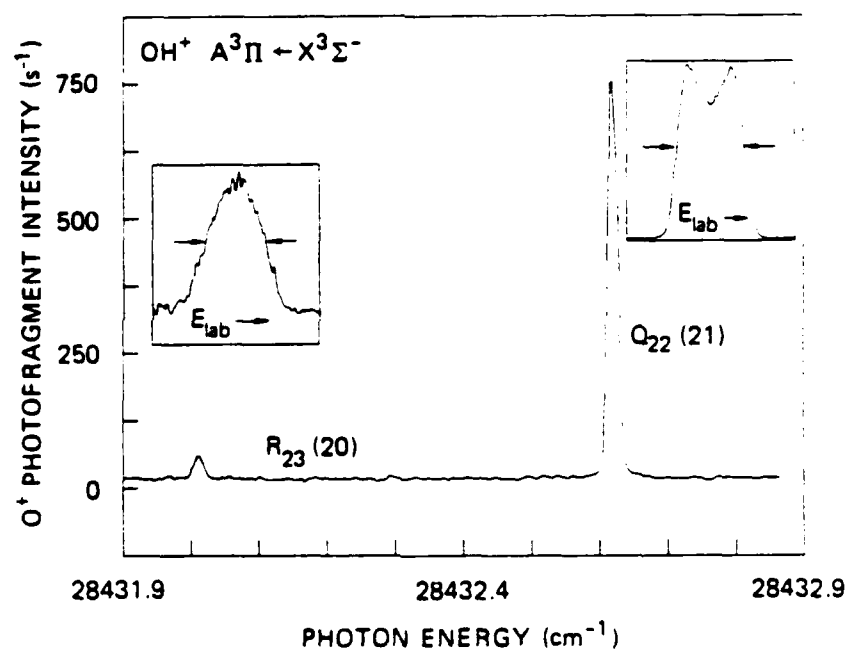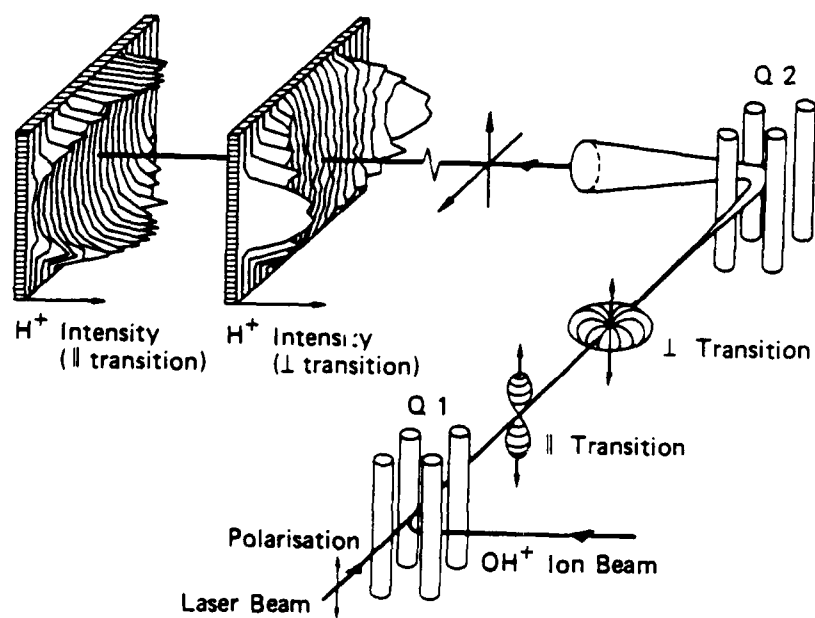## FIGURE CAPTIONS

1. Asymptotic rotationless potential curves for OH^+, with energies expressed relative to $O(^3P_2) + H^+$.

2. Variation in O^+ photofragment intensity from the photodissociation of OH^+ as a function of photon energy. Two transitions in the $A^3\Pi$ $(v=5) \leftarrow X^3\Sigma^- (v=2)$ band appear in this portion of the spectrum. The laboratory kinetic energy spectra of the O^+ photofragments arising from each transition are shown as inserts. The underlying background in the kinetic energy spectrum of the $R_{23}(20)$ transition is due to the near coincidence at this photon energy of a $c^1\Pi \leftarrow a^1\Delta$ transition labeled h in Table I.

3. Schematic of spatial distribution of H^+ photofragments produced from parallel and perpendicular transitions in OH^+.

4. Low-lying electronic states of OH^+ from references 3 and 7. The three groups of observed transitions listed in Table I are indicated by I, II, and III in this figure.

5. Energy level diagram of rotationa. transitions observed in Groups I and II.

6. Asymptotic, rotationally-adiabatic OH^+ potential energy curves for parity "e" levels with J = 18. The solid curves are eigenvalues of the spin-rotation Hamiltonian in Table II. The $^5\Sigma^-$ curves, given by the dashed lines, were calculated separately because they are not mixed with other levels by this Hamiltonian. The solid and dashed horizontal line segments give the energetic location of v = 6 in the bound and barrier regions, respectively, of the $A^3\Pi_1$ substate. All energies are referenced to the $O^+(^4S)$ + H separated atom limit.
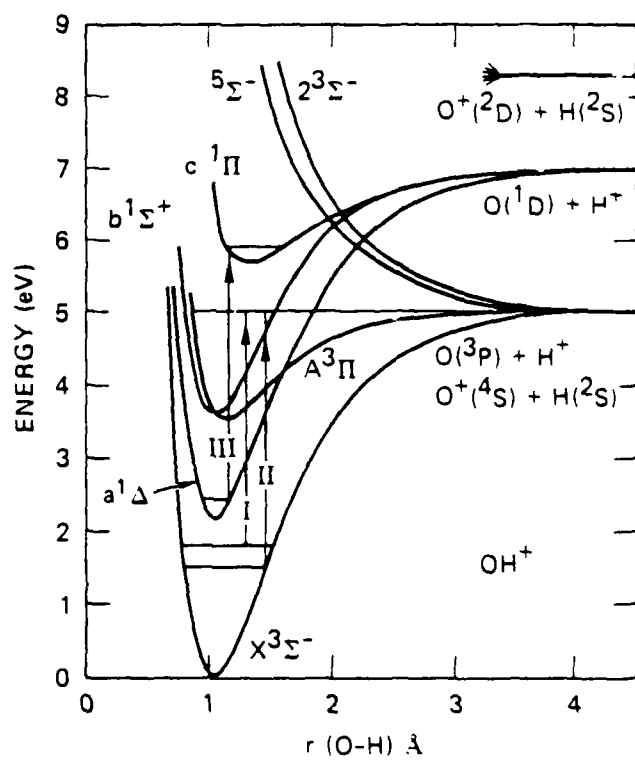
JA-3552-28

OH^+ $A^3\Pi \leftarrow X^3\Sigma^-$

O⁺ PHOTOFRAGMENT INTENSITY (s^{-1})

E_{lab}

E_{lab}

E_{lab}

Q_{22} (21)

R_{23} (20)

PHOTON ENERGY (cm^{-1})

JA-3552-26

C-22

H$^+$ Intensity
(∥ transition)

H$^+$ Intensity
(⊥ transition)

⊥ Transition

∥ Transition

Q 2

Q 1

Polarisation

OH$^+$ Ion Beam

Laser Beam

JA-330583-87B

JA-330583-21R1
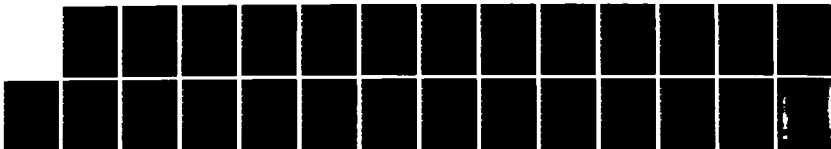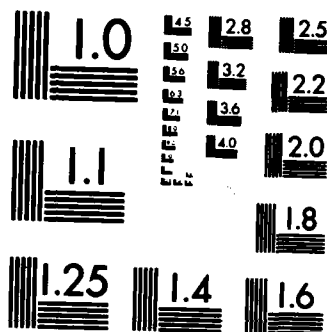
MICROCOPY RESOLUTION TEST CHART

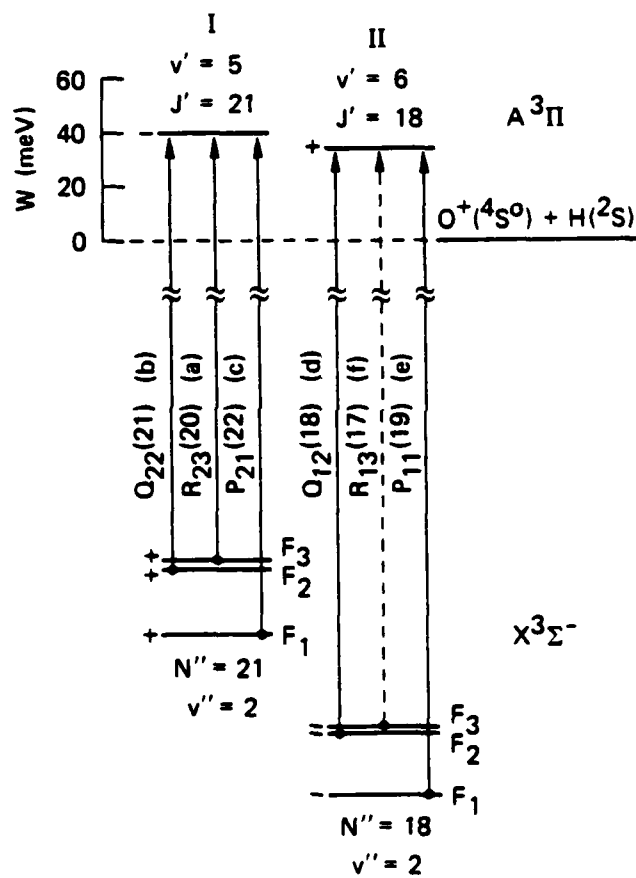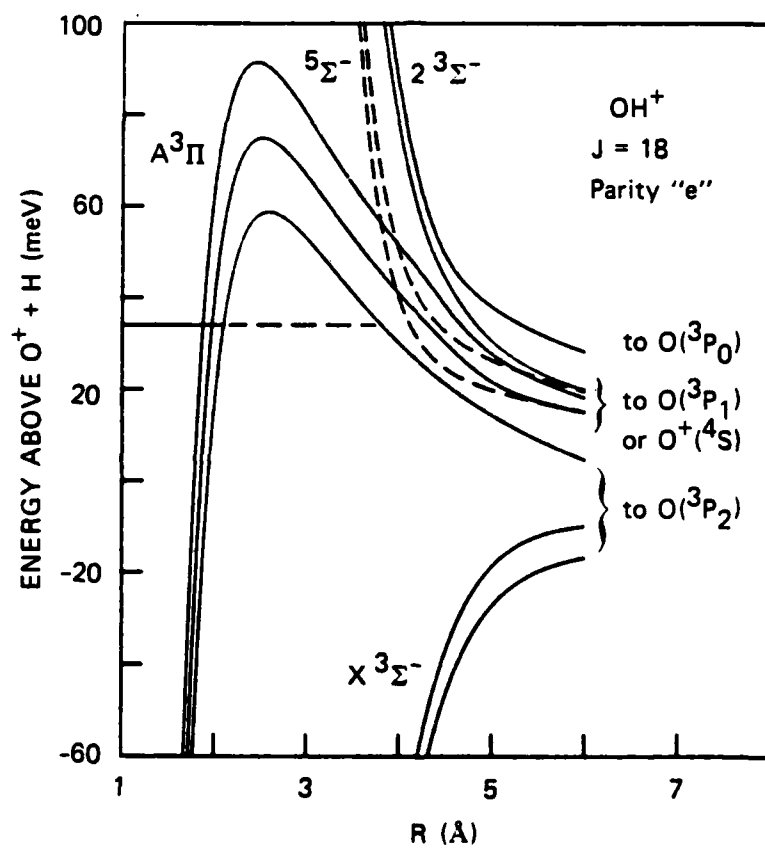NATIONAL BUREAU OF STANDARDS-1963-A

JA-3552-27

JA-3552-29A

PHOTOFRAGMENT SPECTROSCOPY OF SO$^+$

P. C. Cosby

Molecular Physics Department
Chemical Physics Laboratory
SRI International
Menlo Park, CA   94025

ABSTRACT

The SO$^+$ ion, produced by dissociative electron-impact ionization of SO$_2$, is observed to photodissociate into S$^+$ + O over the wavelength range of 6900 - 5750 Å in a series of structured bands. The bands are assigned to the

$$b^4\Sigma^-(v = 7\text{-}12) \leftarrow a^4\Pi(v = 1 - 8)$$

absorption with subsequent predissociation of the b state levels. The predissociation lifetime of the v = 7 level of the b state is found to lie in the range 5 < τ < 26 ps. The predissociation process is attributed to spin-orbit coupling to the 1$^4\Sigma^+$ state. The observed b ← a band locations and photofragment kinetic energy releases are combined with existing photoelectron and emission spectroscopy data to yield improved molecular constants for the a and b states.

I. INTRODUCTION

The SO^+ ion, which is isosteric with O_2^+, but lacks the g–u symmetry restrictions on its electronic states, had not been observed spectroscopically until recently. The photoelectron spectrum[1] of the SO radical has been measured, but numerous features due to impurity species obscured the origins of the lowest quartet state $a^4\Pi$ and the first excited doublet state $A^2\Pi$. Tsuji, Nishimura, and coworkers[2] have made an extensive series of low resolution observations on the fluorescence from a He/SO_2 afterglow and identified the bands $A^2\Pi$ (v=0–11) → $X^2\Pi$ (v=0–10). This established the origin of the A state relative to that of the X. Their work has just been extended to longer wavelengths and higher resolution by Cossart, Lavendy, and Robbe[3], who reported the first observation of emission from SO^+ quartet states. They observed and rotationally analysed the $b^4\Sigma^-$(v=0–2) → $a^4\Pi$(v=0) progression, thus establishing the relative energies of the a and b states. They also give the theoretical and experimental potential energy curves for the lower electronic states of the SO^+ ion.

We observe the photodissociation of SO^+ into S^+ + O over the wavelength region of 6900 – 5750 Å. The spectra are highly structured at moderate resolution and have the rotational structure of a $^4\Sigma$ – $^4\Pi$ transition. From the origin of the b – a system established by photoelectron and emission spectroscopy, we can identify the observed bands as $b^4\Sigma^-$(v=7–12) → $a^4\Pi$(v=1–8). The kinetic energies measured for the photofragments and the spacing of the bands yield an absolute measurement of the dissociation energies for the b and a states and vibrational constants which are valid over an extensive range of the potentials. It is especially notable that the vibrational constants for the $a^4\Pi$ state obtained from our work differ greatly from those reported by Cossart et al., due to their apparent misassignment of the weak (v',v'') = (2,2)

band. When we reassign this band as the (1,1), the data from Cossart et al.,
photoelectron spectroscopy, and photofragment spectroscopy are accurately
described by a single set of vibrational constants. This demonstrates the
unique advantage of photofragment spectroscopy to identify unambiguously the
upper state in a transition on the basis of its photofragment kinetic energy.

II. EXPERIMENTAL

The laser-ion coaxial beams photofragment spectrometer used in the experiment has been described in detail previously.[4] The SO^+ ions were formed by electron impact ($\sim$ 100 eV) dissociative ionization of SO_2 gas, accelerated to 3000 eV, mass selected, and collimated. The ion beam was then merged coaxially using an electrostatic quadrupole with a cw laser beam over a length of approximately 60 cm. The fragment ions produced in the interaction region are separated from the SO^+ ion beam by a second electrostatic quadrupole, energy selected by a hemispherical electrostatic energy analyser, and detected on an electron multiplier.

For most of the work reported here, the laser beam was the intracavity beam of a cw dye laser with a resolution of approximately 2 cm^{-1}. The laser power, which varied between 10 to 50 watts over the spectral range of 6900 – 5750 Å, was monitored by a calibrated photodiode observing the light reflected from the dye jet. Since the SO^+ ion beam passed colinearly through the circulating laser cavity, the ions encountered the opposite Doppler shifts of the copropagating and counterpropagating electromagnetic waves. Consequently, each absorption line appears as a doublet in the photofragment spectra with a separation that varies from 10.7 cm^{-1} at 6900 Å to 12.8 cm^{-1} at 5750 Å.

The extracavity beam of a cw ring dye laser was used to investigate two of the SO^+ bands at high resolution. Operating single mode, the laser had a power of approximately 800 mW , a linewidth of approximately 10 MHz, and a continuous scanning range of 0.4 cm^{-1}. The effective spectral resolution of this system, considering the velocity spread of the ion beam, was better than 0.007 cm^{-1}.

Typical SO^+ ion beam currents of 3×10^{-9} A yielded S^+ photofragment count rates of 6000 s^{-1} for the strong peaks in the spectra using the intra-

cavity dye laser. For comparison, the collision-induced dissociation due to the residual pressure of 5×10^{-9} Torr in the interaction region yielded an S^+ count rate of < 50 s^{-1}. Production of S^+ fragments from spontaneous decomposition of SO^+ was unobservably small. Production of O^+ fragments from any of these processes was not investigated.

III. RESULTS AND DISCUSSION

A. Observed Spectra

The yield of S^+ photofragments that are produced with center of mass (CM) kinetic energies (W) in the range of approximately 0 - 15 meV as a function of laser wavelength is shown in Fig. 1. Three strong bands appear in this wavelength region together with several weaker features. When this wavelength region is scanned with the energy analyser collecting photofragments produced with progressively higher kinetic energies (< 80 meV), all three of the strong bands decrease in intensity, most rapidly at their heads. The uniform variation in band intensity shows that each of the strong bands observed in Fig. 1 accesses the same upper state vibrational level. Consequently, the spacing of these bands represents the vibrational spacing in the lower electronic state (i.e. a v' progression).

Predissociation from higher v' levels could be observed as the energy analyser was adjusted to collect S^+ fragments with still higher CM kinetic energies. An example of this is shown in Fig. 2 which presents a series of dye laser scans over a portion of the wavelength region with the energy analyser set for maximum transmission at W = 0, 14, 28, 94, and 200 meV. It can be seen that as higher energy fragments are collected, the red bandhead decreases in intensity until a new bandhead appears in the W = 94 meV spectrum shifted to the blue by 50 cm^{-1}. Yet another blue-shifted bandhead appears in the W = 200 meV spectrum.

The decrease in the bandhead intensity as the energy analyser transmission is moved from W = 0 to higher values reflects the fact that progressively higher rotational levels in the lowest predissociating vibrational level are probed at the higher energies. The appearance of additional

bandheads in the W = 95 and 200 meV spectra arises from the energy analyser
passing fragments from the predissociation of the lower rotational levels in
the next two higher vibrational levels of the upper electronic state. In
general, v' progressions are observed every 0.1 eV increment in W up to W >
1.2 eV. However, at the higher W values, the bandheads become increasingly
less distinct. This arises because the CM energy resolution of the analyser
decreases with W. Above W ~ 0.5 eV, it can no longer distinguish between low
J transitions of one vibrational level and high J transitions of the next
lower v'.

More precise values of the kinetic energy releases in each band are
obtained by scanning the energy analyzer at fixed values of the laser
wavelength. Kinetic energy spectra of lines in the lowest predissociated
vibrational level show a minimum kinetic energy release of 2 ± 0.5 meV, while
the next higher v' yields a value of W_{min} = 101 ± 10 meV. Thus, the origin of
the lowest v' must lie at an energy < 0.0025 eV above an S^+ + 0 dissociation
limit, where the inequality sign is used because we cannot be certain the very
lowest rotational levels of this v' are predissociated. Secondly, the kinetic
energy spectra indicate that the lowest several predissociated vibrational
levels of the upper electronic state are spaced by 100 ± 10 meV = 806 ± 80
cm^{-1} and that predissociation in the upper state extends at least as high as
994 meV above the S^+ + 0 separated atom limit.

B. Assignment of Bands

The intense bands in the SO^+ photofragment spectrum bear a strong
resemblence to the $b^4\Sigma^-$ → $a^4\Pi$ emission bands observed by Cossart et al.[3] The
potential energy curves of these states are shown in Fig. 3. The photo-
fragment bands also resemble the bands in the analagous $b^4\Sigma_g^-$ – $a^4\Pi_u$ system of

D-7

O_2^+ which has been observed by both emission[5] and photofragment[6] spectroscopies. The $a^4\Pi$ state is expected to be metastable and, therefore, may be significantly populated in the SO^+ ion beam at the time of laser irradiation.

As a check on the consistency of assigning the photofragment bands to the $a^4\Pi \rightarrow b^4\Sigma$ absorption, we can compare the observed transition energies, intensities, and kinetic energy releases with existing data. The photo-electron spectrum of Dyke et al.[1] places the $v = 0$ level of the $b^4\Sigma^-$ state at 14.94 ± 0.05 eV relative to SO $X^3\Sigma^-(v=0)$. From the accepted dissociation energy of the SO X state[7], $D_0^0 = 5.359$ eV, and the ionization potential[8] of $S(^3P_2)$, the lowest dissociation limit of SO^+ is expected at 15.719 eV, hence 0.780 eV above $b^4\Sigma^-(v=0)$ (see Fig. 3). The spacings of the $v = 0-2$ levels of the b state are known accurately from the emission data and approximate absolute locations for $v = 0-4$ are given by the photoelectron spectrum. Since these levels extend only 0.47 eV above $v = 0$, we must extrapolate the levels for the b state into the region of observation. A weighted least-squares fit to the photoelectron and emission data yields $T_e = 120004.6(9.1)$ cm^{-1}, $\omega_e = 972.2(1.4)$ cm^{-1}, and $\omega_e x_e = 6.57(0.46)$ cm^{-1}, where the numbers in parenthesis give one standard deviation uncertainty of the constants. These constants predict $v = 7$ of the b state to lie at 15.7370 ± 0.06 eV, i.e. 18 meV above the lowest $S^+ + O$ separated atom limit. To the degree that the locations of these higher levels can be extrapolated from the known lower levels, which we will later show is quite adequate, the $v = 6$ and $v = 8$ levels are predicted to lie too far (-91 meV and +126 meV, respectively) from the measured photo-fragment energy of < 2 meV to be considered as candidates. Consequently, we identify the first predissociated level of the SO^+ $b^4\Sigma^-$ state as $v = 7$.

The origin of the $a^4\Pi$ state is partially obscured in the photoelectron spectrum by features associated with O and SO_2 impurities. However, the emission bands of Cossart et al. fix the energy of the $v = 0$ level of this state with respect to that of the clearly defined $b^4\Sigma^-$ state. Consequently, an absolute vibrational numbering can be assigned to the $a^4\Pi$ features in the photoelectron spectrum. A weighted least-squares fit to the photoelectron data yields the vibrational constants: $T_e = 108533.9(48.4)$ cm^{-1}, $\omega_e = 799.8(21.6)$ cm^{-1}, and $\omega_e x_e = 5.0(2.2)$ cm^{-1}. These constants for the a state yield the absolute lower state quantum numbers of the observed photofragment bands as shown in Table I and in Fig. 3.

C. Molecular Constants

The spacing of the observed bands and their measured photofragment kinetic energies are fully consistent with the vibrational constants of the $a^4\Pi$ and $b^4\Sigma^-$ states derived from the photoelectron spectrum[1] of SO. However, the constants can be greatly improved by also incorporating the emission data[3] and the photofragment data in a weighted least-squares fit. In the fit, the photoelectron spectra provide absolute locations for the first five vibrational levels with an estimated precision of 70 cm^{-1}, the emission data provide the relative energy differences among the first three vibrational levels with an estimated accuracy of 2 cm^{-1}, and the photofragment data provide relative energy differences between $v = 7-8$, $7-9$, and $11-12$ with an estimated accuracy of 10 cm^{-1}. The photofragment data further provide a measure of the absolute energy of $v = 8$ (and a limit on the energy of $v = 7$) when the measured kinetic energy releases of the photofragments are combined with the known dissociation energy[7] of SO and the ionization potential[8] of S. The mere constants obtained for the b state are given in Table II and

are valid for the v = 0 - 12 vibrational levels of this state. Higher constants in the vibrational expansion were found to be not significant. The T_e value obtained from the absolute photoelectron energies and that from the photofragment kinetic energy releases differed by only 51 cm^{-1} (0.006 eV). Since this difference is well within the uncertainties of both sets of measurements, it confirms the currently accepted value[7] of the SO dissociation energy.

A similar merge of the three sets of data was not possible for the a$^4\Pi$ state. The v = 0 to v = 2 spacing derived from the emission data of Cossart et al.[3] was found to be grossly inconsistant (150 cm^{-1}) with that expected from the photofragment and photoelectron data. In addition to the three strong members of the (v',0) progression, Cossart et al. also observed a fourth, substantially weaker band, which they were unable to rotationally analyse. They considered that it could be either the (1,1) or the (2,2) band, but chose to assign it as the (2,2) because it was calculated from Morse wavefunctions to have a 60% larger Franck-Condon factor and would yield an ω_e for the a state more in agreement with that computed from their ab initio potential energy curve. If we reassign the band as the (1,1), the emission data merges nicely with the photofragment and photoelectron data to yield the vibrational constants given in Table II. We further find that the Morse wavefunction Franck-Condon factors generated from the constants in Table II are nearly equal for the (1,1) and (2,2) bands (0.124 versus 0.147).

The disagreement among the data that arises when the (2,2) band assignment is retained is far more serious than would occur if only the measurement of vibrational spacings were involved. The photoelectron spectrum yields an absolute measure of the energies of v = 0, 1, 2, 3, and 4 of the b state relative to SO X(v=0). The rotationally analysed bands of Cossart et al. fix

the energy of $a^4\Pi$ (v=0) to this same reference. However, the observed

locations of the clearly resolved peaks (correctly) identified in the

photoelectron spectrum as v = 2,3,4, and 6 of the a state are in serious

disagreement with level locations predicted from the vibrational constants of

Cossart et al., but are in full agreement with the level locations predicted

from the constants given in Table II. Consequently, we believe that the

available evidence strongly supports reassigning the weak band observed by

Cossart et al. in the emission spectrum as the (1,1) band.

The constants for the a state in Table II are valid up to v = 11 in this

state, however it should be cautioned that the only information for $v > 4$ is

from the photoelectron spectrum. Due to the spin-orbit splitting in the a

state and the lack of a rotational assignment in the photofragment spectra,

the photofragment kinetic energy measurements do not directly establish the

absolute energy scale in the a state. However, the precise measurement of the

energy difference between the b and a states in Cossart et al.'s spectrum

propagates the accuracy of the b state energies into those of the a state,

thereby yielding a comparable accuracy for the energy of this state.

D. Vibrational Population in $a^4\Pi$ State

Band intensities for photofragments produced with different values of W

are difficult to measure accurately due to variations in the collection

efficiency of the apparatus arising from the angular distribution of the

photofragments. However, within a single v' progression, all of the photo-

fragments are produced with the same values of W. Hence, the relative

intensities of the bands within a progression should depend only on the

relative populations of the absorbing lower state levels and the transition

probability. Table III lists the observed intensities for the (7,v'')

progression together with the appropriate Franck-Condon factors obtained from

Morse wavefunctions and the molecular constants of the b and a states listed

in Table II. In the fourth column of Table III, we have listed the ratios of

the observed intensities to the calculated Franck-Condon factors. These

ratios should be proportional to the relative populations of the $a^4\Pi$

vibrational levels at the time they interact with the dye laser, approximately

20 μs after their formation by dissociative ionization of SO_2. For

comparison, the relative populations expected for these levels of the a state

when produced by direct ionization of SO are listed in the fifth column. It

can be seen that, in contrast to direct ionization, dissociative ionization of

SO_2 preferentially populates the SO^+ a state in its lower vibrational levels.

E. Predissociation Mechanism

It is clear from the photofragment wavelength spectra that levels v = 7,

8, 9, 11, and 12 of the $b^4\Sigma^-$ state are efficiently predissociated. In

addition, levels v = 10 and 13 are observed to predissociate in the photo-

fragment kinetic energy spectra. The kinetic energy spectra further reveal

that predissociation extends at least to levels 994 meV above the S^+ + O

separated atom limit, although the data here are not sufficient to reliably

identify the vibrational levels. Predissociation of the analogous $b^4\Sigma_g^-$ state

in O_2^+ has been studied in considerable detail by both experiment[9] and

theory.[10] There it was found that the first two vibrational levels of the b

state above the $O^+(^4S^o) + O(^3P)$ separated atom limit (v = 4,5) are

predissociated predominantly by the $d^4\Sigma_g^+$ state, whereas the $f^4\Pi_g$ plays an

increasingly important role in the predissociation of higher vibrational

levels. The case of b state predissociation in SO^+ is expected to be somewhat

simpler, because the lack of homonuclear symmetry allows only a single $^4\Pi$

state, the $a^4\Pi$, to arise from the $S^+(^4S^o) + O(^3P)$ separated atom limit. Consequently, the $^4\Sigma^+$ state is the likely candidate for causing the observed predissociation. Cossart et al.[3] have computed the _ab initio_ potential energy curves of the lower quartet and doublet states in SO^+. They find that, as in O_2^+, the repulsive wall of the $^4\Sigma^+$ state passes through the potential well of the b state, as required for an efficient predissociation process. Their calcuated potential energy curve for this state is shown by the dashed curve in Figure 3.

Spin-orbit coupling of the $^4\Sigma^+$ to the $b^4\Sigma^-$ is expected to produce a characteristic pattern[11] of predissociation lifetimes among the rotational and fine-structure levels of the b state. We investigated the (7,2) and (7,3) bands using a single-mode dye laser with the objective of measuring the linewidths of single rotational transtions and, thereby, the lifetime of the $v = 7$ level. Approximately 10 cm^{-1} were investigated within each of these bands by continuously scanning the dye laser over regions of approximately 0.4 cm^{-1}. No resolvable structure could be discerned in either of the bands. This apparent lack of structure at high resolution can be combined with the observation of rotational structure (containing unresolved fine structure) in the lower (1 cm^{-1}) resolution spectra to place approximate limits on the predissociation lifetime of the $v = 7$ level in the b state of between 2.6 x 10^{-11} and 5.0 x 10^{-12} s.

Since rapid predissociation precludes obtaining lifetime measurements for individual rotational levels in $v = 7$ of the b state, a definitive identification of the predissociating state is not possible for this level. We note, however, that the magnitude of the predissociation lifetime inferred here for $v = 7$ is very comparable to that measured for the d state contribution to the predissociation lifetime[9] of $v = 7$ in the b state of O_2^+. This, coupled with

the strong similarities between the electronic states of O_2^+ and SO^+, makes it highly likely that the dominant contribution to predissociation of the SO^+ $b^4\Sigma^-$ state near the lowest separated atom limit is from the $^4\Sigma^+$ arising from this limit.

The short predissociation lifetime of the b state introduces an additional complication in that it is not possible to obtain photofragment kinetic energy spectra for predissociation of a discrete rotational level, which limits the obtainable resolution in the kinetic energy spectra. The lowest separated atom limit $S^+(^4S^o) + O(^3P)$ is in fact three separated atom limits due to the fine-structure splitting of the $O(^3P)$ atom. The energy splittings of $^3P_1 - {}^3P_2$ and $^3P_0 - {}^3P_2$ are 158 and 227 cm^{-1}, respectively, which are easily resolvable in the kinetic energy spectra of discrete rotational levels,[12] but which might not be detected when the photofragments are produced from a distribution of rotational levels in the final state. The $^4\Sigma^+$ state adiabatically correlates to the $^3P_2$ limit, so in the absence of significant long-range coupling of this state to other electronic states correlating to the higher energy fine-structure levels, predissociation to $O(^3P_2)$ can be expected. This indeed is found[13-15] to occur in the predissociation of the O_2^+ b state and we assume here that a similar process occurs in the SO^+ ion.

IV. SUMMARY

We have found that the SO^+ ion produced from dissociative ionization of SO_2 undergoes photodissociation into $S^+ + O$ over the wavelength region of 6900 - 5750 Å. The predissociations occur from $v = 7 - 13$ of the $b^4\Sigma^-$ state. Higher vibrational levels extending to >15000 cm^{-1} above the origin of the b state also appear to predissociate. The predissociation lifetime of $b^4\Sigma^-(v=7)$ is found to be in the range $5 < \tau < 26$ ps, and is likely due to decay by spin-orbit coupling with the $^4\Sigma^+$ state arising from the $S^+(^4S^o) + O(^3P)$ separated atom limit.

Electronic absorptions into the b state are observed from $v = 1 - 12$ of the $a^4\Pi$ state. The population distribution of the SO^+ appears to be nearly uniform among the lower vibrational levels of this state. The short predissociation lifetime of the b state prevents resolution of the complex rotational structure of the b - a absorptions. However, the low resolution spectra of the band envelopes and kinetic energy releases measured for the photofragments are combined with existing data from photoelectron spectra and high resolution emission spectra to yield improved vibrational constants for the $b^4\Sigma^-$ state and revised constants for the $a^4\Pi$ state.

REFERENCES

1. J. M. Dyke, L. Golob, N. Jonathan, A. Morris, M. Okuda, and D. J. Smith, J. Chem. Soc. Faraday Trans. II $\underline{70}$, 1818 (1974).

2. M. Tsuji, C. Yamagiwa, M. Endoh, and Y. Nishimura, Chem. Phys. Letters $\underline{73}$, 407 (1980); I. Murakami, M. Tsuji, and Y. Nishimura, Chem. Phys. Letters $\underline{92}$, 131 (1982).

3. D. Cossart, H. Lavendy, and J. M. Robbe, J. Mol. Spectrosc. $\underline{99}$, 369 (1983).

4. B. A. Huber, T. M. Miller, P. C. Cosby, H. D. Zeman, R. L. Leon, J. T. Moseley, and J. R. Peterson, Rev. Sci. Instrum. $\underline{48}$, 1306 (1977).

5. D. L. Albritton, A. L. Schmeltekopf, W. J. Harrop, R. N. Zare, and J. Czarny, J. Mol. Spectrosc. $\underline{67}$, 157 (1977) and references therein.

6. J. C. Hansen, J. T. Moseley, and P. C. Cosby, J. Mol. Spectrosc. $\underline{98}$, 48 (1983) and references therein.

7. K. P. Huber and G. Herzberg, Molecular Spectra and Molecular Structure IV. Constants of Diatomic Molecules (Van Nostrand Reinhold, N. Y., 1979) p. 620.

8. C. E. Moore, "Ionization Potentials and Ionization Limits Derived from the Analyses of Optical Spectra", Nat. Stand. Nat. Bur. Stand. (U.S.), 34 (Sept. 1970).

9. J. C. Hansen, J. T. Moseley, A. L. Roche, and P. C. Cosby, J. Chem. Phys. $\underline{77}$, 1206 (1982).

10. C. M. Marian, R. Marian, S. D. Peyerimhoff, B. A. Hess, R. J. Buenker, and G. Seger, Mol. Phys. $\underline{46}$, 779 (1982).

11. I. Kovacs, Rotational Structure in the Spectra of Diatomic Molecules (American Elsevier, N. Y., 1969) p. 243. (1980).

12. H. Helm, P. C. Cosby, and D. L. Huestis, J. Chem. Phys. $\underline{73}$, 2629 (1980).

13. C. Pernot, J. Durup, J. B. Ozenne, J. A. Beswick, P. C. Cosby, and J. T. Moseley, J. Chem. Phys. $\underline{71}$, 2387 (1979).

14. M. Tadjeddine, J. Chem. Phys. $\underline{71}$, 3891 (1979).

15. J. Durup, Chem. Phys. $\underline{59}$, 351 (1981).

TABLE I. Observed $b^4\Sigma^-(v') \leftarrow a^4\Pi(v'')$ Bands

(v', v")	Band Center (cm^{-1})
(7,1)	_a)
(7,2)	16356
(7,3)	15584
(7,4)	14823
(8,2)	17169
(8,3)	16395
(9,4)	16432
(11,7)	15742
(12,8)	15777

a) Weak band partially obscured by another feature

TABLE II Molecular Constants of SO$^+$ Quartet States

State	T_e[b]	ω_e	$\omega_e x_e$	v_{max}	D_e(eV)	r_e(Å)[c]	IP(eV)
$a^4\Pi$	108494.6 (49.5)	798.50 (1.71)	4.62 (0.36)	11^d	2.267	1.653	13.501
$b^4\Sigma^-$	120004.9 (48.6)	982.50 (1.35)	10.05 (0.29)	12	2.682	1.533	14.939

a Units are cm^{-1} unless otherwise stated.

b Relative to SO $X^3\Sigma^-$ (v=0).

c Values from Ref. 3.

d Only photoelectron data available above v=4.

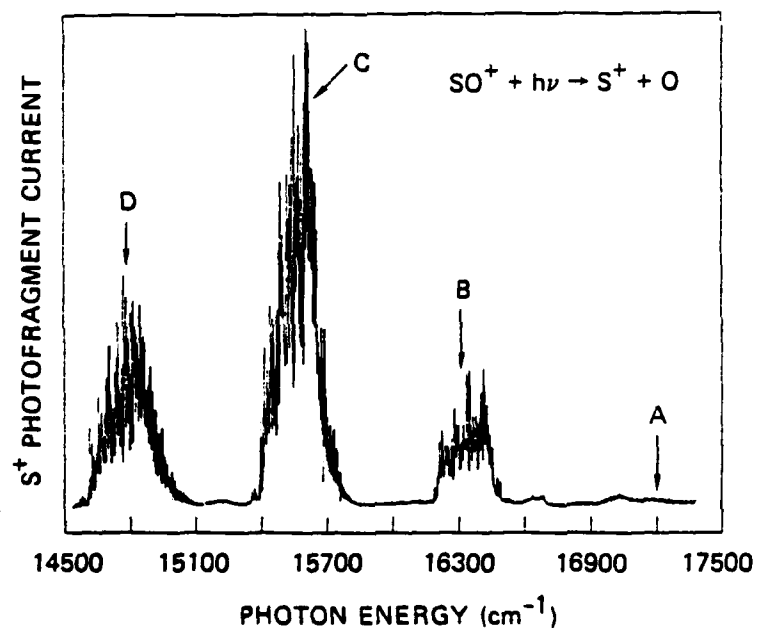TABLE III Relative Vibrational Populations Observed in $SO^+ a^4\Pi(v'')$ Produced by Dissociative Ionization of SO_2

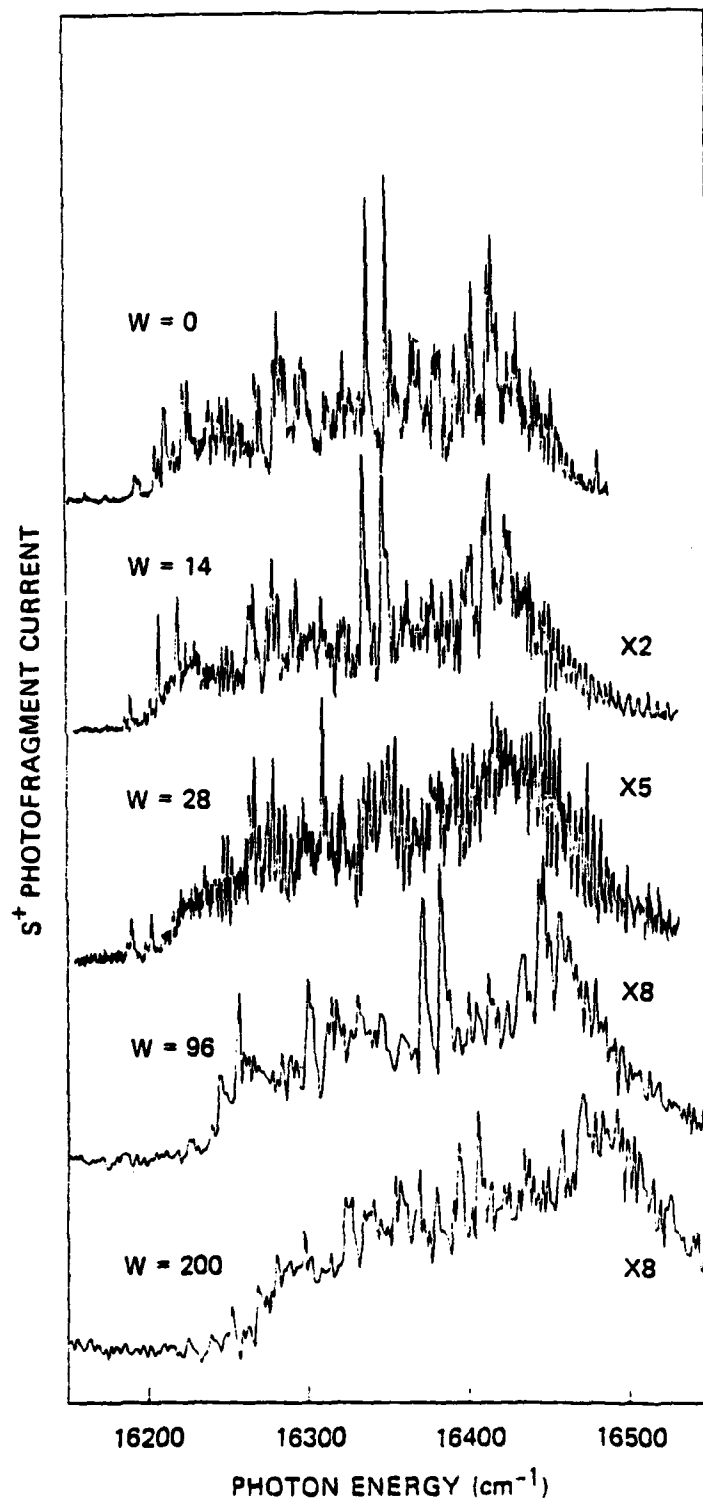| Band (v', v'')	Relative Photofragment Intensity	$b \rightarrow a$ Franck-Condon Factor	Observed Relative Population in v''	$SO^+(a) \rightarrow SO(X)$ Relative Franck-Condon Factor
(7,1)	0.18	0.0025	1.00 ± 0.27	0.29
(7,2)	4	0.0550	0.97 ± 0.10	0.59
(7,3)	15	0.2448	0.82 ± 0.08	0.86
(7,4)	7	0.1211	0.77 ± 0.08	1.00

FIGURE CAPTIONS

Figure 1. Variation in S^+ photofragment current as a function of the photon energy of the intracavity dye laser. Only S^+ photofragments produced with center of mass separation energies in the range $W = 0 - 15$ meV are monitored here. The four bands labeled A - D are identified as the $(v',v'') = (7,1)$, $(7,2)$, $(7,3)$, and $(7,4)$ bands of the SO^+ $b^4\Sigma^-(v') \leftarrow a^4\Pi(v'')$ system.

Figure 2. Variation in S^+ photofragment current as a function of intracavity laser photon energy. The energy analyser was adjusted to pass photofragments with a range of separation energies (W) centered about the value given in meV for each spectrum. The $W = 0$ meV spectrum corresponds to band B in Fig. 1. It is identified as the $(v',v'') = (7,2)$ band of the SO^+ $b^4\Sigma^-(v') \leftarrow a^4\Pi(v'')$ system. The $(8,3)$ and $(9,4)$ bands of this system appear in the $W = 96$ meV and $W = 200$ meV spectra.
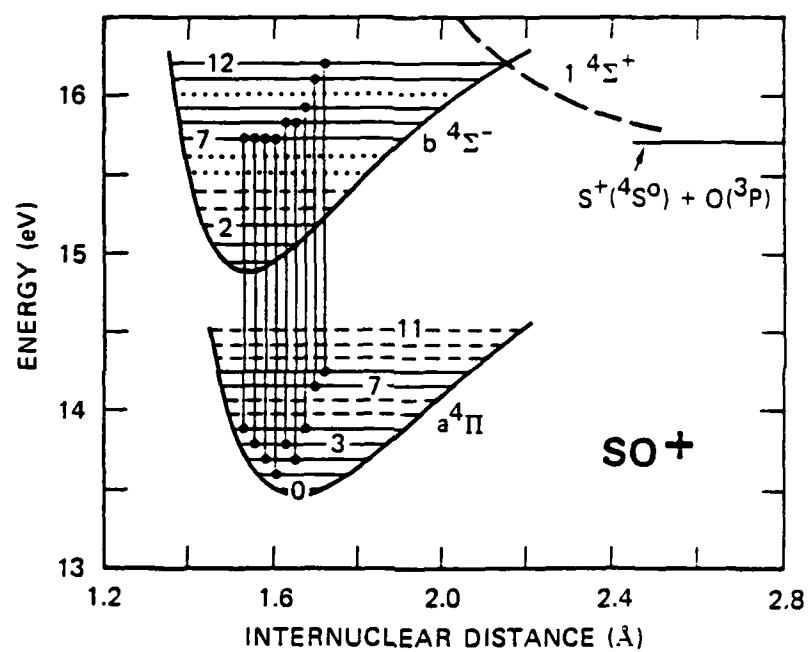
Figure 3 Lowest energy quartet states of SO^+. The potential energy curves of the $a^4\Pi$ and $b^4\Sigma^-$ states and their vibrational level energies are generated from the Morse potential function using the constants listed in Table II. Solid horizontal lines denote vibrational levels observed either by emission (Ref. 3) or photofragment spectroscopy (present work). Levels denoted by dashed lines have been observed only by photoelectron spectroscopy (Ref. 1) and dotted lines represent the unobserved vibrational levels in these states. The dashed curve is the theoretical potential energy curve of the $1^4\Sigma^+$ state given in Ref. 3. The solid vertical lines represent the absorption bands observed in the present work.

$SO^+ + h\nu \rightarrow S^+ + O$

JA-2422-19

Figure showing S⁺ PHOTOFRAGMENT CURRENT versus PHOTON ENERGY (cm⁻¹) with traces labeled W = 0, W = 14 (X2), W = 28 (X5), W = 96 (X8), and W = 200 (X8). Horizontal axis marked at 16200, 16300, 16400, 16500.

JA-2422-20

JA-2422-21

END

FILMED